

University of Alberta

Design of Macromolecular Drug Delivery Systems
Using
Molecular Dynamics Simulation

by

Sarthakkumar Kiritkumar Patel

A thesis submitted to the Faculty of Graduate Studies and Research
in partial fulfillment of the requirements for the degree of

Doctor of Philosophy
in
Chemical Engineering

Chemical and Materials Engineering

©Sarthakkumar Kiritkumar Patel

Spring 2010
Edmonton, Alberta

Permission is hereby granted to the University of Alberta Libraries to reproduce single copies of this thesis and to lend or sell such copies for private, scholarly or scientific research purposes only. Where the thesis is converted to, or otherwise made available in digital form, the University of Alberta will advise potential users of the thesis of these terms.

The author reserves all other publication and other rights in association with the copyright in the thesis and, except as herein before provided, neither the thesis nor any substantial portion thereof may be printed or otherwise reproduced in any material form whatsoever without the author's prior written permission.

Examining Committee

Dr. Phillip Choi (Supervisor); Chemical and Materials Engineering.

Dr. Afsaneh Lavasanifar (Co-supervisor); Faculty of Pharmacy and
Pharmaceutical Sciences.

Dr. Hasan Uludag; Chemical and Materials Engineering.

Dr. Anastasia Elias; Chemical and Materials Engineering.

Dr. Christine Allen; Leslie Dan Faculty of Pharmacy, University of Toronto,
Canada.

*Dedicated
To
My Parents*

Abstract

In recent years, the use of self-associating block copolymer based drug delivery systems have attracted increasing attention as nanoscopic carriers for the encapsulation and the controlled delivery of water insoluble drugs. Currently, most of the drug formulations proceed by “*trial and error*” method with no distinct method to predict the right combination of block copolymers and drugs to give all the desired functional properties. This is simply because such drug delivery systems involve complex intermolecular interactions and geometric fitting of molecules of different shapes. So, in the context of block copolymer design process, quantification and prediction of the interactions between potential block copolymers and the target drug are of great importance. Computer simulations that can predict the level and type of interactions encountered in drug/block copolymer pairs will enable researchers to make educated decisions on choosing a particular polymeric carrier for a given drug, avoiding time consuming and expensive trial and error based formulation experiments.

In the present thesis, we reported the use of molecular dynamics (MD) simulation to predict the solubility of sets of hydrophobic drug molecules having different spatial distribution of hydrogen bond forming moieties in a series of micelle-forming PEO-*b*-PCL block copolymers with and without functionalized PCL blocks. The solubility predictions based on the MD results were then compared with those obtained from the solubility experiments and those obtained

by the commonly used group contribution method (GCM). MD analysis techniques like radial distribution functions provided useful atomistic details to understand the molecular origin of miscibility and/or immiscibility observed between drugs and di-block copolymers. Based on the evidence of reported work, intermolecular specific interactions, intra-molecular interactions, local molecular packing, and stereochemistry of the hydrophobic block all play important roles in inducing miscibility between drugs and block copolymers. Additionally, not only the architecture of block copolymers but also the molecular characteristics of drug molecules, e.g., spatial distributions of hydrogen bond donors and acceptors on their molecules can affect the miscibility characteristics of binary mixtures. Depending on the groups present on drugs and block copolymers, any of the above factors can play vital role in the process of favouring encapsulation. The understanding of relative contributions of these interactions can help us to customize the performance of drug carriers by engineering the structure of block copolymers.

Acknowledgements

It gives me immense pleasure to take this opportunity to thank my academic supervisors Dr. Phillip Choi and Dr. Afsaneh Lavasanifar. The constant motivation and encouragement provided by Dr. Choi is greatly acknowledged. He has provided me technical as well as moral support throughout the span of my doctoral research work. During this long span of more than four years, I have learned a lot about professionalism, personal ethics and troubleshooting phenomena through technical as well as non-technical interactions with him, which is surely going to help me a lot in my future professional career. Dr. Lavasanifar has helped me a lot in making me understand stuffs related to the pharmaceutical field. Without her, it would have been impossible for a chemical engineer like me to grasp many of the pharmaceutical jargons that I know today. Her time-to-time feedbacks related to my research work honed my R&D skills.

I would also like to thank Dr. Hasan Uludag for providing insightful criticism to review my dissertation. My thanks also go to other faculty members, who served as committee members either on my candidacy or defense exams. The names include Dr. A. Elias, Dr. A. Yeung, Dr. L. Unsworth and Dr. C. Allen (external examiner from U of T, Canada)

I would also like to acknowledge the help I received from all the past and present members of research groups of Dr. Choi and Dr. Lavasanifar, with special thanks to Chunli, Abdullah, Mingtao, Liyan, Mingzong, and Xiao.

I would also like to acknowledge the timely help and constant encouragement exemplified by my friends Jigar Patel, Amit Jhala, Japan Trivedi, Mranal Jain, Sundeep, Ketul and Amit Singh. The entertainment (board games and movie nights) that I received by spending weekend time with my friends was most important for relieving the stress of busy weekdays. My special thanks go to my parents Dr. Kirit Patel and Mrs. Sapna Patel and my younger brother Mehul Patel, who have supported me at all times of my life, good and bad.

I would also like to thank '*Tim Hortons*' for providing great coffee everyday, which kept me awake throughout the day to do my research work efficiently.

The financial assistance (funding, awards and scholarships) provided by my supervisor, Natural Sciences and Engineering Research Council of Canada (NSERC), Faculty of Graduate Studies and Research (FGSR), Graduate Students Association (GSA) and Chemical & Materials Engineering (CME) department is gratefully acknowledged.

Table of Contents

Chapter 1	Introduction.....	1
1.1	Block Copolymer Micelles	1
1.2	Block Copolymer-Drug Compatibility	3
1.3	Solubility Parameters	4
1.4	Determination of Solubility Parameters of Polymers and Drugs.....	5
1.5	Interaction Parameters and their Estimation	8
1.6	Scope of the Thesis	10
Chapter 2	Thermodynamic Theories of Polymer Solutions and Mixtures	14
2.1	Thermodynamic Compatibility	14
2.2	Thermodynamics of Mixing.....	15
2.3	Ideal Solution Theory.....	18
2.4	Regular Solution Theory	19
2.5	Hildebrand-Scatchard Equation	22
2.6	Statistical Theories of Liquid Mixtures	24
2.6.1	The Lattice Model of Small-molecule Solutions	25
2.6.2	Flory-Huggins Lattice Theory for Polymer Solutions	29
2.6.2.1	Miscibility predictions based on the Flory-Huggins Theory	31
2.6.2.2	Limitations of the Flory-Huggins Theory.....	34
Chapter 3	Foundations of Molecular Dynamics Simulation.....	36
3.1	Introduction.....	36
3.2	Equations of Motion.....	39
3.3	Force Fields.....	40
3.3.1	Non-bonded Interactions.....	47
3.4	Molecular Dynamics Algorithms.....	48
3.4.1	Integration Algorithms.....	50
3.5	Molecular Dynamics in Various Thermodynamic Ensembles.....	52
3.5.1	Thermal Coupling	53

3.5.2	Pressure Coupling	55
3.6	Periodic Boundary Conditions	57
3.6.1	Ewald Summation	60
Chapter 4	Prediction of Compatibility Between Water Insoluble Drugs and Self Associating PEO-<i>b</i>-PCL Block Copolymers	64
4.1	Introduction	64
4.2	Simulation Details	71
4.2.1	Software and force field	71
4.2.2	Construction of liquid-state models	71
4.2.3	MD Simulation	79
4.2.4	Calculation of Flory-Huggins Interaction Parameters using MD Simulation	80
4.3	Results and Discussion	83
4.4	Summary	96
Chapter 5	Improvement of the Drug Loading Capacity of PEO-<i>b</i>-PCL with Increasing PCL Content for Two Hydrophobic Cucurbitacin Drugs: Roles of Non-Polar and Polar Intermolecular Interactions	98
5.1	Introduction	98
5.2	Simulation Details	102
5.3	Results and Discussion	104
5.3.1	MD Simulation	104
5.3.2	Non-bond Energy Analysis	109
5.3.3	Hydrogen Bond Definition	111
5.3.4	Radial Distribution Functions	117
5.3.5	Implications on <i>in vitro</i> Drug Release Profiles	123
5.4	Summary	124
Chapter 6	Molecular Origin of Solubility of Water Insoluble Drugs in PEO-<i>b</i>-Poly(α-Benzyl Carboxylate ϵ-Caprolactone) with Different Tacticities	126

6.1	Introduction.....	126
6.2	Simulation Details.....	131
6.3	Results and Discussion.....	136
6.3.1	PEO- <i>b</i> -PBCL/Cucurbitacin Drugs.....	136
6.3.1.1	MD Simulation.....	136
6.3.1.2	Intra-molecular Non-bonded Energy	141
6.3.1.3	Specific Interactions.....	144
6.3.1.4	Radial Distribution Function.....	148
6.3.2	PEO- <i>b</i> -PBCL/Fenofibrate & Nimodipine Drugs.....	166
6.4	Summary	171
Chapter 7	Encapsulation Capability of a Multi-block Copolymer Containing Three PCL Blocks Connected to One End of a PEO Block.....	173
7.1	Introduction.....	173
7.2	Model Building and Simulation Methodology	176
7.3	Results and Discussion.....	180
7.4	Summary	192
Chapter 8	Conclusion and Outlook	194
8.1	Cucurbitacin Drugs	196
8.2	Fenofibrate and Nimodipine Drugs.....	198
8.3	Limitations and Assumptions.....	199
8.4	Implications and Future Work	201
	Bibliography	204
	Appendix A Flory-Huggins Lattice Theory for Polymer Solutions	213
	Appendix B Prediction of the Molar Volume of the Repeating Units of Blocks of Copolymer	218
	Appendix C Calculations of Flory-Huggins Interaction Parameters from MD Data.....	220

List of Tables

Table 4.1	Reported experimental solubility of fenofibrate and nimodipine in caprolactone along with the solubility parameters of both the drugs and PCL block calculated by Forrest <i>et al.</i> using the GCM.	69
Table 4.2	Unique torsion angles for the PEO block	76
Table 4.3	Unique torsion angles for the PCL block.	76
Table 4.4	Rotational isomeric states for all torsion angles of PEO- <i>b</i> -PCL.	78
Table 4.5	Computed densities of drugs, block copolymers and their mixtures at 1 atm and 413 K along with the number of drug molecules involved.	86
Table 4.6	Solubility parameters of fenofibrate, nimodipine and different PEO- <i>b</i> -PCL calculated by MD simulation.	87
Table 4.7	χ parameters computed using the δ values listed in Table 4.6 for various drug/block copolymer pairs.	87
Table 5.1	Computed density values of CuB, CuI, PEO- <i>b</i> -PCL and their mixtures (10 – 12 wt% drug) at 1 atm and 473 K along with the number of drug molecules involved.	105
Table 5.2	Contributions of dispersive and electrostatic energy to non-bonded energy of mixtures of both drugs with PEO(2500)- <i>b</i> -PCL(1250) and PEO(1250)- <i>b</i> -PCL(2500).	110

Table 5.3	Locations of the first intermolecular OH peaks obtained from $g_{OH}(r)$ of mixtures containing 12 wt% drug (CuB and CuI) and remaining di-block copolymer with PCL/PEO (w/w) ratio of 0.5 and 2.0.	121
Table 6.1	Rotational isomeric states for all torsion angles of PEO- <i>b</i> -PBCL.	135
Table 6.2	Computed densities of CuB, CuI, all tactic forms of PEO(2500)- <i>b</i> -PBCL(2500) and their mixtures (10 wt% drug) at 1 atm and 473 K along with the number of drug molecules involved.	137
Table 6.3	Numbering of intra-molecular and intermolecular interactions shown in Figure 6.6.	146
Table 7.1	Rotational isomeric states for all torsion angles of PEO- <i>b</i> -3PCL.	179
Table 7.2	Liquid density values of CuB, CuI, Fenofibrate, Nimodipine, PEO(2500)- <i>b</i> -3PCL(2400) and of their binary mixtures (10 wt% drug) computed at 1 atm and two temperatures (473 K and 413 K).	181
Table 7.3	Locations of the first intermolecular OH peaks obtained from $g_{OH}(r)$ of mixtures containing 10 wt% drug (CuB, CuI, fenofibrate, and nimodipine) and remaining block copolymer – PEO(2500)- <i>b</i> -PCL(2500) and PEO(2500)- <i>b</i> -3PCL(2400).	191

List of Figures

Figure 1.1	Schematic Diagram of a Block Copolymer Micelle.	2
Figure 2.1	Three possible types of Gibbs free energy of mixing diagrams for binary mixtures.	16
Figure 2.2	Schematic representation of the lattice model of concentrated binary solutions of small molecules.	26
Figure 2.3	Schematic representation of the lattice model of a polymer solution.	30
Figure 3.1	The global flow scheme for a typical MD Algorithm.	49
Figure 3.2	Periodically repeated images of an original simulation box (solid line) in two dimensions.	58
Figure 4.1	Chemical Structures of (A) PEO- <i>b</i> -PCL; (B) Fenofibrate; and (C) Nimodipine.	68
Figure 4.2	Snapshot of the liquid model of pure PEO(2500)- <i>b</i> -PCL(2500) subjected to 3D periodic boundary conditions.	73
Figure 4.3	Snapshot of the liquid model of binary mixture of PEO(2500)- <i>b</i> -PCL(2500) and fenofibrate drug molecules (40% (w/w) drug/block copolymer) subjected to 3D periodic boundary conditions.	74
Figure 4.4	Conformational energy map of the torsion angle labelled Φ_5 in Table 4.3.	77

Figure 4.5	Flowchart of approaches taken for MD simulation of the pure and binary mixed systems of drugs and block copolymers.	84
Figure 4.6(A)	Concentration dependence of the χ parameters for drugs/PEO(1250)- <i>b</i> -PCL(2500) pairs.	90
Figure 4.6(B)	Concentration dependence of the χ parameters for drugs/PEO(2500)- <i>b</i> -PCL(2500) pairs.	90
Figure 4.6(C)	Concentration dependence of the χ parameters for drugs/PEO(2500)- <i>b</i> -PCL(1250) pairs.	91
Figure 4.7	RDF plots for 70 wt% drug in (I) PEO(1250)- <i>b</i> -PCL(2500) for (A) O atoms of fenofibrate and H atoms of PEO block; (B) O atoms of fenofibrate and H atoms of PCL block; (C) O atoms of nimodipine and H atoms of PEO block; (D) O atoms of nimodipine and H atoms of PCL block and in (II) PEO(2500)- <i>b</i> -PCL(1250) for (E) O atoms of fenofibrate and H atoms of PEO block; (F) O atoms of fenofibrate and H atoms of PCL block; (G) O atoms of nimodipine and H atoms of PEO block; (H) O atoms of nimodipine and H atoms of PCL block.	95
Figure 5.1	Chemical structures of (A) Cucurbitacin B; and (B) Cucurbitacin I.	100

Figure 5.2(A)	Plot of the computed χ values of binary mixtures of two cucurbitacins and three model PEO- <i>b</i> -PCL with different PCL/PEO ratio (w/w).	107
Figure 5.2(B)	Plot of experimentally measured drug loading capacity of PEO- <i>b</i> -PCL micelles with two different PCL/PEO ratio (w/w) for cucurbitacins as reported by Molavi <i>et al.</i>	108
Figure 5.3	Snapshot of H-bond formed between H atom of one of the -OH groups of CuB with O atom of carbonyl group of PCL block of PEO(1250)- <i>b</i> -PCL(2500).	112
Figure 5.4	Snapshot of H-bond formed between H atom of one of the -OH groups of CuB with the O atom of PEO block of PEO(2500)- <i>b</i> -PCL(1250).	113
Figure 5.5	Plot showing the total number of intermolecular H-bonds formed by CuB and CuI with the block copolymers shown in the form of sum of contribution from H-bond with PEO and PCL blocks.	115
Figure 5.6	Partial atomic charges on the atoms of PEO and PCL block monomers.	119
Figure 5.7	Numbering scheme of H and O atoms of Hydroxyl and Carbonyl groups in (A) CuB; and (B) CuI.	120
Figure 6.1	Chemical Structure of PEO- <i>b</i> -PBCL.	128

Figure 6.2	Schematics of the PBCL block with different tacticities. (A) Isotactic; (B) Syndiotactic; and (C) Atactic.	130
Figure 6.3	Schematics of all torsion angles identified in PEO- <i>b</i> -PBCL.	133
Figure 6.4(A)	Plot of the computed χ values of binary mixtures of two cucurbitacins and three tactic forms of PEO- <i>b</i> -PBCL compared with the data for PEO- <i>b</i> -PCL.	139
Figure 6.4(B)	Comparison plot of experimentally measured drug loading capacity of PEO- <i>b</i> -PCL and PEO- <i>b</i> -PBCL micelles for cucurbitacins as reported by Molavi <i>et al.</i>	140
Figure 6.5	Comparison of electrostatic and dispersive energy values for PEO- <i>b</i> -PCL and all the tactic forms of PEO- <i>b</i> -PBCL in their pure state.	143
Figure 6.6	Different types of intra-molecular and intermolecular interactions probable in the binary mixtures of PEO- <i>b</i> -PBCL and cucurbitacin drug molecules.	145
Figure 6.7	RDF plots for Interaction No. 1 (listed in Table 6.3) in (A) pure di-block copolymer system; and (B) mixture system of drug/di-block copolymer.	149
Figure 6.8(A)	RDF plot of CuB drug in PEO- <i>b</i> -PBCL for Interaction No. 2.	151

Figure 6.8(B)	RDF plot of CuB drug in PEO- <i>b</i> -PBCL for Interaction No. 3.	151
Figure 6.8(C)	RDF plot of CuB drug in PEO- <i>b</i> -PBCL for Interaction No. 4.	152
Figure 6.8(D)	RDF plot of CuB drug in PEO- <i>b</i> -PBCL for Interaction No. 5.	152
Figure 6.9(A)	RDF plot of comparison of CuB and CuI drugs in PEO- <i>b-s</i> PBCL for Interaction No. 2.	155
Figure 6.9(B)	RDF plot of comparison of CuB and CuI drugs in PEO- <i>b-s</i> PBCL for Interaction No. 3.	155
Figure 6.9(C)	RDF plot of comparison of CuB and CuI drugs in PEO- <i>b-s</i> PBCL for Interaction No. 4.	156
Figure 6.9(D)	RDF plot of comparison of CuB and CuI drugs in PEO- <i>b-s</i> PBCL for Interaction No. 5.	156
Figure 6.10(A)	RDF plot of comparison of CuB and CuI drugs in PEO- <i>b-a</i> PBCL for Interaction No. 2.	157
Figure 6.10(B)	RDF plot of comparison of CuB and CuI drugs in PEO- <i>b-a</i> PBCL for Interaction No. 3.	157
Figure 6.10(C)	RDF plot of comparison of CuB and CuI drugs in PEO- <i>b-a</i> PBCL for Interaction No. 4.	158
Figure 6.10(D)	RDF plot of comparison of CuB and CuI drugs in PEO- <i>b-a</i> PBCL for Interaction No. 5.	158

Figure 6.11	RDF plot showing the comparison of correlation between –OH groups of CuB and CuI and aromatic rings of the di-block copolymer.	161
Figure 6.12	Numbering scheme of H and O atoms of Hydroxyl and Carbonyl groups in (A) CuB; and (B) CuI.	162
Figure 6.13	RDF plot showing correlations between all the –OH groups of CuI, the –OH(1) group of CuB and aromatic rings of the di-block copolymer.	163
Figure 6.14	Partial atomic charges of –OH(1) group on (A) CuB; and (B) CuI.	164
Figure 6.15	Plot of the computed χ values of binary mixtures of fenofibrate and nimodipine and three tactic forms of PEO- <i>b</i> -PBCL compared with the data for PEO- <i>b</i> -PCL.	167
Figure 6.16	RDF plot showing correlation of H(Chain) atoms with (A) Fenofibrate; and (B) Nimodipine.	169
Figure 6.17	RDF plot showing correlation of H atoms of PEO block with (A) Fenofibrate; and (B) Nimodipine.	170
Figure 7.1	Chemical Structure of PEO- <i>b</i> -3PCL.	174
Figure 7.2	Schematics of all torsion angles identified in PEO- <i>b</i> -3PCL.	178

Figure 7.3	Plot of the computed χ values of binary mixtures of cucurbitacin (Set-I) drugs and PEO- <i>b</i> -3PCL along with the data for PEO- <i>b</i> -PCL.	183
Figure 7.4	Plot of the computed χ values of binary mixtures containing PEO- <i>b</i> -3PCL and fenofibrate and nimodipine (Set-II) drugs along with the data for PEO- <i>b</i> -PCL.	184
Figure 7.5	Plot showing the total number of intermolecular H-bonds formed by CuB and CuI with the PEO- <i>b</i> -3PCL in the form of sum of contributions from H-bond with PEO and PCL blocks.	186
Figure 7.6	Plot showing the total number of intermolecular H-bonds formed by fenofibrate and nimodipine drugs with the PCL blocks of the PEO- <i>b</i> -PCL and PEO- <i>b</i> -3PCL.	187
Figure 7.7	Numbering scheme of H-bond acceptor atoms of (A) CuB; (B) CuI; (C) Fenofibrate; and (D) Nimodipine.	190

List of Abbreviations

Cohesive Energy Density	CED
Critical Micelle Concentration	CMC
Cucurbitacin B	CuB
Cucurbitacin I	CuI
Degree of Polymerization	DOP
Electrostatic Potentials	ESP
Femtosecond	fs
Food and Drug Administration	FDA
Group Contribution Method	GCM
Hydrogen Bond	H-bond
Lennard Jones	LJ
Methyl Red	MR
Molecular Dynamics	MD
Monte Carlo	MC
Nanometres	nm
Nuclear Magnetic Resonance	NMR
Periodic Boundary Conditions	PBC
Picosecond	ps
Poly(ethylene oxide)- <i>b</i> -Poly(ϵ -caprolactone)	PEO- <i>b</i> -PCL
Poly(ethylene oxide)- <i>b</i> -Poly(α -benzyl carboxylate ϵ -caprolactone)	PEO- <i>b</i> -PBCL

Poly(ethylene oxide)- <i>b</i> -Poly(lactide)	PLA
Poly(methyl methacrylate)	PMMA
Poly(methylene oxide)	PMO
Polypropylene	PP
Poly(propylene oxide)	PPO
Polystyrene	PS
Poly(vinyl acetate)	PVAc
Radial Distribution Functions	RDF
Reticuloendothelial System	RES
Rotational Isomeric State	RIS
Small Angle Neutron Scattering	SANS
Tetramethyl Bisphenol-A Polycarbonate	TMPC
Van der Waals	VdW

Chapter 1

Introduction

1.1 Block Copolymer Micelles

Amphiphilic block copolymers consist of hydrophilic and hydrophobic blocks that can spontaneously self-assemble in aqueous solutions above a threshold concentration, the critical micelle concentration (CMC), to form micelles. These polymeric micelles are several tens of nanometres in size and have emerged as novel nanoscopic vehicles for the delivery of water insoluble drugs in a controlled manner [1-5]. These micelles are characterized by their unique core-shell structure, in which the core is composed of hydrophobic blocks that are surrounded by a corona of hydrophilic blocks (Figure 1.1). Generally, the hydrophobic core acts as a micro reservoir for the solubilisation of water insoluble drugs while the hydrophilic outer shell provides stealth properties.

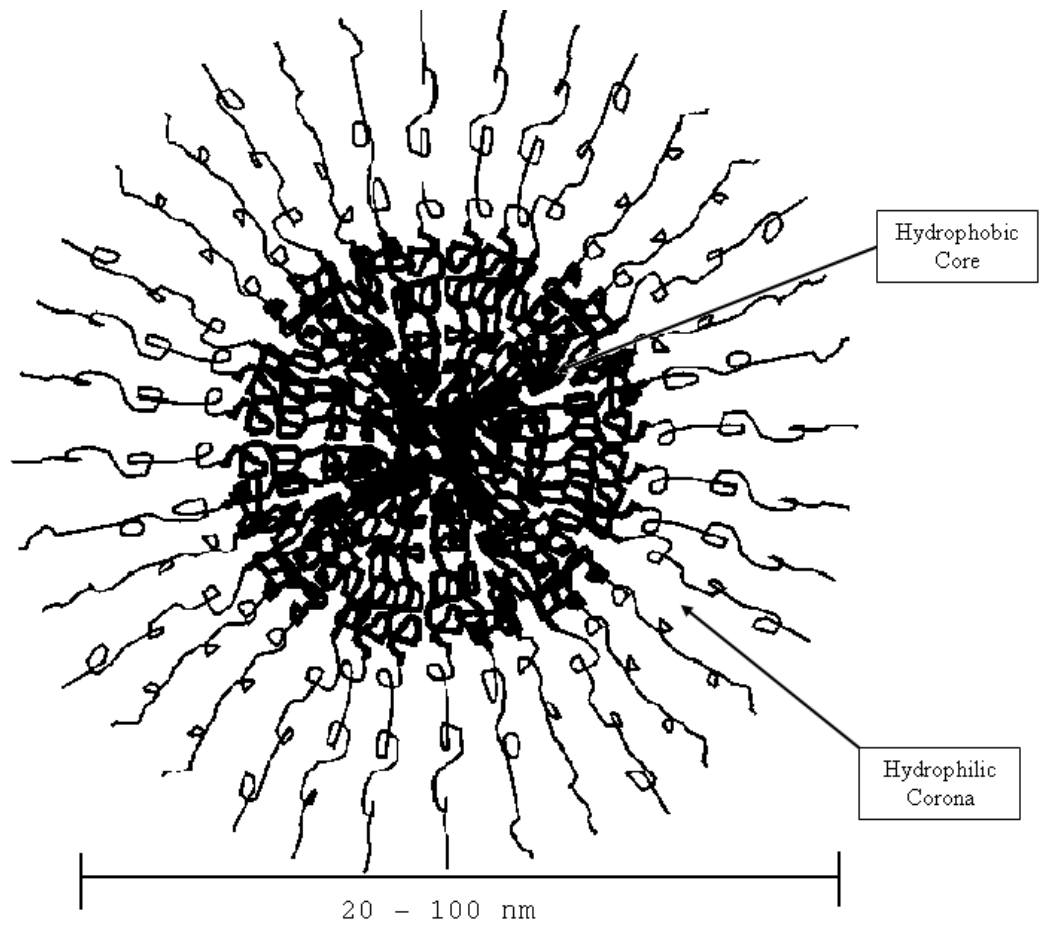


Figure 1.1 Schematic Diagram of a Block Copolymer Micelle.

Drug carriers at this scale (< 200 nm) escape from being detected and eliminated by the reticuloendothelial system (RES). Moreover, their sizes are large enough (> 10 nm) to avoid renal excretion. As a consequence, these drug carriers possess a very desirable property of being able to circulate in the vasculature for extended periods of time after intravenous administration and show facilitated extravasation at sites with leaky vasculature, e.g., tumour sites.

Poly(ethylene oxide)-*b*-poly(ϵ -caprolactone) (PEO-*b*-PCL) is one of the most widely studied and applied micelle-forming block copolymer system in drug delivery. Since PEO is biocompatible, non-toxic and has a high degree of hydration, it has been approved by the Food and Drug Administration (FDA) in the United States. PEO chains form shell and offer “stealth” behaviour *in vivo* due to its ability to minimize cell and protein interactions, whereas PCL due to its high hydrophobicity, biocompatibility and biodegradability forms an ideal reservoir for hydrophobic drugs.

1.2 Block Copolymer-Drug Compatibility

The degree of compatibility between the block copolymer and the drug in such micelle-based drug delivery systems can affect their performance related characteristics like stability of the micelle, drug encapsulation efficiency and drug release kinetics [1, 6]. The knowledge of block copolymer-drug compatibility is important for designing drug formulations and determining the effectiveness of polymeric delivery systems. In practice, the Flory-Huggins interaction parameter (χ) is used to assess the extent of compatibility between the core of the micelle

and the solute (drug). Lower the χ value, more compatible the drug is with the core of micelle and hence higher the predicted amount of drug solubilisation. This interaction parameter has been used to qualitatively elucidate the different levels of solubilisation of various water insoluble drugs in block copolymer micelles based drug delivery systems [1, 6-10]. The Flory-Huggins interaction parameter can be calculated either based on the knowledge of the solubility parameters of pure components used in the formulation or from the enthalpy of mixing both components. The concept of solubility parameters and interaction parameters along with their methods of measurement will be reviewed briefly in the next few sections.

1.3 Solubility Parameters

The concept of solubility parameter is used to quantify the strength of intermolecular interactions. The two most common solubility parameters used are the Hildebrand (δ) and Hansen solubility parameters (δ_d , δ_p and δ_h). This concept was introduced for the first time by Hildebrand and Scott [11]. They defined the solubility parameter (δ) as the square root of cohesive energy density as shown in the following expression:

$$\delta = \sqrt{\frac{\Delta E_v}{V}} = \sqrt{\frac{\Delta H_v - RT}{V}} \quad (1.1)$$

where δ is the Hildebrand solubility parameter; ΔE_v , ΔH_v , and V are energy of vaporization, heat of vaporization and molar volume of the material, respectively. Unfortunately, this equation is only suitable for non-polar fluids containing non-directional dispersion forces.

A polar fluid, generally, has three major components of intermolecular forces: Dispersion (London) forces (d); Polar/Electrostatic forces (p); and Hydrogen bonding forces (h). Utilizing these three intermolecular attractions, Hansen divided the cohesive energy, i.e., the Hildebrand solubility parameter, into three components as shown in the following expression:

$$\delta^2 = \delta_d^2 + \delta_p^2 + \delta_h^2 \quad (1.2)$$

Hansen solubility parameters are also referred to as 3D solubility parameters. The decomposition of cohesive energy into three components does not have a simple experimental analogue and this concept seems appealing only from the application point of view. The three components are empirically adjusted to define the miscibility characteristics of the solvent. In general, compatible materials tend to have comparable solubility parameters (either δ or δ_d , δ_p and δ_h).

1.4 Determination of Solubility Parameters of Polymers and Drugs

The Hildebrand and Hansen solubility parameters of materials can be determined using various experimental methods as reviewed by Hancock *et al.*[12]. In particular, the solubility parameters of low molecular weight compounds are

determined by direct measurement of heat of vaporization (ΔH_v) using calorimetry. However, polymer, owing to their extremely low vapour pressures, cannot be vaporized. Hence, in another approach, polymer's solubility/miscibility is measured in solvents with known cohesive energies [13]. The solubility parameter of the solvent which swells the polymer sample the most is assigned to the polymer. This approach is quite subjective and gives different results for the same polymer, depending on the polarity and hydrogen bonding characteristics of the solvent. Moreover, the indirect experimental procedures employed are usually time consuming and tedious as described by Archer [14]. Additionally, because of the thermal instabilities of polymer/drug systems, in many circumstances, this approach fails to provide their solubility parameters.

The most convenient way to obtain a quick estimation of solubility parameters is to use group contribution tables [15]. The Group Contribution Method (GCM) is based on the idea that the total intermolecular interactions between the molecules in a liquid are linear sum of the contributions from various chemical moieties within the molecules. Following equations signify such an idea.

$$\delta_d = \frac{\sum F_{di}}{V} \quad (1.3)$$

$$\delta_p = \frac{\sqrt{\sum F_{pi}^2}}{V} \quad (1.4)$$

$$\delta_h = \frac{\sqrt{\sum E_{hi}}}{V} \quad (1.5)$$

Here, F_{di} , F_{pi} and E_{hi} refer to the contributions from various chemical moieties and such values can be obtained from the Hoftyzer-Van Krevelen's method [16]. The molar volume (V) of the material can be determined by the Fedors method [17] or by a newly developed group contribution method GCVOL [18-20] as described in the Appendix B. The GCM is simple to use and generally provides reasonable solubility predictions for compounds with simple chemical architectures involving non-directional intermolecular interactions like dispersion forces. Nevertheless, the GCM fails to provide a good estimation for the solubility of complex drug molecules and copolymers for the following reasons [16, 21]: a) the method fails to take into consideration the geometry of the molecules involved, b) it also fails to take into account the excluded volume interactions which are especially prevalent for long chain copolymers, c) The GCM would yield the same values of solubility parameters for isomers due to their inability to distinguish between isomers that have identical chemical structures but different constitution and/or configuration, and d) the GCM tends to underestimate δ_p [22]. More details on the use of GCM in the pharmaceutical research will be discussed later in Chapter 4.

Recently, a computational approach (Molecular modelling) has also been applied to determine the Hildebrand and Hansen solubility parameters of various polymers and surfactants [21-26]. Molecular dynamics (MD) simulation is one of the most widely used molecular modelling techniques to obtain the molecular level insights into the problem of interest. Utilizing the simple laws of classical mechanics, MD simulations compute the motions of individual molecules in the

models of solids, liquids and gases. This approach shows a great potential especially in the case of polymer/drug binary systems and the simulation results are usually in good agreement with the experimental results. The MD approaches seem to outperform the GCM [21]. The fundamentals behind the working of MD simulation will be discussed in Chapter 3. Later in Chapter 4, we will compare the two different MD approaches to predict the solubilities of a selected polymer/drug system. Generally, the major limiting factors in such computational approaches are proper choice of force field parameters and the system size we can study. However, continuously improving computational facilities have improved the accuracy of such calculations.

1.5 Interaction Parameters and their Estimation

The importance of the prediction of compatibility between block copolymers and drug molecules was described in the Section 1.2. Since the interaction parameter approach is used to assess the extent of compatibility, we hereby briefly review this concept. The origin of these parameters lies in the various statistical thermodynamic theories of polymer solutions and mixtures, which will be further discussed in details in Chapter 2.

Within this approach, the miscibility prevails if the measured parameter lies below a critical value. The interaction parameter originates from the statistical mechanical theory of liquids – the lattice model of concentrated solutions. The concept of interaction parameter was introduced for the first time for small

molecules mixtures by Bragg and Williams [27] and later Flory and Huggins independently generalized the theory to polymer solutions [28-31].

Interaction parameters describe the relative strength of cohesive and adhesive interactions (intermolecular interactions) and hence the enthalpic interactions (enthalpy change on mixing) are reflected in this term (Chapter 2). Entropic component of the Gibbs free energy of mixing is generally not considered in this approach. Nonetheless, the mixing process is entropically favourable process and hence will always favour the miscibility. Hence, in the framework of the Flory-Huggins lattice theory, the enthalpic interaction between the components will be reflected in the sign and magnitude of the interaction parameter which will eventually determine the miscibility between the components of a mixture. Generally, the system having strong cohesion interactions will be characterized by positive interaction parameters, while the system having stronger adhesive interactions (favouring miscibility) will be described by negative interaction parameters. This point will be further elaborated in Chapter 2.

The polymer-solvent interaction parameter has been estimated using several experimental methods like small angle neutron scattering (SANS), melting point depression (for semi-crystalline polymers), osmotic pressure, and inverse gas chromatography (IGC). Interested readers should refer the book by Olabisi *et al.* [32] and references therein for detailed descriptions of aforementioned methods. Unfortunately, most of these experimental techniques are not applicable to the polymer-drug systems, due to their viscous and non-volatile characteristics. Hence, using the expressions derived in appropriate polymer solution

thermodynamic theory (Chapter 2), we can estimate the polymer-drug interaction parameter either using the pure component properties, i.e., the solubility parameters of drugs and polymers or using the mixture properties, i.e., the enthalpy of mixing both components. Again, the solubility parameters can be predicted using one of the methods described in the Section 1.4, while the enthalpy of mixing can be estimated using the computational approaches described in Section 4.2.4.

1.6 Scope of the Thesis

General hypothesis and objective of research:

As the title of this thesis indicates, we are interested in the application of MD simulation in predicting the solubility of different drugs in polymeric micellar delivery systems. Polymeric micelles are of great interest for encapsulating hydrophobic drugs and their controlled delivery. In order to achieve maximum solubility and control over release, for any given drug molecule, a certain polymer structure showing maximum compatibility with the drug of interest should be designed. The challenge is to identify the molecular structure of the blocks in the block copolymer that can encapsulate the drug of interest and at the same time would provide the desired release properties. As discussed earlier, the knowledge of block copolymer-drug compatibility is important for designing drug formulations and determining the effectiveness of such delivery systems. Additionally, such drug delivery systems involve complex intermolecular interactions and fittings of molecules of different shapes. Obviously, being able

to quantify such interactions between various drugs and block copolymers with different chemical moieties will definitely facilitate the block copolymer design process. Hence, the crux of this thesis is to develop valuable tools for predicting binary interactions between di-block copolymers and hydrophobic drugs that provide useful atomistic details related to forces contributing to the thermodynamic compatibility. Molecular simulation seems to be the method of choice.

Specific objectives:

The first objective of this thesis is to test if the MD simulation would be a better method to determine the compatibility of drug/block copolymer systems than the GCM that is commonly used in the pharmaceutical research. Owing to the several disadvantages associated with the GCM (Section 1.4), it fails to predict the solubility of complex drugs in block copolymers. In order to overcome these limitations of the GCM, we will be developing two different MD approaches. The pros and cons of both the approaches in predicting the polymer-drug compatibility will also be discussed. Using MD approach, the Flory-Huggins interaction parameters between drugs and block copolymers will be computed in order to assess the power of this approach in predicting the experimental solubility trends. The effect of drug loading on the interaction parameter will also be studied.

The second objective of this work is to generate useful information related to the molecular origin of the miscibility observed between hydrophobic drugs and di-block copolymers. The relative contributions of non-polar and polar intermolecular interactions in inducing the miscibility will also be discussed.

Various MD analysis techniques will be applied to generate useful atomistic details related to intermolecular specific interactions. The effect of molecular weights of the blocks of block copolymer on the interaction parameters will also be studied.

The third objective of this thesis is to study the interactions between the tailor-made di-block copolymers and hydrophobic drugs. We will apply the developed MD simulation technique to various engineered block copolymers having controlled molecular architecture either by introducing functional groups or by introducing branches of homologous segments to generate multi-hydrophobic block copolymers. Introduction of various functional groups on the blocks of block copolymer is also known to introduce stereochemistry into the block copolymer, which indirectly affects the interactions of these block copolymers with drug molecules. Hence, we will also study the role of stereochemistry in the process of inducing polymer/drug miscibility.

To properly address all the above-described objectives, we selected two different sets of model hydrophobic drugs with distinctively different molecular structures. Set-I consists of cucurbitacin drugs (Cucurbitacin B and Cucurbitacin I) having multiple hydrogen bond donors and acceptors (hydroxyl and carbonyl groups) evenly distributed on their molecules while Set-II consists of fenofibrate and nimodipine drugs having essentially only clustered hydrogen bond acceptors. In particular, these different sets of hydrophobic drugs will help us to study the relative contributions of polar and non-polar intermolecular interactions to the process of inducing polymer/drug compatibility. The study performed in the

present thesis will serve as the first attempt to provide an atomistic understanding of the differences in the encapsulation mechanisms of linear as well as engineered block copolymers.

The thesis is organized into four major sections. Section 1, which is mainly composed of Chapter 2, describes various statistical theories related to polymer solutions and mixtures along with a brief review of concepts of solubility parameters and interaction parameters. The Chapter 3 forms the part of Section 2, which covers various methodologies used in MD simulation that were used in the present work. Section 3 (Chapters 4 to 7) forms the major part of the thesis, where we apply MD simulation techniques to the systems of various hydrophobic drugs (Set-I and Set-II) and di-block copolymers and their engineered forms. Atomistic details obtained from results and discussion in the Section 3 helps to achieve three major objectives of the thesis described above. In the final section (Chapter 8) major conclusions along with the future outlook is provided.

Chapter 2

Thermodynamic Theories of Polymer Solutions and Mixtures

2.1 Thermodynamic Compatibility

In general, the term miscibility applies to the case where constituents mix on a molecular scale and mixture exist in single phase with uniform chemical composition throughout. An ideal solution signifies such situation. Nonetheless, in real solutions, even those containing only low molecular weight substances, exhibit non-ideal behaviour. In the case of polymers, it is very rare that we can observe miscibility at molecular scale and instead, we observe miscibility at the segmental scale with the formation of micro domains. In fact, various techniques like small angle neutron scattering (SANS) and Nuclear magnetic resonance (NMR) have provided the evidence of the mixing at segmental level for various polymer blends [33, 34]. However, thermodynamics offers a unique definition of miscibility for both low and high molecular weight substances.

2.2 Thermodynamics of Mixing

For mixing processes at constant temperature and pressure, equations (2.1) and (2.2) describe the thermodynamic criteria for achieving the miscibility between the components in a mixture.

$$\Delta G_m < 0 \quad (2.1)$$

$$\left(\frac{\partial^2 \Delta G_m}{\partial \phi_i^2} \right)_{T,P} > 0 \quad (2.2)$$

ΔG_m is Gibbs free energy of mixing and equation 2.2 describes the second derivative of ΔG_m with respect to the concentration (mole or volume fraction) of one of the components, across the entire composition range. Equation (2.1) is a necessary requirement for any spontaneous mixing process, while the equation (2.2) ensures the stability of the mixture. Figure 2.1 illustrates three possible kinds of Gibbs free energy of mixing diagrams for a binary mixture. The curve (i) is the only one which obeys both equations (2.1) and (2.2) for the entire range of compositions and hence indicates a miscible mixture. The curve (ii) disobeys both the criteria and hence would yield immiscible mixtures for the entire range of compositions.

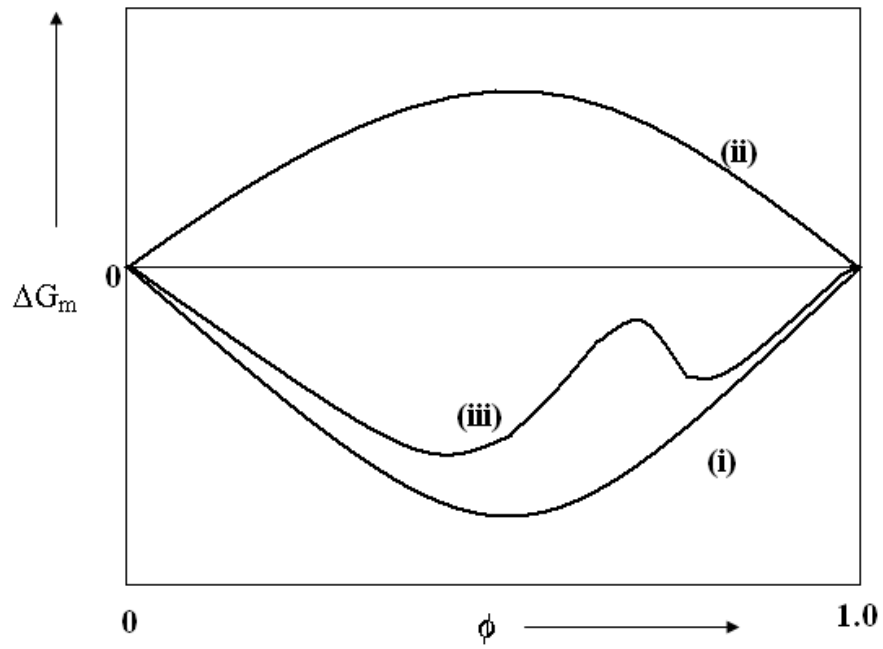


Figure 2.1 Three possible types of Gibbs free energy of mixing diagrams for binary mixtures.

The curve (iii) follows equation (2.1) but does not follow equation (2.2) for the composition range where the slope is positive and hence they form partially miscible mixture with miscible and immiscible regions at different concentrations.

The Gibbs free energy of mixing represents the algebraic sum of the two contributions – the enthalpic and the entropic contributions as shown in the following expression:

$$\Delta G_m = \Delta H_m - T\Delta S_m \quad (2.3)$$

where ΔG_m , ΔH_m , and ΔS_m represent the free energy, enthalpy, and entropy changes on mixing, respectively. The entropic contribution is always favourable (i.e., $\Delta S_m > 0$) for any spontaneous mixing process, since the mixing process generates more available configurations for the whole system. However, the enthalpic contribution can be positive, negative or even zero depending on the nature of intermolecular interactions between the components. For the polymeric systems, owing to their high molecular weight, there is less dependence of the free energy of mixing on the entropic contributions as compared to the enthalpic contributions. As a result, the sign of ΔG_m depends essentially upon the sign and magnitude of the ΔH_m . Several solution theories of varying complexity have been developed to describe the changes in Gibbs free energy of mixing. The primary problem in any solution theory is to estimate thermodynamic properties of a given mixture based on intermolecular forces. We start with the solutions of low molecular weight compounds which are described by the ideal solution theory and

later we develop upon this theory to attain the final goal of discussing the polymer solution theory.

2.3 Ideal Solution Theory

An ideal solution is defined as the one in which the intermolecular interactions between all the components are comparable. This is simplest theory based on three basic assumptions:

- a) The sizes of molecules of all the components are approximately the same.
- b) The intermolecular interactions are non-directional (e.g., dispersion forces) and comparable in magnitude.
- c) The mixing is totally a purely statistical process (i.e., random mixing condition).

As a result of the assumption (b), we have $\Delta H_m = 0$ for ideal solutions and hence, in such cases, the change in the free energy of mixing is given by

$$\Delta G_m = -T\Delta S_m^{ideal} \quad (2.4)$$

The ideal entropy of mixing, ΔS_m^{ideal} , for binary mixtures can be derived using the lattice theory of solutions and the Boltzmann law of entropy. For details, please refer to Section 2.5.1. For now, we directly accept the following final expression for the ideal entropy of mixing.

$$\Delta S_m^{ideal} = -R(x_1 \ln x_1 + x_2 \ln x_2) \quad (2.5)$$

Here, R is ideal gas constant and x_i is mole fraction of the component i . Since the mole fractions are always less than 1, ΔS_m^{ideal} will always be positive.

In an ideal solution, mainly due to the assumption (c) of random mixing condition, the molecules distribute themselves uniformly in the mixture according to the Boltzmann law. But in real solutions and/or polymer solutions involving the mixing of low molecular weight solvent with a high molecular weight polymer, the individual repeating units are linked along a polymer chain or sometimes molecules of one type may tend to associate and hence this leads to a loss of conformational entropy. Due to this, the entropy change on mixing in real solutions is lower than that predicted by the random mixing condition signified in the equation (2.5).

2.4 Regular Solution Theory

The term ‘regular’ solutions was coined for the first time by Hildebrand in 1927 [35] and later in 1929 [36], he discussed the thermodynamic significance of such solutions. The regular solution deviates only moderately from the ideal solution. All the deviations from ideality are ascribed to the enthalpic effects and hence in this case, the enthalpy of mixing, $\Delta H_m \neq 0$. But, still the assumption of random mixing condition (i.e., random distribution and orientation of molecules) holds true and hence, the entropy effects are still ideal in this theory. The regular solution theory of liquid mixtures is based on the following major assumptions as

described by Longuet-Higgins [37]: (i) the molecules are arranged in a regular lattice, (ii) liquid components have ordered structures of the same type, and (iii) the intermolecular potential energy is the sum of contributions from nearest neighbours in the lattice and these contributions depend only on their chemical nature (i.e., non-directional).

The entropy of mixing is approximated by ΔS_m^{ideal} expression (2.5) derived in the ideal solution theory. The non-zero ΔH_m is given by:

$$\Delta H_m = nzw x_1 x_2 \quad (2.6)$$

where z , the coordination number, describes the effective number of nearest neighbours, and w is pair interaction energy. For a binary mixture of components 1 and 2, the pair interaction energy is defined using the mean field expression as follows:

$$w = \frac{1}{2} w_{11} + \frac{1}{2} w_{22} - w_{12} \quad (2.7)$$

w_{ij} is interaction energy between components i and j . We derive expressions (2.5) and (2.6) in Section 2.5.1, utilizing the lattice models of concentrated solutions with Bragg-Williams mean-field approximation. Combining equations (2.5) and (2.6), we get the following expression for the free energy of mixing for real solutions:

$$\Delta G_m = nzw x_1 x_2 + RT(x_1 \ln x_1 + x_2 \ln x_2) \quad (2.8)$$

The pair interaction energy, w , may be regarded as the free energy of formation of a single contact between two molecules of different types. The physical meaning and thermodynamic properties of w has been studied in detail by Guggenheim [38]. The fundamental approximation in the regular solution theory is that w is independent of the composition and temperature of the mixture. Later, it was shown by Guggenheim that w has to vary with temperature. This is understandable, since the temperature-independent w would always lead to negative values of excess entropy of mixing which eventually shows a quantitative disagreement with the experiment. Nonetheless, the mixing is not really a purely statistical process due to intermolecular interactions and local concentration fluctuations and hence, such a variation is to be expected. But, the regular solution theory provides no clue to the actual value of dw/dT . It is worth noting that the applicability of the ideal entropy approximation is no longer guaranteed, if the constituents of a mixture experiences strong attractive or repulsive forces (a large absolute value of w). The greater the w value is, the larger the deviation of the entropy expression. It is worth noting that the theory of regular solutions has been successful in describing the mixtures of only non-polar liquids lacking directional intermolecular forces.

2.5 Hildebrand-Scatchard Equation

The enthalpy of mixing (ΔH_m) expression (2.6), in its present form, is not of any practical use, due to the presence of experimentally immeasurable terms. Thus, we need to transform this expression in order to make the enthalpy of mixing calculations feasible from the experimental point of view. Hildebrand-Scatchard equation serves this purpose and is utilized to develop the concept of Hildebrand solubility parameters described in the Section 1.3. The pair interaction energy, w in the expression of ΔH_m is calculated from the equation (2.7). In this equation, interaction energies, w_{11} and w_{22} are the energy changes involved in transferring molecules of types 1 and 2 to their vapour states at infinite dilution, respectively, and w_{12} corresponds to the energy liberated by considering molecules 1 and 2 back into the solution state. So, the first step involves proper approximation of the values of w_{12} . Here, if w_{12} is the arithmetic mean of w_{11} and w_{22} (i.e., $w_{12} = (w_{11}+w_{22})/2$), then ΔH_m equals zero which is not true for the case of regular solution. However, if w_{12} is the geometric mean of w_{11} and w_{22} (i.e., $w_{12} = (w_{11}w_{22})^{1/2}$), then w can be written as $(w_{11}^{1/2} - w_{22}^{1/2})^2$. This approximation is also known as the Scatchard geometric mean assumption and works well for low molecular weight non-polar materials. When dealing with the mixtures, in which there is a large disparity between the sizes of various kinds of molecules; e.g., polymer solutions, an alternative and more appropriate way to express the relative amounts of the various components is volume fraction (ϕ_i) rather than the mole fraction (x_i). [39]. Replacing mole fractions with volume fractions in equation

(2.6) and introducing the geometric mean approximation, one can re-write it to obtain the heat of mixing per unit volume of mixture:

$$\frac{\Delta H_m}{V} = \phi_1 \phi_2 [\delta_1 - \delta_2]^2 \quad (2.9)$$

where δ_i is defined as the solubility parameter of component i , V is total volume of mixture and ϕ_i is volume fraction of component i . The solubility parameter is the square root of w_{ii} which is also called cohesive energy density (CED). CED (sum of intermolecular energies per unit volume) is defined as the energy required to vaporize a molar volume of the material at constant temperature. The relationship between the Hildebrand solubility parameters and CED is expressed in equation (1.1).

From the inspection of equation (2.9), it is clear that this formula always predicts $\Delta H_m > 0$ (i.e., endothermic heats of mixing), which holds true only for the regular solutions. Since, ΔS_m^{ideal} in equation (2.5) is always positive, the components of a mixture are assumed to be compatible only if $\Delta H_m \leq T\Delta S_m$. Thus, the miscibility can be predicted based on the pure component property δ_i . In general, if the absolute value of $(\delta_1 - \delta_2)$ difference is zero or small i.e., if two materials have approximately same Hildebrand solubility parameters, they would be thermodynamically compatible. The convenience of the solubility parameter approach lies in the feasibility of assigning δ values a priori to the individual

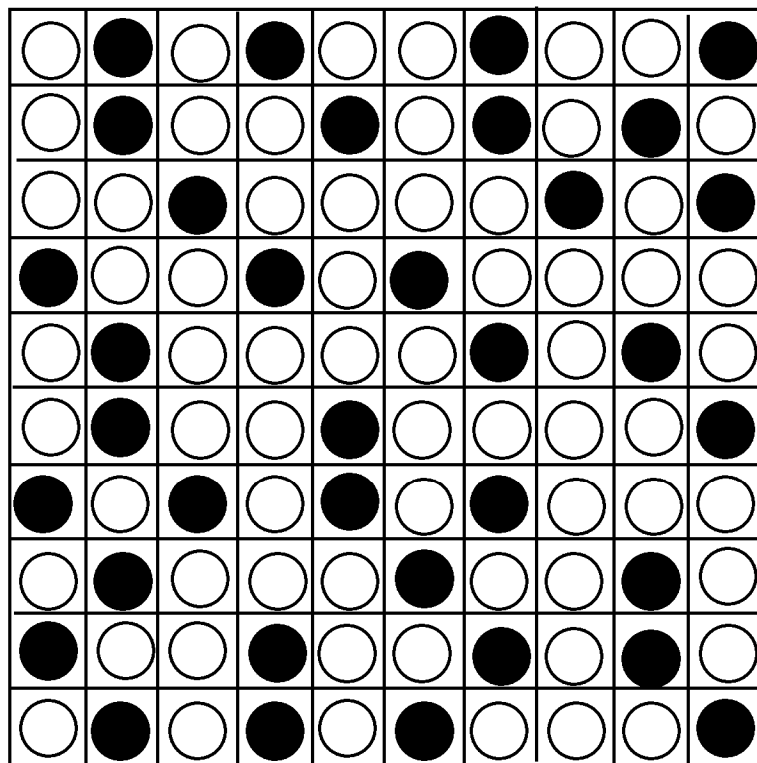
components of the mixture. Various techniques used to determine the solubility parameters of polymers and drugs have been described in the Section 1.4.

2.6 Statistical Theories of Liquid Mixtures

Statistical thermodynamics provide molecular theory of the macroscopic properties of a thermodynamic system. Dilute and concentrated solutions behave quite differently and hence their statistical mechanical treatments are also different. In a dilute solution, the solute molecules are surrounded by many pure solvent molecules so that the interactions between solute molecules can be neglected. These solutions behave very similar to dilute gases and hence application of an exact approach like a series expansion approach is possible [27]. On the other hand, for a concentrated solution, the solute-solute interactions are too strong to be neglected. In fact, if a phase separation occurs in the solution at a higher concentration, then the series expansion often diverges beyond the concentration of phase separation. One way to describe such solutions is to utilize various approximate theories. Prevailing theories of concentrated solutions utilize highly idealized ‘coarse-grained’ lattice models to capture important aspects of their behaviour. In the next section, we will work through the basic assumptions and features of the lattice theory for concentrated solutions of small molecules. The discussion of this theory will eventually form the base for developing the Flory-Huggins Lattice theory for polymer solutions.

2.6.1 The Lattice Model of Small-molecule Solutions

Consider a simple example of a binary mixture comprising of low-molecular weight solute (component 1) and low-molecular weight solvent (component 2). A schematic representation of a two-dimensional lattice model of concentrated binary solutions of small molecules is illustrated in Figure 2.2. In such a simple lattice model of solutions, the following major assumptions are involved: (a) The sizes and shapes of solute and solvent molecules are assumed to be approximately the same with preferably a spherical shape. Therefore, only one solute or one solvent molecule can occupy a single lattice site at any given instant, (b) The determination of probable statistical mechanical states depends solely on translational degrees of freedom, i.e., the states of the system are simply defined by the number of unique ways the molecules can be arranged on such lattice, (c) The volume of each lattice site is fixed under the condition of constant temperature, (d) The lattice is assumed to be incompressible and hence all the pressure-volume effects due to mixing are neglected, and (e) No vacant sites are allowed. The different spatial arrangements of all the molecules in the lattice give rise to the *configurational entropy* term or the entropy change on mixing expression (Equation (2.5)) that is valid for both ideal and regular solutions. Additionally, an expression for the enthalpy change on mixing (Equation (2.6)) can also be derived based on this lattice model.



● = SOLUTE MOLECULES

○ = SOLVENT MOLECULES

Figure 2.2 Schematic representation of the lattice model of concentrated binary solutions of small molecules.

The *configurational entropy* is related to the total number of distinguishable ways of arranging molecules (Ω) by following *Boltzmann relation*:

$$\Delta S_m = k_b \ln \Omega \quad (2.10)$$

where k_b is Boltzmann's constant (1.38×10^{-23} J/K). Here, Ω is the number of distinguishable ways of arranging n_1 solute molecules and n_2 solvent molecules on the lattice with $N = n_1 + n_2$, being the total number of sites. In order to evaluate Ω , we utilize the Bragg-Williams mean-field approximation, which simply states that the arrangement of the molecules is totally random despite the presence of intermolecular interactions. The Ω is given by the following expression:

$$\Omega = \frac{N!}{n_1!n_2!} \quad (2.11)$$

Using the Stirling's approximation:

$$\ln n! = n \ln n - n \quad (2.12)$$

And combining equations (2.10) and (2.11), leads to the following expression for the *configurational entropy*:

$$\Delta S_m = -R(x_1 \ln x_1 + x_2 \ln x_2) \quad (2.13)$$

Next, based on the random mixing approximation, we derive the expression for ΔH_m in following way. The lattice coordination number, z , is the number of cells that are first neighbours to a given cell. Now, the average number of type 2 molecules being nearest neighbour to a chosen type 1 molecule is zx_1 . Multiplying this with the n_1 will provide the average number of 1-2 interactions. Therefore,

$$\text{The average number of 1-2 interactions is:} \quad n_1zx_1$$

$$\text{The average number of 1-1 interactions is:} \quad n_1zx_1/2$$

$$\text{The average number of 2-2 interactions is:} \quad n_2zx_2/2$$

Now, the change in energy of mixing (ΔU_m) is given by:

$$\Delta U_m = U_{mix} - [U_1 + U_2] \quad (2.14)$$

As a result, the energy change on mixing can be expressed as follows:

$$\Delta U_m = \left[n_1zx_1w_{12} + \frac{1}{2}n_1zx_1w_{11} + \frac{1}{2}n_2zx_2w_{22} \right] - \left[\frac{1}{2}n_1zw_{11} + \frac{1}{2}n_2zw_{22} \right] \quad (2.15)$$

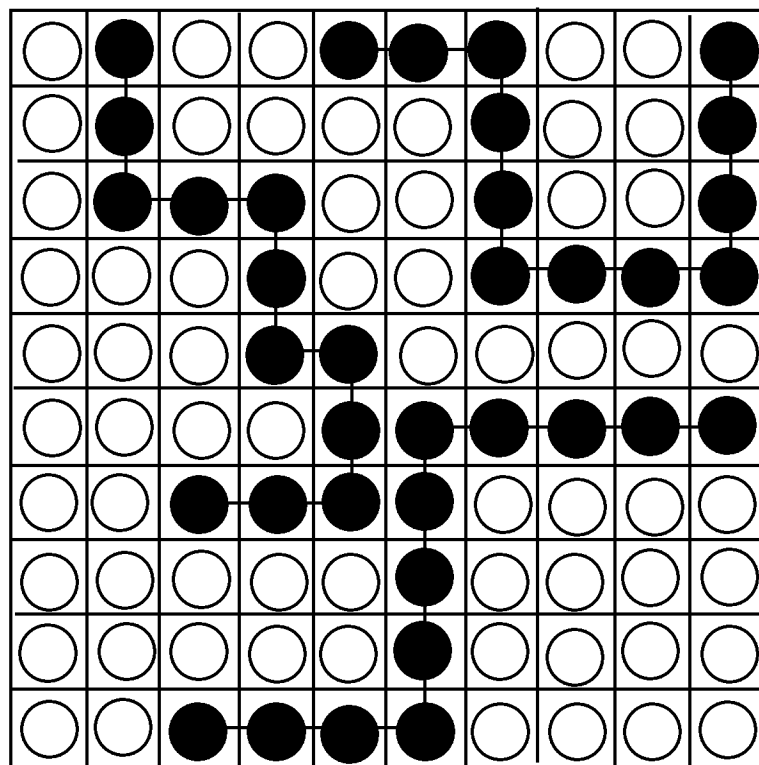
Simplification of the above expression and utilizing the assumption (d) for lattice models, will lead to expression (2.16).

$$\Delta H_m = (n_1 + n_2)zwx_1x_2 \quad (2.16)$$

Here, w is energy change associated with the formation of one solute-solvent contact and is estimated based on the equation (2.7).

2.6.2 Flory-Huggins Lattice Theory for Polymer Solutions

In the last section, the lattice model of small-molecule solutions was described. In this section, we extend those mechanics to statistically more complex systems of polymer solutions. The lattice theory of polymer solutions is known as the Flory-Huggins theory, which was independently developed by Flory and Huggins as a generalization of Bragg-Williams lattice model of concentrated binary solutions [28-31]. This theory was developed to provide a molecular theoretical basis for the free energy predictions which will in turn allow the predictions of miscibility behaviour of such polymer solutions. Hence, this theory provides the simplest approximation for terms ΔH_m and ΔS_m appearing in the free energy expression of equation (2.3). Figure 2.3 represents a schematic representation of the lattice model of polymer solutions. Each filled circle represents a chain segment, a piece of polymer that is about the same size of a solvent molecule. A chain segment is not necessarily a monomer. All the assumptions related to the lattice theory (Section 2.6.1) still apply here. In the case of polymer solutions, the mixing occurs at the segmental level due to presence of connected polymer segments instead of individual molecules.



● = CHAIN SEGMENTS OF POLYMER MOLECULES
○ = SOLVENT MOLECULES

Figure 2.3 Schematic representation of the lattice model of a polymer solution.

The expressions for entropy change and enthalpy change on mixing are given as follows (Please see Appendix A for detailed derivation)

$$\Delta S_m = -R \left(\frac{\phi_1}{DP_1} \ln \phi_1 + \frac{\phi_2}{DP_2} \ln \phi_2 \right) \quad (2.17)$$

$$\Delta H_m = \chi RT \phi_1 \phi_2 \quad (2.18)$$

Here, it is worth noting that ΔH_m and ΔS_m are defined per mole of lattice sites. ϕ_i and DP_i are volume fraction and degree of polymerization of component i , respectively. R is universal gas constant and T is absolute temperature. χ , the Flory-Huggins interaction parameter, is defined as $z\omega/RT$. The z is coordination number of a lattice site while ω is pair interaction energy per mole of lattice sites. Although, this theory considers χ as a dimensionless concentration-independent quantity, inversely proportional to the temperature, the experimental data reveals that this parameter largely depends on the concentration [39].

2.6.2.1 Miscibility predictions based on the Flory-Huggins Theory

Combining equations (2.3), (2.17) and (2.18), we obtain the free energy of mixing expression for polymer solutions:

$$\Delta G_m = RT \left[\chi \phi_1 \phi_2 + \frac{\phi_1}{DP_1} \ln \phi_1 + \frac{\phi_2}{DP_2} \ln \phi_2 \right] \quad (2.19)$$

The last two terms originated from the expression (2.17) of entropy change on mixing. The entropy gain predicted based on this expression can be thought of as the maximum achievable entropy gain through the mixing process since this expression was deduced based on the *athermal mixing* condition assumption. This assumption requires that the polymer molecules in the mixture have no preferred conformations on molecular level and do not interact with each other through orientation-dependent interactions. Unfortunately, this mixing condition would be appropriate only for the mixtures of two non-polar amorphous polymers interacting mainly through non-directional interactions like dispersive interactions. In polymer mixture systems, if components possess strong correlations in their local structures or interact through directional interactions like electrostatic or hydrogen bonding interactions, then the entropy gain through mixing will be significantly less than that predicted by the equation (2.17). For polymers with high molecular weight ($DP_i \rightarrow \infty$), the entropic contribution is very small or very near to zero and hence for such systems, the miscibility predictions would mainly depend on the values of enthalpy change on mixing which mainly depends upon the nature of intermolecular interactions between the components of the mixture. Hence, within the context of the Flory-Huggins lattice model, the miscibility prediction will be mainly dependent on the values of the interaction parameters. Therefore, in the present case, we require very small or negative values of χ in order to achieve miscibility. In general, for binary mixtures of long polymers, the miscibility is achieved when the χ values are less than the χ value at critical point ($\chi_{critical}$). The expression for $\chi_{critical}$ (Equation (2.20)) can be

obtained by applying the definition of critical point on equation (2.19), i.e., setting the 2nd and 3rd derivatives of ΔG_m with respect to volume fractions (ϕ_i) equal to zero.

$$\chi_{critical} = \frac{1}{2} \left(\frac{1}{\sqrt{DP_1}} + \frac{1}{\sqrt{DP_2}} \right)^2 \quad (2.20)$$

This expression implies that the miscibility of binary polymer blend depends only on the chain length or degree of polymerization of the components. In the case of polymer blends, $DP_1 \approx DP_2 \approx \infty$, and hence the $\chi_{critical} = 0$. This implies that the polymer mixing always takes place if the χ parameter is negative. Miscible polymer mixtures with negative χ exist due to specific interactions like electrostatic charge, hydrogen bonding, etc., between given polymer segments. For a polymer solution, $DP_1 = 1$ and $DP_2 \approx \infty$, the $\chi_{critical} = 0.5$.

For polymer blends, the presence of orientation-dependent interactions (i.e., specific interactions) can possibly induce miscibility in spite of an extremely small entropy gain [40]. On the other hand, for non-polar polymers, the miscibility can only be achieved through near to zero values of the enthalpy change on mixing. From the Hildebrand-Scatchard equation discussed earlier, this implies that the Hildebrand solubility parameters of the constituent polymers should be very close. Thus, one can easily relate the ΔH_m from the Hildebrand-Scatchard equation (Equation (2.9)) with the ΔH_m from the Flory-Huggins theory (Equation (2.18)) to get a useful working relationship between interaction

parameters and solubility parameters of polymers. This concept is best illustrated by the following approximate equation [15]:

$$\chi_{12} = \frac{V_r}{RT}(\delta_1 - \delta_2)^2 \quad (2.21)$$

Here, δ_1 and δ_2 are Hildebrand solubility parameters of polymers 1 and 2, respectively. V_r is reference molar volume. The choice of this reference volume is somewhat arbitrary, but it is usual practice to choose the smallest volume among the molar volumes of the components of polymer blends or solutions. The equation (2.21) provides means of predicting a mixture's property (χ) from pure component properties (δ). Thus, equation (2.21) in conjunction with the equation (2.20) provides a straightforward scheme for predictions of polymer miscibility; once the solubility parameters and molecular weights of the polymers are known.

2.6.2.2 Limitations of the Flory-Huggins Theory

The Flory-Huggins theory captures some essential features of the mixing process of polymer blends and solutions and provides a simple expression for describing its thermodynamics through the introduction of an important parameter, χ_{12} . Yet, there are number of limitations to the original formulation of this theory. It is worth noting that this theory is a mean-field theory (assumption used while deriving the expression for the internal energy change of mixing, equation (2.18)). Many of the deficiencies are related to the major approximations and assumptions associated with treating such polymeric systems using the simple lattice models.

In particular, no vacant sites are allowed in the lattice, no pressure volume effects, polymer molecules are of same size (i.e., mono disperse). Moreover, due to the fitting of molecules on a fixed lattice, this theory fails to take into account the molecular characteristics like: the size and shape of the polymer segments, the flexibility and local structures of the chain molecules, and the van der Waals radii of atoms. The major deficiencies of the Flory-Huggins theory have been reviewed in great detail in articles by Dudowicz *et al.* [41, 42].

Over the last few decades, numerous developments to the original theory have been made by many authors [43-46]. Most of these theories fall into the category of equation-of-state theories which adopts statistical thermodynamics approach based upon the equation of state to include the pressure volume effects on mixing and to take into account the polydispersity of the polymers. Due to the intricate nature of equations resulting from these modified theories, they are rarely used for practical purposes. Hence, the Flory-Huggins theory is still the most widely used thermodynamic theory with interaction parameters being extensively used to judge the miscibility in many practical situations.

Chapter 3

Foundations of Molecular Dynamics Simulation

This chapter briefly describes some of the major aspects of molecular dynamics (MD) simulation, with a main focus put on the calculation methods used in the current thesis. Most of the methodologies used are well-established techniques and are extensively explained in classical texts on molecular simulation [47-49]. Therefore, only the basic foundations of these subjects will be treated here.

3.1 Introduction

The macroscopic properties of interest are generally the result of statistical averages over many microstates over a much longer time scale than rapid electronic motions. Depending on the mechanical approach we use, the definition of microstate varies. For example, in terms of quantum mechanics, the wave functions are referred to as microstates. Theoretically, these wave functions/microstates can be obtained by solving the Schrodinger equation. On the other hand, classical mechanics uses positions and momenta of constituent

atoms of the material to specify microstates. The collection of position and momentum variables constitute a phase space. The quantum mechanical approach, because of the limited computational resources, fails to describe systems containing large number of atoms and molecules (e.g., polymeric systems). Hence, approximate methods like Monte Carlo (MC) or Molecular Dynamics (MD), which uses classical mechanics, are more popular methods to generate such microstates. These microstates can be averaged using the tools of statistical mechanics to compute the desired macroscopic property. The MC method generates microstates by exploring positions of atoms through ‘energy directed’ random walks, by placing molecular models mostly on cubic lattices. The combination of all the accessible positions is termed as the “*Configuration Space*” and the average equilibrium thermodynamic property obtained is usually referred to as an ensemble average. On the other hand, MD methods are deterministic and all the generated states are connected in time since they are obtained by numerically solving the Newton’s equation of motion. The MD method generates microstates by exploring the “*Phase Space*”, i.e., both positions and velocities of the constituent atoms in the continuous space as compared to the lattices in the MC method. Due to this, the MD method is preferable for computational studies of systems containing molecules having complex structures (e.g., drug molecules used in present thesis), which tend to lose important atomistic details if fitted on simple lattices. An additional advantage of MD methods is that it allows the study of time-dependent or transport properties like diffusion and viscosity.

In statistical mechanics, an average value is defined in terms of an ensemble average, an average taken over large number of replicas of systems considered simultaneously. Generally, this average corresponds to an experimentally observable quantity. MD simulation, generally, yields time average values of a particular quantity. Equation (3.1) illustrates an expression for the time average (\bar{A}) of a thermodynamic quantity A .

$$\bar{A} = \lim_{\tau \rightarrow \infty} \frac{1}{\tau} \int_0^{\tau} A(t) dt \quad (3.1)$$

According to the ergodic hypothesis, the ensemble average computed from MC simulation should be equal to the time average obtained from a comparable MD simulation [50]. This hypothesis simply states that if one allows the system to evolve in time indefinitely, then the system will eventually pass through all the possible states. In other words, the time average should not depend on the chosen initial configuration. In practice, the ergodicity of a system is always assumed but non-ergodic systems do exist. If a realistic initial configuration is selected, it is very likely that the MD trajectory would satisfy the equality of ergodic hypothesis. The MD scheme that we adopted in this work has been shown to be ergodic by Cho and Jonnaopulos [51].

MD simulation requires numerical solutions of second order differential equations of Newtonian mechanics at every time step along with the generation and storage of positions and velocities of all constituent atoms in MD trajectory files. Due to this, MD simulations are computationally expensive and are often

limited by the speed of computers used. Additionally, these simulations are often limited to the systems containing 1000 to 1500 atoms. MD simulations for systems with large number of atoms typically require days or weeks to perform even with the use of current high end workstations. Consequently, only hundred or thousand of picoseconds simulation regime is accessible by this technique. Unfortunately, this is insufficient time for many systems such as polymers in the condensed state to undergo very drastic reorientation and relaxation. It is therefore imperative that the initial state of the system be as representative of the equilibrated state as possible. The Rotational Isomeric State (RIS) theory has been often used to generate initial structures in order to overcome these difficulties. This theory will be discussed in detail in Section 3.6 and later in Section 4.2.2, we will describe the application of this theory to generate equilibrated initial structures of block copolymers used in the present thesis.

3.2 Equations of Motion

The MD simulation neglects quantum effects and treats all atoms as classical particles and hence it depicts the dynamic behaviour of molecules based on classical Newton's second law of motion.

$$F = ma = m \frac{dv}{dt} = m \frac{d^2r}{dt^2} \quad (3.2)$$

where m is mass of the particle, a is its acceleration and r is its position or coordinates and F is force acting on each atom, which can be obtained from the

potential energy, $U(r)$, which is function of all atomic positions. Since the force is conservative, it is defined as negative gradient of the potential energy function of the system, which is readily differentiable with respect to the atomic positions.

$$F = -\frac{\partial U(r)}{\partial r} \quad (3.3)$$

Generally, the potential energy, $U(r)$, is defined by a force field, constructed out of a combination of pair wise interactive terms, as described in the next section. Given a set of initial conditions (velocities and positions), the equation (3.2) can be integrated numerically in discrete time steps using finite difference methods (Section 3.4.1) for all the particles in the simulated system, to yield the positions and momenta of these particles as functions of time, which are stored in a *trajectory*. From this trajectory, the average values of properties can be determined. The MD method is deterministic in the sense that once the positions and velocities of each atom are known at time $t = 0$, the state of the system can be predicted at any later time.

3.3 Force Fields

The functional form along with the parameter sets used to describe the potential energy of a system within MD simulation is referred to as force field [52]. The force field uses a set of empirical formulas to mimic all interactions between atoms that are covalently bonded as well as non-bonded interactions between atoms and molecules in molecular systems. Their development and application

lies on the validity of several assumptions [49]. The most important assumption is the Born-Oppenheimer approximation, which assumes that the electrons attain their optimum distribution fast enough to adjust to any movement of nuclei based on the fact that the nuclear mass is far greater than the electronic mass. In other words, we ignore the electronic motions and express the energy of a system as a function of the nuclear coordinates only. Transferability is another key issue in application of such force fields, since the set of parameters derived from relatively small number of cases of probably small molecules needs to be applied to much wider range of molecular systems. Finally, we make an approximation that interactions among atoms and molecules can be described using simple analytical functions and their corresponding parameters can model the chemistry. Force field functions and associated parameter sets are derived from both experimental work and high-level *ab initio* (first principle quantum mechanical) calculations. The quality of the force field determines the quality of the resultant data and hence different force fields are designed for different purposes. Roughly, force fields are classified into three classes:

Generic Force Fields: They are all purpose force fields used for all types of materials including organic, inorganic and metallic materials. They contain simplified form of the potential energy function in order to enhance their general applicability. But these types of force fields have limited transferability. DRIEDING I and II [53], and Universal Force field (UFF) [54] are few examples of force fields belonging to this class.

Classical First Generation Force Fields: These force fields were mainly developed for specific applications in the field of biochemistry. Major force fields belonging to this class are AMBER [55] and CHARMM [56]. These force fields were mainly applied to the simulations of biological macromolecules like proteins and DNA.

Second Generation Force Fields: These types of force fields have extended form of the potential energy function mainly including the cross terms. This increases their transferability. Examples include, MMFF [57], MM2 [58], CFF [59]. The parameters in the CFF force field were modified to extend its applicability into the field of organic polymers and zeolites. The resultant force field was termed as the PCFF [60, 61]. Later, to extend the applicability of this force field to condensed phase applications, the COMPASS (Condensed-phase Optimized Molecular Potentials for Atomistic Simulation Studies) [62] force field was developed, where the non-bond parameters were re-parameterized and optimized to fit the condensed-phase properties. This is a classical force field but since most of its parameters were derived based on *ab initio* data; this is sometimes also referred to as an *ab initio* force field.

It has been shown that the COMPASS force field is able to make accurate predictions of structural, conformational, cohesive, and other physical properties for a wide range of molecules and polymers [62]. Rigby has demonstrated that the COMPASS force field is able to reproduce liquid density for a variety of substances with complex molecular structures [63]. In this thesis, we are mainly

interested in studying the role of non-bond interactions in inducing compatibility between di-block copolymers and drugs having complex molecular structures. Hence, the COMPASS force field has been selected as a force field of choice.

The functional form of total potential energy of the system, as described by the COMPASS force field, is composed of several terms arising from the parameterization of the bonding and non-bonding interactions as shown in the following equation:

$$E_{total} = E_b + E_\theta + E_\phi + E_\tau + E_{cross} + E_{vdW} + E_Q \quad (3.4)$$

The first five valence terms parameterize the short ranged intra-molecular interactions which correspond to internal coordinates bond (b), angle (θ), torsion angle (ϕ), Wilson out-of-plane angle (τ), and cross-coupling terms (E_{cross}). These cross-coupling terms are generally included in the second generation force fields to achieve higher accuracy. They include combinations of two or more internal coordinates (e.g., bond-bond, bond-angle and bond-torsion) that would predict vibration frequencies and structural variations associated with the conformational changes. The last two terms of equation (3.4) represent non-bonded interactions consisting of Lennard Jones (LJ) 9-6 function for the dispersive interactions and Coulombic function for electrostatic interactions.

The COMPASS force field uses quartic polynomials for bond stretching (E_b) and angle bending (E_θ) as shown in expressions (3.5) and (3.6).

$$E_b = \sum_b [k_2(b - b_o)^2 + k_3(b - b_o)^3 + k_4(b - b_o)^4] \quad (3.5)$$

$$E_\theta = \sum_\theta [k_2(\theta - \theta_o)^2 + k_3(\theta - \theta_o)^3 + k_4(\theta - \theta_o)^4] \quad (3.6)$$

where b_o and θ_o are equilibrium bond length and angle, respectively. Torsion angles or dihedral angles (ϕ) existing between four atoms is described using a three-term Fourier expansion as given in the equation (3.7).

$$E_\phi = \sum_\phi [k_1(1 - \cos \phi) + k_2(1 - \cos 2\phi) + k_3(1 - \cos 3\phi)] \quad (3.7)$$

An out-of-plane angle or improper torsion coordinate, defined according to Wilson *et al.* [64], arises when the local molecular structure consists of four atoms with three valence bonds formed to one center atom. It is easy to visualize the presence and importance of such angles in ammonia (NH_3) molecule having trigonal pyramid structure. This type of angle is also useful in molecular systems involving aromatic rings in their structure. The expression describing improper torsion angle (τ) is shown in the equation (3.8).

$$E_\tau = \sum_\tau k_2 \tau^2 \quad (3.8)$$

The expression for E_{cross} (Equation (3.9)) includes six cross-coupling terms arising from interactions among above four types of internal coordinates.

$$\begin{aligned}
E_{cross} = & \sum_{b,b'} k(b-b_o)(b'-b_o') + \sum_{\theta,\theta'} k(\theta-\theta_o)(\theta'-\theta_o') + \\
& \sum_{b,\theta} k(b-b_o)(\theta-\theta_o) + \\
& \sum_{b,\phi} (b-b_o)[k_1 \cos \phi + k_2 \cos 2\phi + k_3 \cos 3\phi] + \\
& \sum_{\theta,\phi} (\theta-\theta_o)[k_1 \cos \phi + k_2 \cos 2\phi + k_3 \cos 3\phi] + \\
& \sum_{\theta,\theta,\phi} k(\theta-\theta_o)(\theta'-\theta_o') \cos \phi
\end{aligned} \tag{3.9}$$

Induced dipole interactions in a molecule are defined by dispersion terms in the force field. These dispersion interactions along with short distance repulsions are described by LJ-9-6 function (Equation (3.10)), which is collectively referred to as van der Waals (vdW) interactions. A steep repulsion at short separations is caused by Pauli repulsion associated with the overlap of electron clouds belonging to the approaching non-bonded atoms/molecules.

$$E_{vdW} = \sum_{i,j} \varepsilon_{ij} \left[2 \left(\frac{r_{ij}^o}{r_{ij}} \right)^9 - 3 \left(\frac{r_{ij}^o}{r_{ij}} \right)^6 \right] \tag{3.10}$$

where ε_{ij} is interaction strength and r_{ij}^o is equilibrium intermolecular distance. These LJ-9-6 parameters are given for like atom pairs. For unlike atom pairs, a 6th-order combination rule [65] is used to calculate the off-diagonal parameters:

$$r_{i,j}^o = \left(\frac{(r_i^o)^6 + (r_j^o)^6}{2} \right)^{\frac{1}{6}} \quad (3.11)$$

$$\varepsilon_{i,j}^o = 2\sqrt{\varepsilon_i \bullet \varepsilon_j} \left(\frac{(r_i^o)^3 \bullet (r_j^o)^3}{(r_i^o)^6 \bullet (r_j^o)^6} \right)$$

The electrostatic interaction energy (E_Q) is described using the Coulombic function as shown in the equation (3.12).

$$E_Q = \sum_{i,j} \frac{q_i q_j}{r_{ij}} \quad (3.12)$$

Here, q_i and q_j are partial atomic charges on atoms i and j . In certain force fields (e.g., DRIEDING II [53]), an additional term describing the interactions due to hydrogen bonding is used. But in the COMPASS force field, there is no explicit term in the potential energy function to describe such interactions and in fact the term E_Q describes such interactions along with the interactions between the point charges. In this force field, the partial atomic charges of a molecule are calculated from the charge bond increment, δ_{ij} , which represents the charge separation between two valence-bonded atoms i and j [62]. Thus, the net partial atomic charge q_i on an atom i is considered to be the summation of all the charge bond increments.

$$q_i = \sum_j \delta_{ij} \quad (3.13)$$

where j represents all the atoms that are valence-bonded to atom i . The charge bond increment parameters were derived by fitting to *ab initio* electrostatic potentials (ESP) of the molecule. More details on calculating q_i can be found in the reference by Sun H. [62]. Briefly, the *ab initio* data includes ESP, energies, and the first and second derivatives of the energies. In order to maintain the transferability of these charge parameters, a constrained ESP (CESP) method is employed in which all the previously determined bond increments are fixed and are transferred while only the unknown ‘new’ parameters are relaxed to fit the ESP. The default parameters of the COMPASS force field available in the commercial software package Materials Studio (MS Modeling version 4.2, Accelrys) have been used for all the simulation work reported in this thesis.

3.3.1 Non-bonded Interactions

In a typical MD simulation, most of the CPU time is invested in the calculations of non-bonded interactions. In order to evaluate all non-bonded pairs in a molecular system of N atoms, we need to perform the $O(N^2)$ calculation (i.e., CPU time $\propto N^2$). The dispersion interactions are short-ranged and hence, a cut-off method is employed to reduce the computational requirement. On the other hand, the electrostatic interactions are long-ranged and truncation using cut-offs affect the results significantly [66]. Hence, such interactions need to be treated with special methodologies. Generally, the Ewald procedure [48, 67] is employed to deal with electrostatics in simulations. Note that this procedure can only be

performed on the systems subjected to periodic boundary conditions. This will be discussed in more detail in Section 3.6.1.

3.4 Molecular Dynamics Algorithms

The heart of any MD algorithm is to numerically integrate the Newton's second law of motion (Equation (3.2)) in discrete time steps (Δt). Generally, the finite difference method is used to solve this second-order differential equation. Given a set of initial positions (r_i) and velocities (v_i) at time t , the positions and velocities at time $t+\Delta t$ are calculated. All the atoms are assigned initial velocities according to the Maxwell-Boltzmann distribution at the temperature of interest. In Figure 3.1, a global flow scheme for a typical MD algorithm is given. Utilizing appropriate force field, forces on each atoms are calculated from the functions describing the distance-derivative of the interaction potentials (i.e., $\partial U(r_i)/\partial r_i$). Usually, three-body and/or higher body interactions are ignored in order to keep the computation in a manageable manner, since CPU time $\propto N^n$ for n -body interactions. Hence, pair-wise additive assumption is used during force/interaction calculations. The Materials Studio software package used in this thesis applies velocity Verlet algorithm to integrate the equation of motion as explained in the next section. The collection of positions and velocities of the atoms for the pre-determined period of simulation time (i.e., the number of time steps) is called MD trajectory. The properties of interest can then be averaged, over the whole trajectory, using equation (3.1) to obtain the final results.

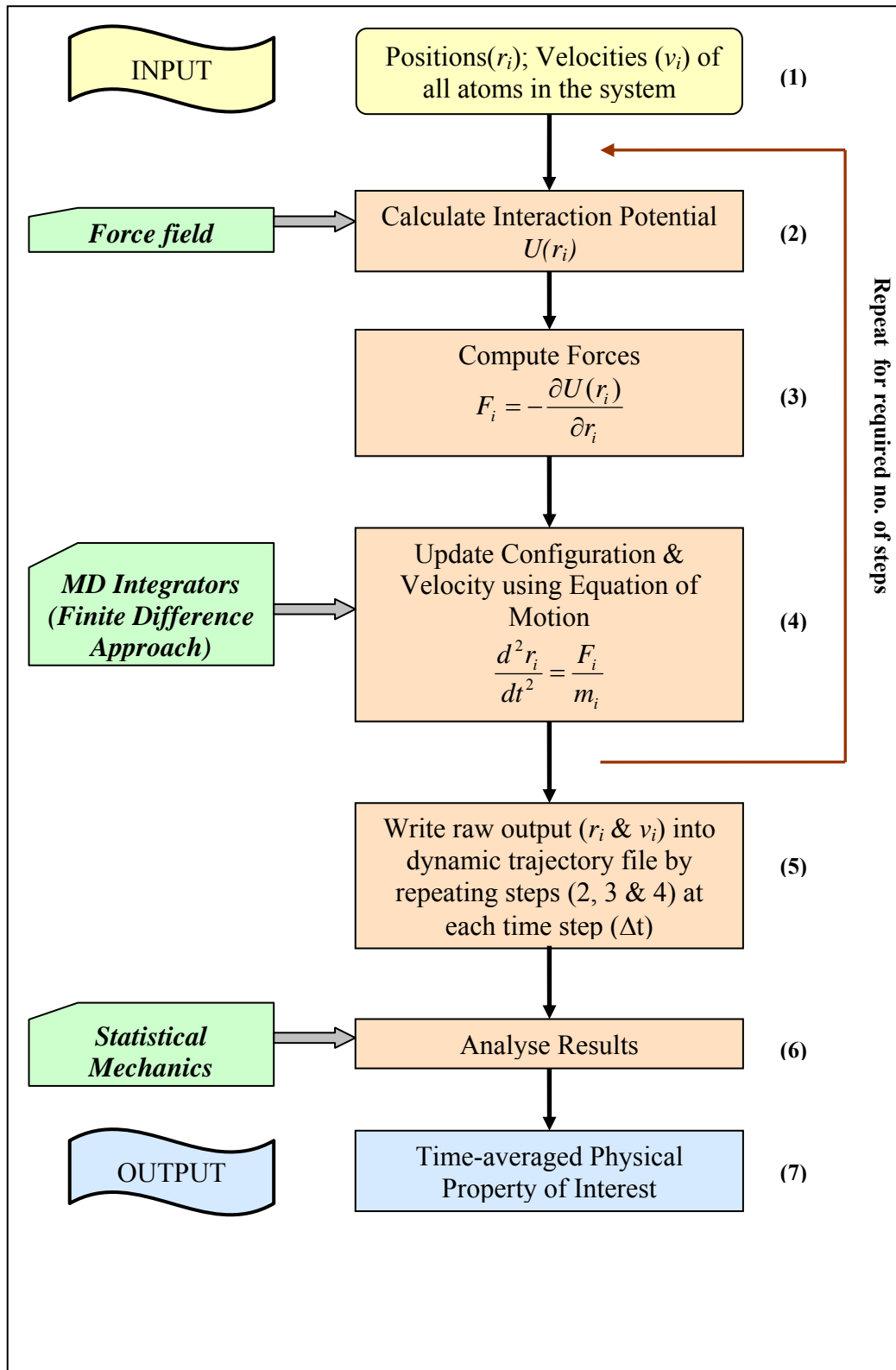


Figure 3.1 The global flow scheme for a typical MD Algorithm.

3.4.1 Integration Algorithms

Integration algorithms utilize finite difference methods to perform the dynamics incrementally making use of constant time-steps Δt . The Verlet algorithms [68] are perhaps the most widely used integration algorithms in MD simulations. The Verlet algorithm uses positions, accelerations at time t and positions from the previous time step to determine new positions. This algorithm is stable, accurate and simple to implement. A problem with this version of Verlet algorithm is that the velocities are not calculated explicitly at each time step, which are normally required to evaluate the values of kinetic energy in order to test the conservation of energy at all points of simulation time. To overcome this difficulty, some variants of Verlet algorithm has been developed, which mainly differs in terms of what variables are stored in memory at what times. The leap-frog algorithm is one of such variants where velocities are handled explicitly but unfortunately, they are not defined at the same time as the positions and are half a time step out of synchrony. As a result, in this scheme, kinetic and potential energy are not defined at the same time, and hence one cannot compute the total energy directly. The velocity Verlet algorithm overcomes this shortcoming of the leap-frog algorithm. In the velocity Verlet algorithm, for given positions, velocities and accelerations at time t , we can compute:

$$\begin{aligned}
r(t + \Delta t) &= r(t) + v(t)\Delta t + \frac{1}{2}a(t)\Delta t^2 \\
a(t + \Delta t) &= \frac{F(t + \Delta t)}{m} \\
v(t + \Delta t) &= v(t) + \frac{1}{2}[a(t) + a(t + \Delta t)]\Delta t
\end{aligned}
\tag{3.14}$$

Hence, we get positions, velocities and accelerations at the same time. Consequently, this algorithm consumes less memory compared to previous algorithms because one does not need to keep track of velocities at different time steps. Since, these integration methods are approximate methods derived based on the Taylor expansions, they involve truncation as well as round-off errors. These errors are generally dependent on the values of integration time step (Δt). For example, in the Verlet algorithm, the truncation error is proportional to Δt^4 . Thus, the integration time step (Δt) is a key parameter determining the accuracy and stability of any integration algorithm. It is obvious that a short time step would generate a stable trajectory but the time scale of a process that can be accessed would be rather limited. The choice of a particular time step depends on the integrators as well as the system. The main assumption involved in the Verlet algorithm is that the accelerations and velocities are constant over a time step used. Hence, in order to satisfy this assumption, we must split the highest vibrational frequency in a particular molecular system into 8 to 10 segments. For most of the molecular systems, the highest vibrational frequency is 10^{-14} s (i.e., 10 femtosecond) for C-H bond stretching. Therefore, the time step should be about 0.5 to 1 femtosecond (fs). Though longer time steps upto 5 fs can be used for

studying much simpler molecular systems. For all the simulations in this thesis, we have used 1 fs integration time step.

3.5 Molecular Dynamics in Various Thermodynamic Ensembles

MD studies are based on statistical thermodynamics rules and hence they provide direct route from microscopic details of a system to macroscopic properties of interest. To serve this purpose, it is crucial to imitate the dynamics similar to the experimental conditions using the corresponding correct ensemble for the property of interest. In classical mechanics, Newton's equation of motion conserves energy and hence conventional MD describes a system with constant number of particles (N), volume (V), and energy (E) (i.e., NVE or microcanonical ensemble). However, this ensemble does not resemble standard experimental conditions where a system is generally exposed to external pressure and/or exchanges heat with the environment and therefore, several other algorithms are available to sample in different ensembles. In most cases, temperature (T) and pressure (P) are most crucial properties which one would like to control. Most common thermodynamic ensembles relevant to the experimental conditions are canonical (NVT) or isothermal-isobaric (NPT) ensembles. One needs to reformulate the equations of motion by adding new degrees of freedom in order to regulate temperature and pressure of the system. Simulations performed in this work has been carried out in NVT and NPT ensembles using the temperature and pressure couplings as described in next few sections.

3.5.1 Thermal Coupling

In MD simulation, most of the thermostats essentially belong to three major classes: (a) Scaling velocities (e.g., velocity-scaling and Berendsen Thermostat); (b) Adding stochastic forces and/or velocities (e.g., Andersen, Langevin, and Dissipative Particle Dynamics Thermostats); and (c) Using “*extended Lagrangian*” formalisms (e.g., Nosé-Hoover thermostat). Each of these classes of schemes has advantages and disadvantages, depending on their application.

Velocity-scaling procedure is one of the earliest methods used to perform canonical simulations. This scheme works by scaling the velocities of particles at each time step in order to keep the effective system temperature constant. However, this procedure suppresses the natural fluctuations of kinetic energy of the system and hence they do not produce realistic canonical trajectories. On the other hand, the stochastic methods work by adding a friction and noise term to the Newton’s equation of motion. This scheme generates an exactly defined canonical ensemble, but the presence of random noise does disturb the actual dynamics of the system.

The extended system (ES) methods (Nosé-Hoover thermostat) belonging to the class (c) was introduced by Nosé [69, 70] and subsequently reformulated by Hoover [71] to eliminate the time scaling so that the trajectories in real time and with evenly spaced time points can be obtained. This is one of the most widely used methods for performing canonical simulations that produces true canonical ensembles. Since this thermostat was used to control temperature in all the simulations described in the present thesis, we hereby briefly review this

thermostat algorithm. In this method, one incorporates an additional (fictitious) degree of freedom to the real physical system to represent interaction of the system with heat bath. The additional dynamic variable is believed to have mass Q , whose magnitude determines the coupling between the reservoir and the real system and hence influences the temperature fluctuations. The Lagrangian expression for the total system (reservoir + real system) is given by:

$$L_{NOSE} = \sum_{i=1}^N \frac{m_i}{2} s^2 \dot{r}_i^2 - U(r^N) + \frac{Q}{2} \dot{s}^2 - (f+1)k_B T \ln s \quad (3.15)$$

where f is degrees of freedom of the physical system (e.g., $3N$) and T is the desired temperature. The parameter s is a dynamical variable that represents the extra degree of freedom of the reservoir. It is worth noting that if $s = 1$, the original Lagrangian is recovered. The third and fourth terms in the above Lagrangian expression represent the kinetic energy and (negative) potential energy of the reservoir, respectively. Equations of motion, in terms of the virtual variables for the system, are derived from the Hamiltonian, which is in turn derived from the above extended Lagrangian (Equation (3.15)). Equations of motion can be written in real as well as virtual variable but for the sake of convenience, real-variable formulation is recommended. Introducing the thermodynamic friction coefficient $\xi = s'p'_s / Q$, equations of motion in terms of the real variables can be recovered as follows:

$$\begin{aligned}
\dot{r}_i &= \frac{p_i}{m_i} \\
\dot{p}_i &= -\frac{\partial U(\mathbf{r}^N)}{\partial r_i} - \xi p_i \\
\dot{\xi} &= \frac{1}{Q} \left(\sum_{i=1}^N \frac{p_i^2}{m_i} - (f+1)k_B T \right) \\
\xi &= \frac{\dot{s}}{s}
\end{aligned} \tag{3.16}$$

The choice of this user-defined fictitious mass Q of additional degree of freedom is rather arbitrary and is generally based on the balance between the stability of the solution and the highest-frequency motions of the system. If Q is high (i.e., loose coupling), the flow of energy between the physical system and the reservoir will be too slow and consequently, infinite Q corresponds to a NVE MD system. On the other hand, if Q is too low (i.e., tight coupling), then the energy oscillates unphysically, causing equilibration problems. If the energy of the extended system is conserved, then the Nosé-Hoover thermostat reproduces the canonical ensemble of the real physical system in every respect.

3.5.2 Pressure Coupling

Pressure can only be defined when the system is placed in a container having a definite volume. In a computer simulation, the unit cell subjected to periodic boundary conditions is viewed as a container. We describe the important features of periodic boundary conditions in the next section. To control the pressure in MD simulation, the volume of the simulation box is considered as a dynamical variable. For NPT simulation performed in the present thesis, the Andersen

barostat [72] has been used to control the pressure, and hence this method is described briefly over here. Andersen method was developed to adjust the pressure in a simulation of interacting particles. Here, the volume of cell is allowed to change but its shape is preserved by allowing the cell to change isotropically. In a simulation box of volume V , Andersen proposed to replace the coordinates r_i by scaled coordinates ρ_i defined by:

$$\rho_i = \frac{r_i}{V^{1/3}} \quad (3.17)$$

Consider the following new Lagrangian, in which a new variable Q appears:

$$L(\rho^N, \dot{\rho}^N, Q, \dot{Q}) = \frac{1}{2} m Q^{2/3} \sum_{i=1}^N \dot{\rho}_i^2 - \sum_{i<j=1}^N U(Q^{1/3} \rho_{ij}) + \frac{1}{2} M \dot{Q}^2 - \alpha Q \quad (3.18)$$

If one interprets Q as the volume V , the first two terms on the right are just the Lagrangian of unscaled system. The third term is kinetic energy for the motion of Q , and the fourth term represents the potential energy associated with Q . Here, α and M are constants. A physical interpretation of these additional terms in equation (3.18) would be: Assume that the system is simulated in a container which can be compressed by a piston. Thus, Q , whose value is volume V , is coordinate of the piston. αV is potential derived from the external pressure α acting on the piston and M is mass of the piston. In the process of constructing modified Lagrangian of scaled system, we have to decide upon the values of

constants α and M . The value of α is chosen to be the value of pressure of the fluid and M is mass of the piston whose motion expands or compresses the fluid. The trajectory averages calculated from a simulation are independent of the value of M , as long as M is finite and positive. Hence, if the only goal of a simulation is to calculate the equilibrium averages, then any finite positive value of M can be chosen [72].

3.6 Periodic Boundary Conditions

Periodic boundary conditions are employed to simulate bulk liquid state properties by eliminating the unnecessary surface effects. These boundary conditions are implemented by replicating a cubic simulation box of volume V (primary cell) throughout the space to form an infinite lattice. The replicated cells are called image cells and have the same number of particles as the primary cell. A two dimensional version of such a periodic system is shown in Figure 3.2. It is worth noting that there are no surface molecules and no walls at the boundary of each cell and hence particles are free to enter or leave any cell. However, the number of particles in each cell is kept constant. During the course of simulation, as an atom moves in the primary cell, its periodic images in all the image cells move in exactly the same way. Since all the images are just shifted copies of an original atom, it is not necessary to store the coordinates of all the images in a simulation and we only keep the track of coordinates of the atoms in the primary cell. When an atom leaves the primary cell by crossing a boundary, attention is switched to the image just entering.

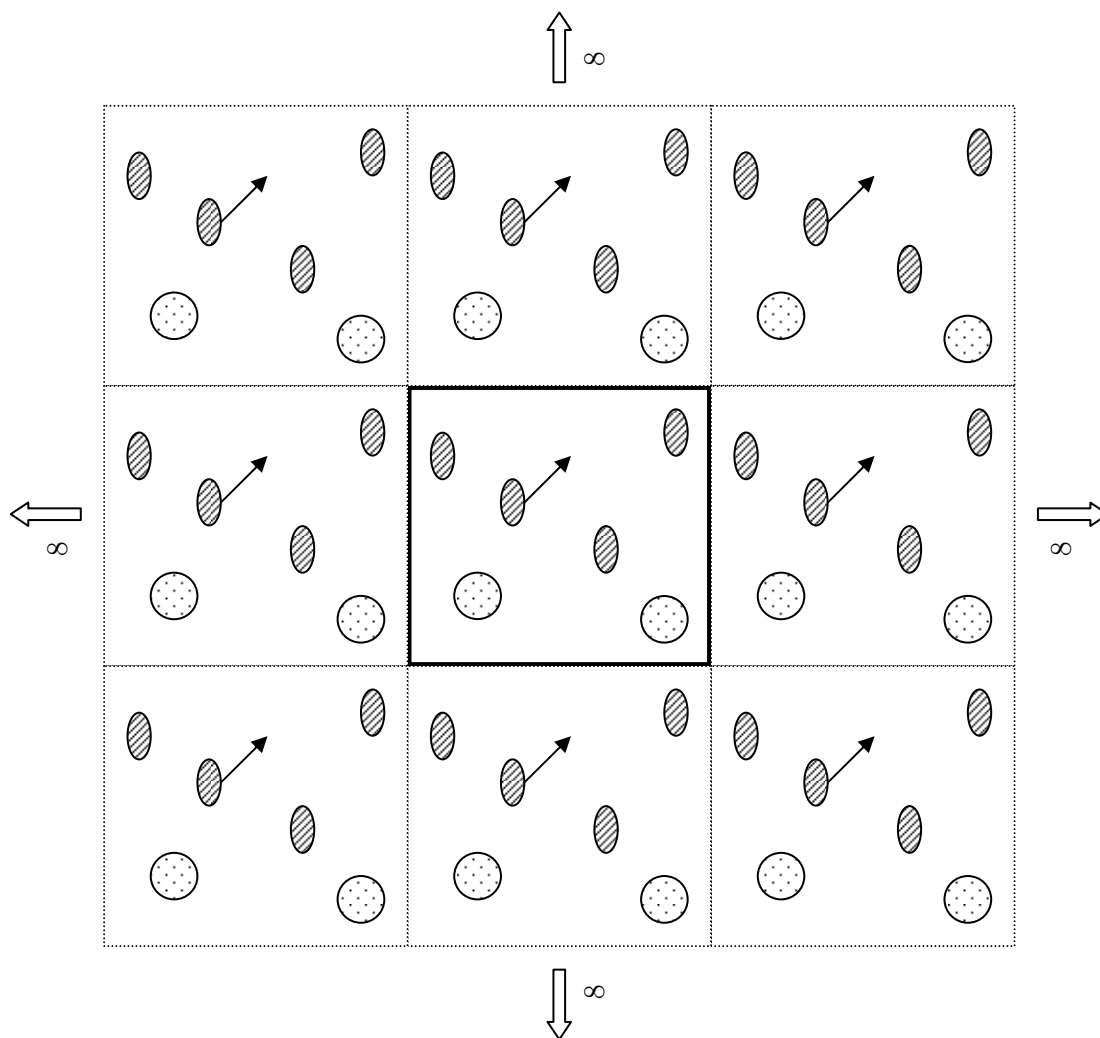


Figure 3.2 Periodically repeated images of an original simulation box (solid line) in two dimensions.

For short-range interactions, we normally apply a spherical cut-off in order to improve the computational efficiency. The cut-off radius should be chosen such that a particle in the primary cell does not see its own image in the surrounding image cells. The atoms within this cut-off are kept in neighbour lists, which are named Verlet list, and updated at certain time intervals. In order to reduce the computational cost for long-range electrostatics, special tricks like Ewald summation are applied, which will be discussed in the next section.

In the present thesis, we apply periodic boundary conditions to construct amorphous state models of block copolymers, drugs and their binary mixtures. The liquid state models are built using the methodologies developed by Theodorou and Suter [73]. In order to model the bulk liquid states of block copolymers, single chain conformations in the unit cell subjected to periodic boundary conditions are used. First, a unit cell is created whose size is determined based on the density, the molecular weight and the number of polymer chains. Then, the centre of each molecule is placed in a random position within the unit cell and structures are grown from the middle outwards. As the single chain conformations are grown, several constraints are imposed. Hard overlaps are avoided by ascribing a hard core radius to each atom equal to 0.3 times of its van der Waals radius.

For systems with large number of atoms (e.g., block copolymers), the number of MD time steps one can access in practice is still rather limited. Hence, to properly sample the conformation of the block copolymer to generate average final properties free from any artefacts of the input initial structure, it is very

important to use a realistic way to generate initial structures which are close to ‘true’ structures. In other words, we need to fulfil the important condition of ergodic hypothesis discussed in Section 3.1. For this purpose, the use of RIS model developed by Flory [74] is inevitable in order to generate realistic copolymer configurations. The RIS theory is standard method used to compute the conformational statistics of polymer chains based on the Boltzmann distribution. In this theory, each bond is assumed to adopt a small number of discrete torsion angles representing the lowest energy. One can easily identify such RIS energy states based on the distribution of torsion angles of skeletal bonds of the copolymers. More details on the RIS theory [74] and its application to the system of di-block copolymers used in the present thesis will be presented later in the Section 4.2.2.

3.6.1 Ewald Summation

Ewald summation [75] was introduced in 1921 as a technique to sum the long-range electrostatic interactions between particles and all their infinite periodic images efficiently. This method is based on the representation of the electrostatics in a system by Coulombic point charges q . Hence, first, we assume a collection of N charged particles in a cubic box with side length L , with periodic boundary conditions. The total electrostatic energy in this system is given by:

$$U_{ELEC} = \frac{1}{2} \sum_n \sum_{i=j=1}^N \frac{q_i q_j}{|r_{ij} + nL|} \quad (3.19)$$

The prime ' in the sum over periodic images n indicates that the particle self-interaction $i = j$ should be skipped when i and j are in the same periodic image ($n=0$). The above sum in the equation (3.19) is conditionally convergent and hence the main idea in the Ewald summation is to convert one conditionally convergent sum into two absolutely convergent sums. To evaluate U_{ELEC} efficiently, we break it into two parts: (i) a short-ranged potential treated with a simple cut-off; and (ii) a long-ranged potential which is periodic and slowly varying, which can therefore be represented to an acceptable level of accuracy by a finite Fourier series. This is achieved by surrounding each discrete point charge using the Gaussian charge distribution of opposite sign and equal magnitude. In this way, the interactions are screened so that they are short-ranged and then the sum of interactions is absolutely convergent. After this, a compensating charge density is added so that the overall potential is identical to the original one. Summation of this compensating distribution is performed in a reciprocal space so that it is absolutely convergent. This part is treated using the Fourier series. The Ewald sum (Equation (3.20)) is therefore written as the sum of three parts, the short-ranged real (direct) space sum (U^r), the long-ranged calculated in the reciprocal (imaginary or Fourier) space sum (U^m), and a self-interaction constant term (U^o).

$$U_{Ewald} = U^r + U^m + U^o \quad (3.20)$$

The reciprocal space part extends infinitely over all periodic images. The actual charge distribution is described by a set of Gaussian charge clouds, for which an interaction in reciprocal space can be written as sum over the set of k vectors:

$$U^m = \frac{1}{2} \sum_{k \neq 0} \frac{4\pi}{k^2} e^{-k^2/4\alpha} |\rho(k)|^2 \quad (3.21)$$

Here, α is the inverse length (an Ewald parameter), which is used to determine the relative weight of real and reciprocal space contributions. $\rho(k)$ is given by:

$$\rho(k) = \sum_{i=1}^N q_i e^{ik \cdot r} \quad (3.22)$$

The real space part is calculated in a similar way as normal Coulomb interactions, except that the Gaussian functions ($erf(\alpha|r_{ij} + nL|)$) needs to be subtracted from the point charges, in order to cancel charges added to the system in equation (3.21). Hence U^r is given by the equation (3.23).

$$U^r = \frac{1}{2} \sum_{i \neq j}^N \frac{q_i q_j}{r_{ij}} \frac{erfc(\alpha|r_{ij} + nL|)}{|r_{ij} + nL|} \quad (3.23)$$

Here, $erfc$ is complimentary error function defined as $erfc(x) \equiv 1 - erf(x)$. The error function is defined as follows:

$$erf(x) = \frac{2}{\sqrt{\pi}} \int_0^x e^{-r^2} dr \quad (3.24)$$

The system now contains both point charges and Gaussian charge clouds around a single charge point, and for a single charge point there can be a charge interaction with itself. To remove this term, a self-interaction correction is performed:

$$U^o = -\frac{\alpha}{\sqrt{\pi}} \sum_{i=1}^N q_i^2 \quad (3.25)$$

Chapter 4

Prediction of Compatibility between Water Insoluble Drugs and Self Associating PEO-*b*-PCL Block Copolymers¹

4.1 Introduction

Block copolymers can self-associate to form polymeric micelles, which can serve as nanoscopic vehicle for the delivery of water insoluble drugs in a controlled manner [1, 3, 5, 6]. The challenge is to identify the molecular structure of the blocks in the block copolymer that can encapsulate the drug of interest and provide the desired release properties. It is believed that compatibility between a drug and the hydrophobic block of a block copolymer determines the encapsulation capacity of the micelles [6, 76, 77]. Nonetheless, use of drug compatible moieties in the micellar core has been shown to lower the rate of drug release from the carrier [6]. To optimize the properties of polymeric micelles and

¹ A version of this chapter has been published. Patel, S.; Lavasanifar, A.; Choi, P. (2008). *Biomacromolecules*. 9, 3014-23.

achieve maximum encapsulation and sustained rate of drug release from these carriers, the current practice is to synthesize the target block copolymer and examine the solubility of drugs by carrier using a trial and error approach. This is simply because such drug delivery systems involve complex intermolecular interactions and fittings of molecules of different shapes. Obviously, being able to quantify such interactions between various drugs and block copolymers with different chemical moieties will definitely facilitate the block copolymer design process. This will, in turn, avoid cumbersome and expensive trial and error formulation studies. The molecular simulation seems to be the method of choice in this regard. Ideally, one would like to simulate block copolymer micelles to determine how block copolymer structure and its block lengths affect drug loadings and encapsulation efficiency for the drug of interest. Nevertheless, simulating such systems at the atomistic level on a routine basis is totally impossible at the time being as the computational costs are prohibitively high. Therefore, we have focused on studying binary interactions between the drugs and the block copolymers of interest in their liquid state rather than in a micelle environment. In particular, the aim of the present work is to test if MD simulation would be a better method to determine the compatibility of drug/block copolymer systems than the GCM that is commonly used in the pharmaceutical research. And as shown in this chapter, the MD approaches we used seem to outperform the GCM.

The concept of solubility parameter is used to quantify the strength of intermolecular interactions. The details on the Hildebrand (δ) and Hansen

solubility parameters (δ_d , δ_p and δ_h) can be found in Sections 1.3 and 1.4. According to different formalism of the solubility parameter as depicted in equation (4.1), it is related to the interaction energy potential, $u(r)$ and the local arrangement of molecules in the liquid state, $g(r)$ (i.e., the radial distribution function).

$$\delta = \sqrt{\frac{\Delta E_v}{V}} = \sqrt{\frac{2\pi n^2}{V^2} \int_0^\infty u(r)g(r)r^2 dr} \quad (4.1)$$

where $\Delta E_v/V$ is cohesive energy density (CED); n is number of molecules. Equation (4.2) shows the relationship between the Hildebrand and Hansen solubility parameters.

$$\delta^2 = \delta_d^2 + \delta_p^2 + \delta_h^2 \quad (4.2)$$

Here, the subscripts d , p and h refer to the contributions due to dispersion forces, polar forces, and hydrogen bonding, respectively. In general, compatible materials tend to have comparable solubility parameters (either δ or δ_d , δ_p and δ_h). One common method to obtain the Hildebrand and Hansen solubility parameters is the GCM. The details on the GCM method can be found in the Section 1.4. The GCM is simple to use and generally provides reasonable compatibility predictions for compounds with simple chemical structures. Nevertheless, the GCM fails to provide a good estimation for the solubility of complex drug

molecules and copolymers owing to several disadvantages as described in the Section 1.4.

Forrest *et al.*[78] used the GCM to calculate the Hildebrand solubility parameters of a few lipophilic drugs and of the hydrophobic block (i.e., the PCL block) of a commonly used block copolymer poly(ethylene oxide)-*b*-poly(ϵ -caprolactone) (PEO-*b*-PCL, see Figure 4.1(A)). Using such δ , they calculated the Flory-Huggins interaction parameters (χ), which quantify the difference in intermolecular interactions of the components in a binary mixture, thereby the compatibility for various pairs of drugs and the PCL block of PEO-*b*-PCL. According to the Flory-Huggins solution theory, lower χ values indicate better solubility. It is evident in their results that χ between hydrophobic drugs such as fenofibrate and nimodipine (see Figures 4.1(B) and 4.1(C)) and the PCL block of PEO-*b*-PCL predicted using the GCM are inconsistent with their solubility in caprolactone obtained by experimental means (see Table 4.1). In particular, the Hildebrand solubility parameters of fenofibrate and nimodipine computed by the GCM are 22.5 and 21.6 (J/cm³)^{1/2}, respectively, and the corresponding χ values between them and the PCL block are 0.539 and 0.250, respectively. However, the caprolactone solubility of fenofibrate and nimodipine was 120 and 20 mmol:mol, respectively (see Table 4.1). Higher solubility of fenofibrate in PEO-*b*-PCL was unexpected because their χ parameter is greater than that of nimodipine/PCL block of PEO-*b*-PCL pair.

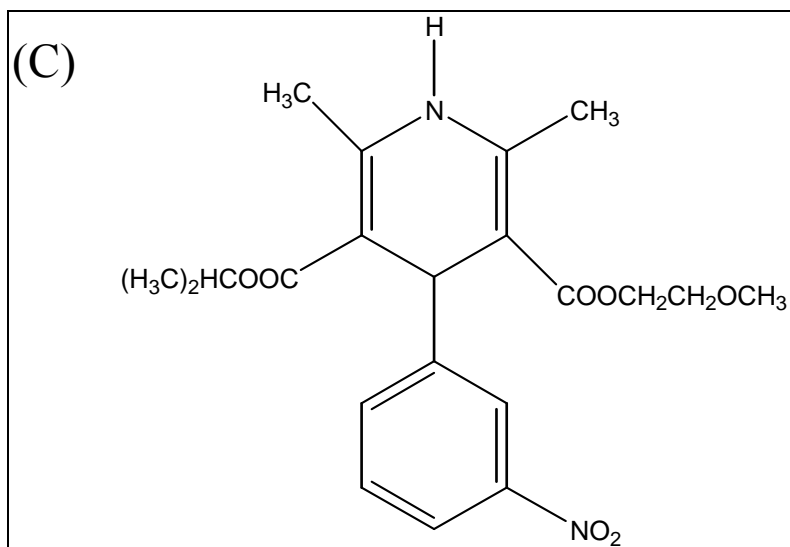
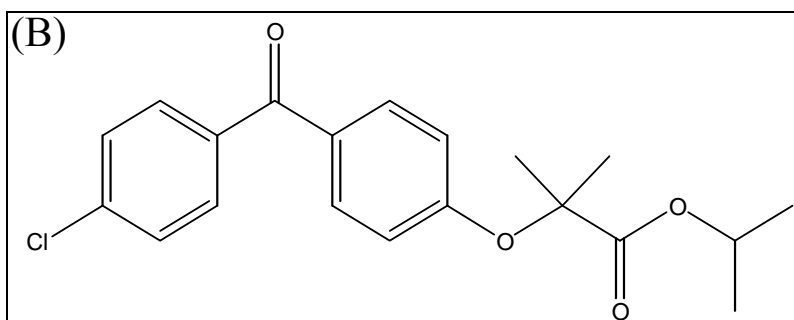
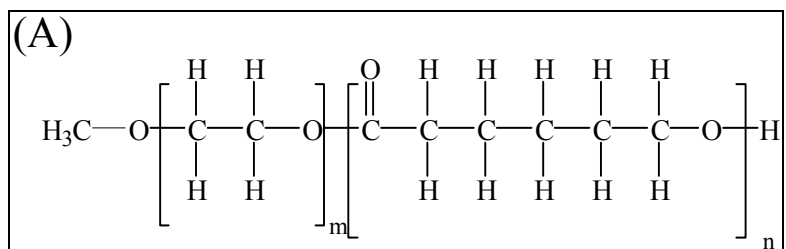


Figure 4.1 Chemical Structures of (A) PEO-*b*-PCL; (B) Fenofibrate; and (C) Nimodipine.

Table 4.1 Reported experimental solubility of fenofibrate and nimodipine in caprolactone along with the solubility parameters of both the drugs and PCL block calculated by Forrest *et al.* using the GCM.

Drug	δ (J/cm³)^{1/2}	$\chi_{\text{drug-PCL}}$	Drug:Caprolactone (mmol:mol)^a
PCL	20.20	-	-
Fenofibrate	22.50	0.539	120
Nimodipine	21.60	0.250	12

^a solubility reported based on maximum incorporation reported by referenced authors in PEG-*b*-PCL or PEG-*b*-PCL-*b*-PEG nanocarrier (See text for details)

It is worth noting that the experimental solubility data reported by Forrest *et al.* was obtained from Jette *et al.* [79] and Ge *et al.* [80] and it signifies the amount of drug soluble in the micelles formed by the corresponding di-block and tri-block block copolymers made up of PEO and PCL blocks for fenofibrate and nimodipine respectively but was converted to a basis of mmol drug/mol of caprolactone. In the case of nimodipine, no drug loading data is available for di-block PEO-*b*-PCL.

Considering the inadequacy of the GCM, in the present work, we therefore applied the technique of MD simulation to determine whether MD simulation would provide better compatibility predictions for the systems that the GCM yielded incorrect results. The motivation originates from the work of Choi *et al.* [22-25] in which the authors have utilized the MD simulation to obtain better estimation of the solubility parameters of surfactants as compared to the GCM and have shown that such an approach can rectify some of the drawbacks of the GCM. Because one can account not only for the interactions between the drug and the PCL block but also for the interactions between the drug and the PEO block in the MD simulation, we carried out simulations using PEO-*b*-PCL with different hydrophilic (PEO) and hydrophobic (PCL) block lengths.

Recently, an *in silico* model has been proposed by Huynh *et al.* [26], which involves calculations of the solubility parameters, of an anticancer agent docetaxel and various small molecule excipients, using semi-empirical methods and MD simulation. The relative *in silico* solubility of Docetaxel in various excipients was in good agreement with the experimental solubility data and hence

validated the use of computational model as a reliable tool for designing drug-excipient mixture formulations. Nevertheless, our study concentrates on the prediction of thermodynamic compatibility between drug and long chain block copolymer. Two different MD strategies were used so that the effects of drug loading and of hydrophilic and hydrophobic block lengths of PEO-*b*-PCL on drug/PEO-*b*-PCL compatibility could be investigated.

4.2 Simulation Details

4.2.1 Software and force field

All MD simulations were performed using Materials Studio Software package (MS Modeling Version 4.0 from Accelrys Inc.) run on a Silicon Graphics (SGI) workstation cluster. The initial block copolymer conformations were generated using the rotational isomeric state (RIS) theory. The COMPASS force field [62] was used throughout to describe bonded and non-bonded interactions (See Section 3.3 for details). Based on first principle quantum mechanical calculations, the partial atomic charges on the molecules were preset by the COMPASS force field. The electrostatic interaction was calculated using the Ewald summation method (Section 3.6.1) since it provides a more effective way of handling long-range interactions. [67]

4.2.2 Construction of liquid-state models

The liquid state models of the block copolymers, drugs and their mixtures were built using the methodologies developed by Theodorou and Suter. [73] Such

structures were constructed using the amorphous builder module available in Cerius². Three PEO-*b*-PCL block copolymers with different hydrophilic (PEO) and hydrophobic (PCL) block lengths were used. They were PEO(1250)-*b*-PCL(2500), PEO(2500)-*b*-PCL(2500) and PEO(2500)-*b*-PCL(1250), where the number in the bracket signifies the molecular weight of the block. Snapshots of liquid state models of PEO(2500)-*b*-PCL(2500) block copolymer and mixture of PEO(2500)-*b*-PCL(2500) block copolymer and fenofibrate drugs [40% (w/w) drug/polymer] are shown in Figures 4.2 and 4.3, respectively.

In the cases of block copolymers, single chain conformations in unit cells subjected to three-dimensional periodic boundary conditions were used. Here, the periodic boundary conditions provide means to model bulk liquid state using only single chains. As single chain conformations were grown, several constraints were imposed. Hard overlaps were avoided by ascribing a hard core radius to each atom equal to 0.3 times of its van der Waals radius. The unit cell was also subjected to the density constraint. Since experimental density values of the drugs and their mixtures with various block copolymers at 140 °C (i.e., 413 K) were not available, we carried out an isobaric-isothermal (NPT) ensemble MD simulation ($P = 1 \text{ atm}$; $T = 413 \text{ K}$) using the density values from the GCM as the initial values to determine their density. Here, the Nose thermostat [69] and Andersen barostat [72] were used to control the temperature and pressure of the systems. In the NPT MD simulation, the volume of the periodic unit cell (i.e., density) is allowed to fluctuate.

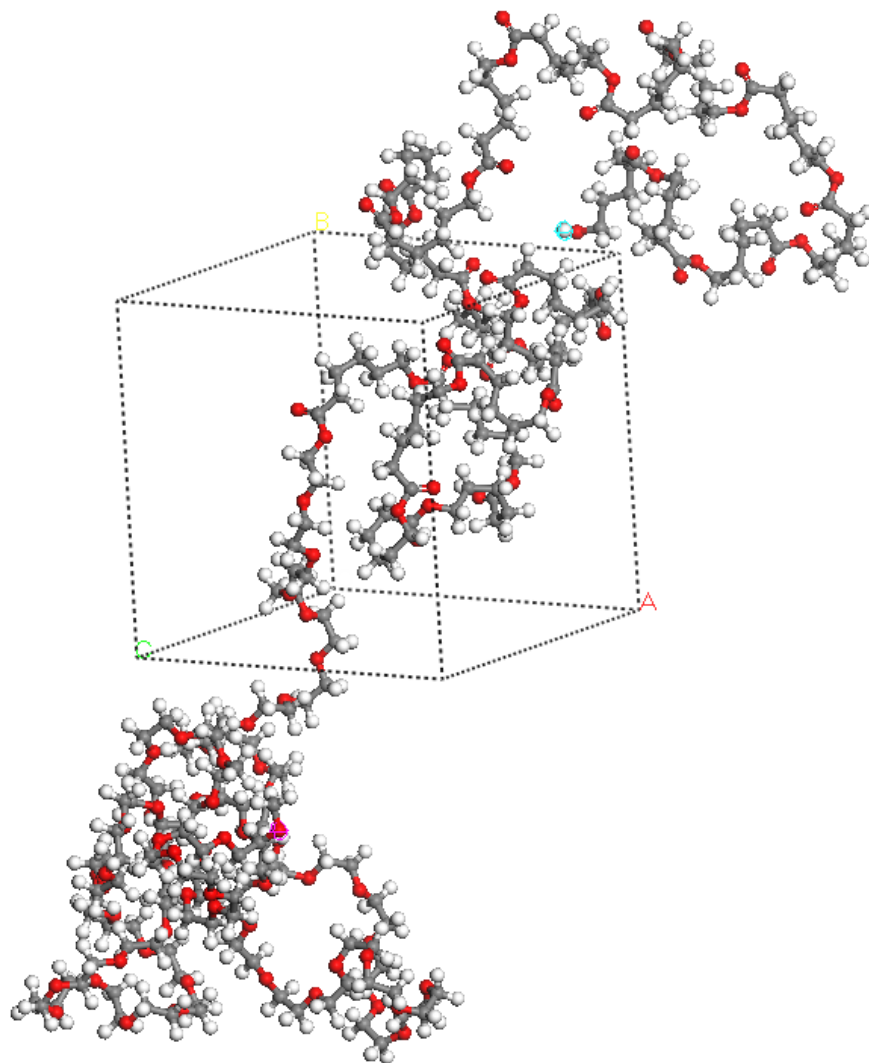


Figure 4.2 Snapshot of the liquid model of pure PEO(2500)-*b*-PCL(2500) subjected to 3D periodic boundary conditions.

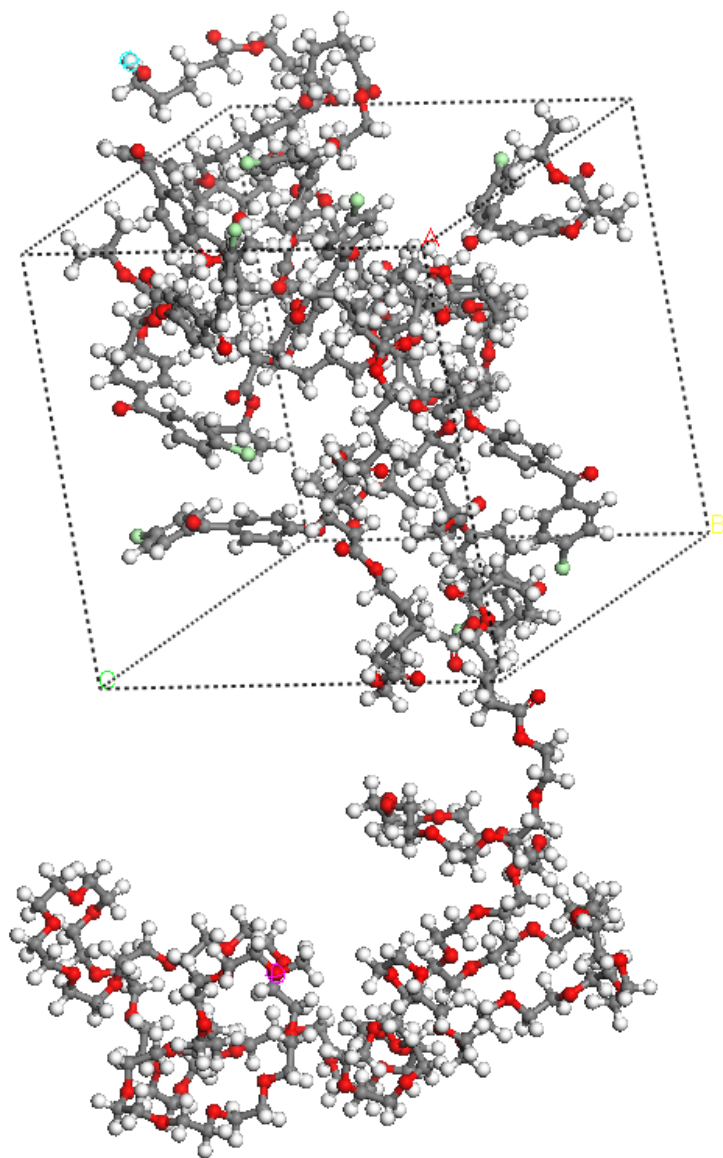


Figure 4.3 Snapshot of the liquid model of binary mixture of PEO(2500)-*b*-PCL(2500) and fenofibrate drug molecules (40% (w/w) drug/block copolymer) subjected to 3D periodic boundary conditions.

The final, and perhaps the most important constraint imposed, was the distribution of the torsion angles of the skeletal bonds in the copolymers, which was determined using the RIS theory [81, 82]. Nevertheless, it should be noted that the RIS theory cannot be used for polymers in their crystalline state. In particular, the torsion angle distribution was determined by applying the Boltzmann weighting factor to the energies of the RIS minima. In this work, the initial distribution of torsion angles was determined by the following method. We identified a total of seven torsion angles for PEO-*b*-PCL and they are described in Tables 4.2 and 4.3. A conformational energy map was constructed for each of these torsion angles by rotating the torsion angle through 360 degrees in ten-degree intervals while simultaneously relaxing all other degrees of freedom to achieve a root mean square force of below 1.0 kcal/(mol Å). A representative conformational energy map is shown in Figure 4.4 for the torsion angle Φ_5 . From this figure, one can readily identify two rotational isomeric states and they are two minima at approximately 60 and 240 degrees. Next, we determined the width of each RIS at a point 0.6 kcal/mol above the minimum. This value was used as the torsion angle tolerance $\Delta\Phi_5$, for constructing the amorphous structures. In Table 4.4, we list the values of RIS minima and respective tolerances for all seven torsion angles that have significant influence to the conformation of the copolymer. Once the RIS state distribution was determined, the RIS states were populated allowing for angle tolerances stated in Table 4.4.

Table 4.2 Unique torsion angles for the PEO block.

Angle Terminology	Torsion Angle
Φ_1	
Φ_2	
Φ_3	

Table 4.3 Unique torsion angles for the PCL block.

Angle Terminology	Torsion Angle
Φ_4	
Φ_5	
Φ_6	
Φ_7	

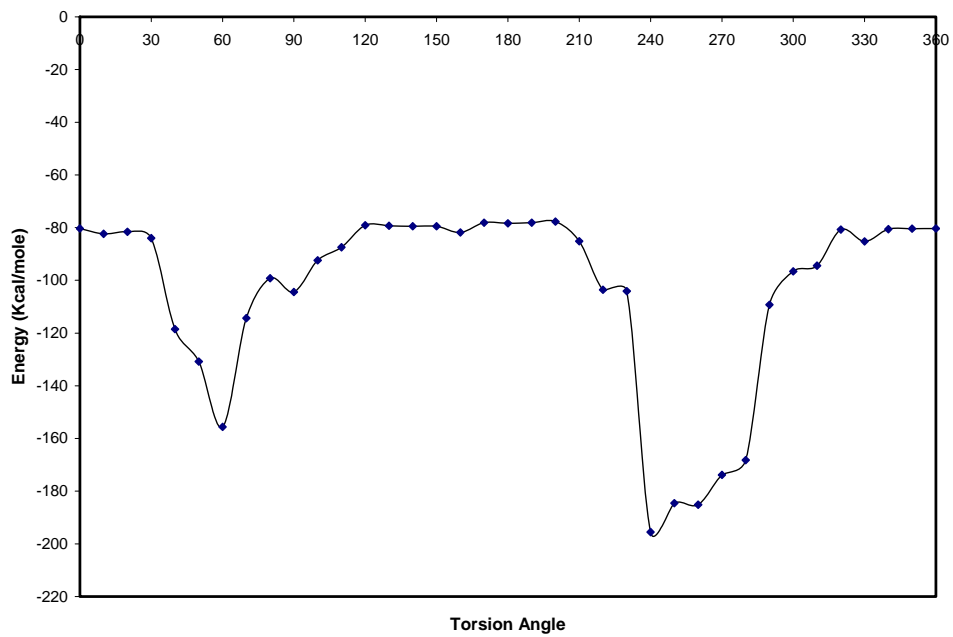


Figure 4.4 Conformational energy map of the torsion angle labelled Φ_5 in Table 4.3.

Table 4.4 Rotational isomeric states for all torsion angles of PEO-*b*-PCL.

Skeletal Bond	State 1*	State 2*	State 3*	State 4*
Φ_1	170 ± 20	300 ± 10	330 ± 10	N/A
Φ_2	40 ± 10	60 ± 10	280 ± 10	350 ± 10
Φ_3	80 ± 10	250 ± 10	N/A	N/A
Φ_4	170 ± 10	200 ± 10	N/A	N/A
Φ_5	60 ± 10	240 ± 15	N/A	N/A
Φ_6	70 ± 15	180 ± 10	230 ± 5	N/A
Φ_7	190 ± 10	220 ± 10	N/A	N/A

*Data are Torsion angle \pm Tolerance

It is worth noting that the initial conformations of the copolymers used in the NPT MD simulations were subjected to the RIS constraints as well.

The reason for using the RIS theory in the construction of the liquid state models was discussed in Section 3.6. In our simulations, we have utilized the fact that the distribution of torsion angles, in the bulk amorphous state, are the same as those of an isolated molecule; that is, the molecular conformation in the bulk is unperturbed by the excluded volume effect and non-bonded intermolecular interactions. This approximation, which is attributed to Flory [83], has been supported by extensive experimental data in the polymer field [74]. Other conformational features such as bond lengths and bond angles were set based on their experimental values. These values generally adjust very quickly during the course of a MD simulation. Upon application of the aforementioned constraints, the size of the simulation cells obtained was about 3 nm which is generally sufficient to represent the bulk amorphous state of the systems, especially subjected to three dimensional periodic boundary conditions. And conformation of the block copolymers is fairly close to that in equilibrium.

4.2.3 MD Simulation

The initial amorphous structure formed using the method described above is in a relatively high energy state and hence before performing MD, energy minimization was carried out using the conjugate gradient method. This minimization step often helps to remove strong van der Waals overlaps.

Canonical (NVT) MD simulations for all the structures were carried out using the Nose thermostat [69] at a constant temperature of 413 K. The temperature is well above the melting points of fenofibrate, nimodipine, and the block copolymers to ensure that all materials are in the liquid (i.e., amorphous) state. A time step of 1 fs was used to ensure the stability of the simulation. The simulations were carried out until the total energy of the systems stabilized. Simulations of drug molecules were carried out for 1000 ps, while the simulations of the block copolymers and mixtures were carried out for 2000 ps. The last few hundred ps of the trajectory files were used to calculate the physical properties of interest. The simulation time used for the pure drug systems should be long enough for the drug molecules to equilibrate. It is worth noting that the computed root mean square displacement over a time period of 1000 ps of fenofibrate and nimodipine are 7.0 and 5.0 Å, respectively, which are comparable to that their radii of gyration, 6.0 and 4.5 Å, respectively, indicating that equilibration was achieved. Finally, to get potential energy in vacuum state (E_{vac}), a single chain of copolymer or a single drug molecule without being subjected to periodic boundary conditions was simulated for 2000 ps at 413 K.

4.2.4 Calculation of Flory-Huggins Interaction Parameters using MD Simulation

Hildebrand solubility parameter (δ) is the square root of cohesive energy density (CED).

$$\delta = \sqrt{CED} = \sqrt{\frac{(E_{vac} - E_{bulk})}{V}} \quad (4.3)$$

where E_{vac} is potential energy in the vacuum state, E_{bulk} is potential energy in the amorphous state, and V is molar volume given by the ratio of density to molecular weight. E_{vac} and E_{bulk} were calculated from MD simulation and were used to calculate the corresponding δ . The Flory-Huggins interaction parameter χ was then calculated using following equation (derived in Section 2.6.2.1):

$$\chi = \frac{V_r(\delta_1 - \delta_2)^2}{RT} \quad (4.4)$$

where R is universal gas constant and V_r is reference volume. The choice of reference volume is somewhat arbitrary but it is a usual practice to choose the smallest one among the molar volumes of drugs and of repeating units of the blocks of the block copolymer. The molar volumes of the drug molecules can be computed directly from the knowledge of their densities and molecular weights. The molar volumes of fenofibrate and nimodipine at 413 K were found to be 322.17 cm³/mol and 391.06 cm³/mol, respectively. But, since the densities of repeating units of the blocks of the copolymer are not known, we predict their molar volumes using a group contribution method called GCVOL [18-20] as described in the Appendix B. The predicted values of the molar volumes of repeating units of PEO and PCL blocks at 413 K were 91.41 cm³/mol and 108.46 cm³/mol, respectively. Since, the molar volume of the repeating unit of PEO

block was the smallest, it was chosen as the V_r . Although this is the simplest method to calculate χ , it suffers from several disadvantages. In particular, it yields only positive χ values and secondly, it is unable to describe the concentration dependence of χ (i.e., local molecular packing effect in a mixture environment) as χ is calculated using the properties of pure components.

Considering the drawbacks of the first approach, another approach was used in which the internal energy changes on mixing for drug/block copolymer pairs were calculated. The internal energy change on mixing can be readily calculated from MD simulation by comparing the internal energies of mixture and pure state block copolymer and pure state drugs as shown below:

$$\Delta E_m = E_{mixture} - n_1 E_1 - n_2 E_2 \quad (4.5)$$

where $E_{mixture}$ is the enthalpy of block copolymer and drug mixtures; E_1 and E_2 are enthalpies of pure state block copolymer and drugs, respectively; n_1 and n_2 are moles of pure block copolymer and drug, respectively. While performing NPT MD simulations on such mixtures, we noted negligible volume changes on mixing and hence we ignored the $\Delta(PV)$ effect. The $P\Delta V$ for most of the systems was found to be on the order of 10^{-3} (kcal/mol). As a result, ΔH_m is approximately equal to ΔE_m . Subsequently, the Flory-Huggins interaction parameter can be calculated using following equation (Section 2.6.2):

$$\Delta H_m = \chi RT \phi_1 \phi_2 \quad (4.6)$$

where ϕ_1 and ϕ_2 are the volume fractions of the block copolymer and drug. It is evident from the equation (4.6) that the second approach allows us to study the concentration dependence of χ . The simulation methodology for pure and binary mixed systems is outlined in Figure 4.5.

As mentioned earlier, since the equilibration of block copolymers both in the pure and mixture states could not be achieved over the simulation times we could practically use, we used the RIS theory to generate their initial conformations that should not be far from equilibrated structures. Conformations generated in this way follow the spirit of the Flory-Huggins theory. Obviously, it would be better if we could carry out more MD simulations using more initial conformations generated by the RIS theory for each mixture. Nevertheless, the computational cost is prohibitively high.

4.3 Results and Discussion

Table 4.5 shows computed density values of PEO-*b*-PCL, drugs and their mixtures in their liquid state obtained from the NPT MD simulations at 1 atm and 413 K. The experimental density values were not available. Nevertheless, Rigby has demonstrated that the COMPASS force field is able to reproduce liquid density for a variety of substances with complex molecular structures. [63]. We feel that computed density values for drugs and drug/block copolymer mixtures should be reliable. The density was then used in the subsequent NVT MD simulations to determine δ and χ .

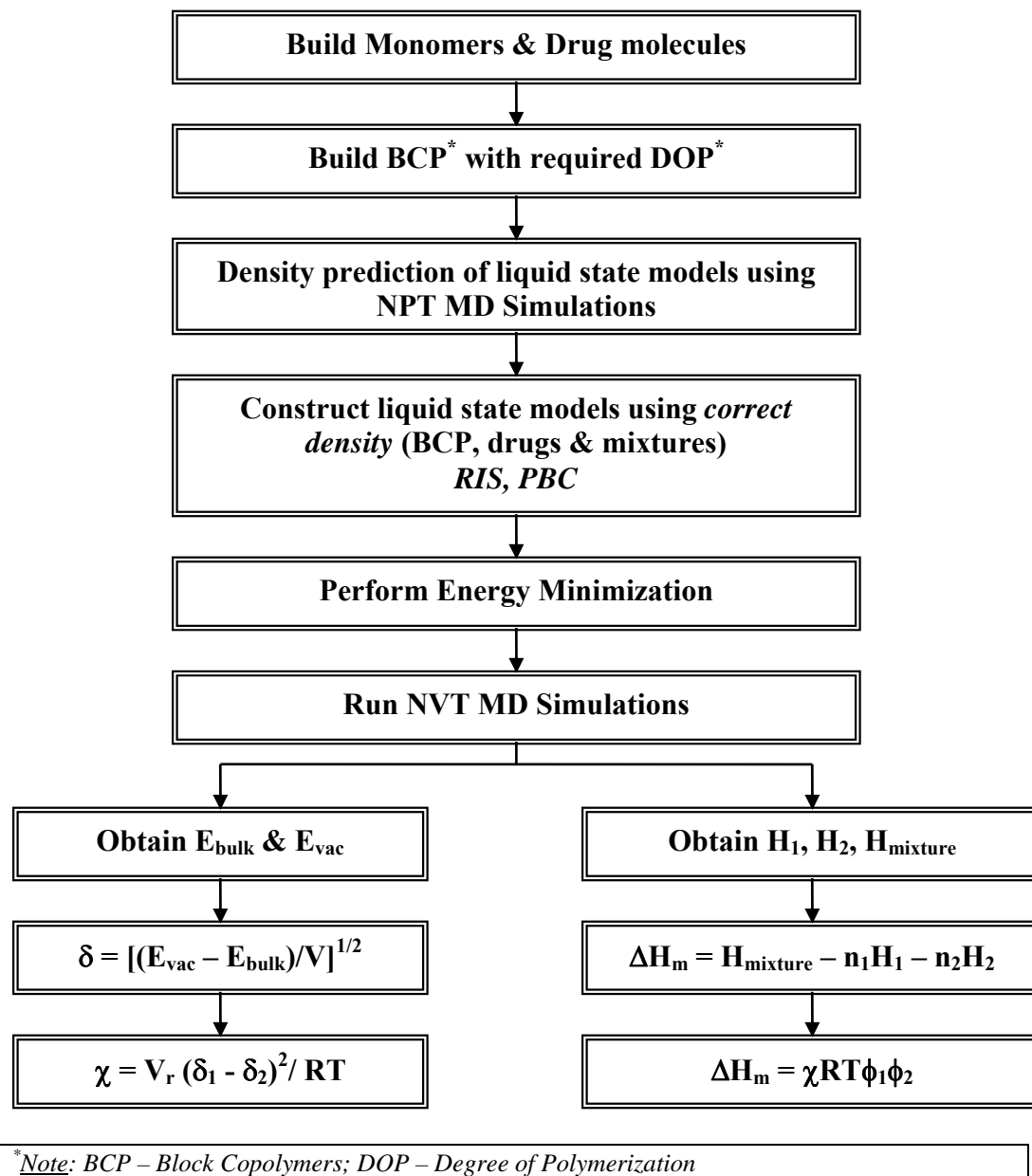


Figure 4.5 Flowchart of approaches taken for MD simulation of the pure and binary mixed systems of drugs and block copolymers.

The NVT MD trajectory files were created for each structure in the amorphous and vacuum states. The mean potential energies of the bulk and vacuum states were then calculated by using time average of the potential energy over the last 100 ps of the trajectory.

Table 4.6 summaries the computed solubility parameters of both drugs and of three model PEO-*b*-PCL block copolymers. And such values were used to calculate the corresponding χ parameters for various drug/block copolymer pairs using equation (4.4) and results are listed in the Table 4.7. The higher χ values for nimodipine/PEO-*b*-PCL pair than those of fenofibrate/PEO-*b*-PCL pair (especially those two PEO-*b*-PCL models with long PCL blocks) by MD simulation reflect that nimodipine exhibits lower solubility than fenofibrate in three PEO-*b*-PCL block copolymers, which are consistent with the experimental solubility results of the above systems.

For both drugs, an increase in the molecular weight of the PCL block was also shown to decrease the χ values, an indication for higher drug solubility in PEO-*b*-PCL micelles with longer PCL blocks, which has also been observed experimentally by Jette *et al.*[79] and Ge *et al.*[80]. The MD results suggest that it is desired to include the PEO block in the calculation of δ , thereby χ to yield the correct compatibility predictions. Paradoxically, Table 4.7 also shows that an increase in the molecular weight of the PEO block (same PCL molecular weight) has almost no effect on the χ values.

Table 4.5 Computed densities of drugs, block copolymers and their mixtures at 1 atm and 413 K along with the number of drug molecules involved.

Block copolymer/Drug/mixture	Density (g/cm³)	No. of drug molecules
Fenofibrate (F)	1.12	-
Nimodipine (N)	1.07	-
PEO(1250)- <i>b</i> -PCL(2500) (P ₁)	1.15	-
Mixture of P ₁ & F (70 wt% drug)	1.14	24
Mixture of P ₁ & F (40 wt% drug)	1.15	7
Mixture of P ₁ & F (10 wt% drug)	1.15	1
Mixture of P ₁ & N (70 wt% drug)	1.13	21
Mixture of P ₁ & N (40 wt% drug)	1.13	6
Mixture of P ₁ & N (10 wt% drug)	1.14	1
PEO(2500)- <i>b</i> -PCL(2500) (P ₂)	1.15	-
Mixture of P ₂ & F (70 wt% drug)	1.14	32
Mixture of P ₂ & F (40 wt% drug)	1.14	9
Mixture of P ₂ & F (10 wt% drug)	1.15	2
Mixture of P ₂ & N (70 wt% drug)	1.12	28
Mixture of P ₂ & N (40 wt% drug)	1.14	8
Mixture of P ₂ & N (10 wt% drug)	1.14	1
PEO(2500)- <i>b</i> -PCL(1250) (P ₃)	1.20	-
Mixture of P ₃ & F (70 wt% drug)	1.18	24
Mixture of P ₃ & F (40 wt% drug)	1.20	7
Mixture of P ₃ & F (10 wt% drug)	1.20	1
Mixture of P ₃ & N (70 wt% drug)	1.15	21
Mixture of P ₃ & N (40 wt% drug)	1.17	6
Mixture of P ₃ & N (10 wt% drug)	1.18	1

Table 4.6 Solubility parameters of fenofibrate, nimodipine and different PEO-*b*-PCL calculated by MD simulation.

Drug/Block copolymer	Solubility Parameters (δ) (J/cm^3)^{1/2}
Fenofibrate	16.06 \pm 0.51
Nimodipine	14.49 \pm 0.40
PEO(1250)- <i>b</i> -PCL(2500)	17.49 \pm 0.18
PEO(2500)- <i>b</i> -PCL(2500)	17.57 \pm 0.10
PEO(2500)- <i>b</i> -PCL(1250)	19.55 \pm 0.18

Table 4.7 χ parameters computed using the δ values listed in Table 4.6 for various drug/block copolymer pairs.

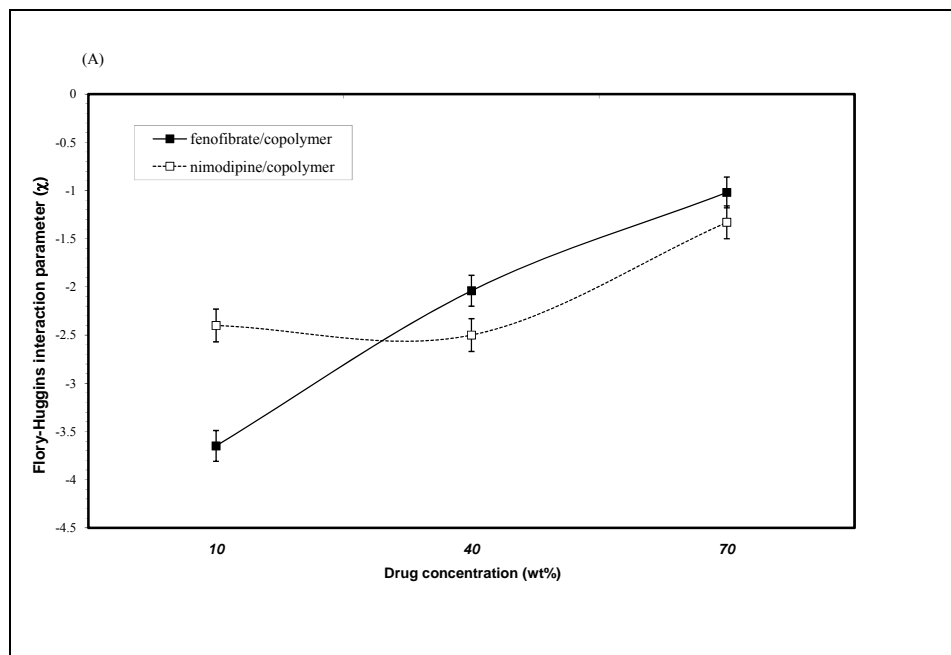
Drug	Flory-Huggins interaction parameter (χ) for various drug/block copolymer pairs		
	PEO(1250)-<i>b</i>-PCL(2500)	PEO(2500)-<i>b</i>-PCL(2500)	PEO(2500)-<i>b</i>-PCL(1250)
Fenofibrate	0.05 \pm 0.02	0.06 \pm 0.03	0.33 \pm 0.09
Nimodipine	0.23 \pm 0.05	0.26 \pm 0.05	0.68 \pm 0.11

This observation is also consistent with the conventional drug/block copolymer solubility studies in which only the interaction between the drug and the hydrophobic block of a block copolymer is considered. [6, 78].

The above MD approach (i.e., the calculation of χ using the δ of pure components) yield better compatibility predictions as compared to the GCM, possibly due to rectification of many of the drawbacks of the GCM discussed earlier (in Section 1.4) by the MD simulation approach. One key difference between these two approaches is that the GCM basically uses only the interaction energy potential $u(r)$ to obtain the δ while MD simulation includes not only the interaction energy potential, $u(r)$, but also the local arrangement of the molecules (i.e., $g(r)$) to compute the δ (Equation (4.1)). Nevertheless, χ computed using the above MD approach still suffers from the drawback that it cannot capture the $g(r)$ of the molecules, both drug and block copolymer molecules, in a mixture environment (i.e., the concentration dependence of χ cannot be assessed). We therefore used the second approach (i.e., Equations (4.5) and (4.6)) to investigate the concentration dependence of χ . The enthalpy changes on mixing between block copolymer and drug molecules were computed using NVT MD simulation to obtain ΔE_m ($\cong \Delta H_m$) and were used to calculate the χ values for various drug/block copolymer pairs at the concentrations of 10, 40 and 70 wt% of drugs. The average total energy is more commonly expressed per mole of copolymer or mixture. To calculate the χ , all the calculated enthalpy changes on mixing were converted to per mole of the lattice sites as described in the Appendix C. In calculations of the free energy of the pure drugs, we have accounted for the drug-

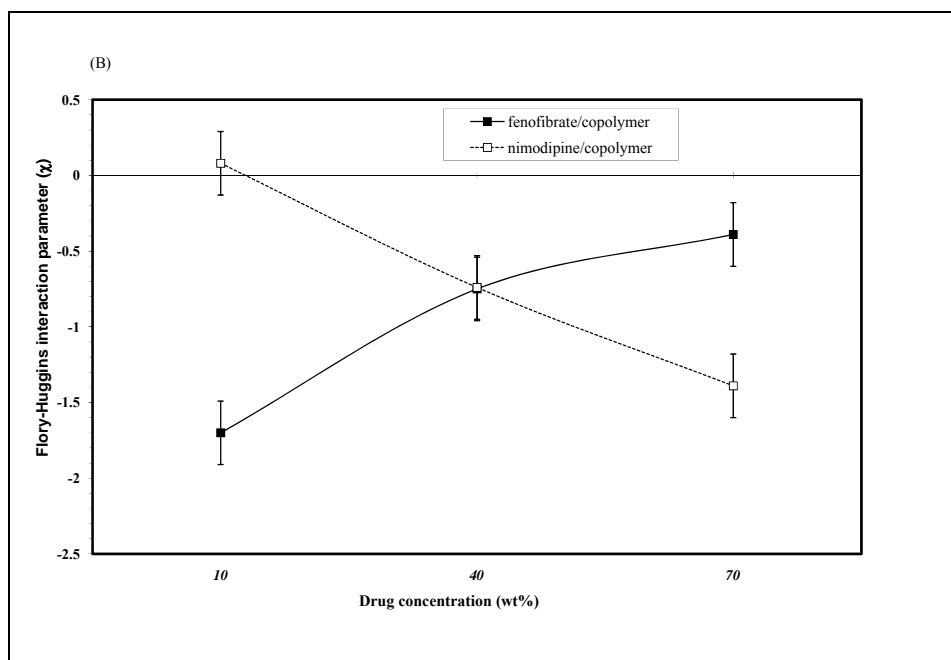
drug interactions by using 25 molecules to represent their pure liquid state. The relationship between the χ values and polymer concentrations in drug/block copolymer pairs are plotted in Figures 4.6(A), 4.6(B), and 4.6(C). The error bars shown in the figures are ensemble fluctuations determined based on the data of MD trajectories.

The above described procedure is justified by the finding of Gadelle *et al.* In particular, they have shown, using the example of the solubilization of aromatic solutes (benzene and chlorobenzene) in PEO-*b*-PPO-*b*-PEO micelles, that the interaction parameter between the solute and the hydrophobic cores (PPO core in their case) is insufficient to characterize the solubilization in micelles formed by block copolymers [84]. According to their observation, such interaction parameters can be quite misleading and there are equal chances of existence of interactions between aromatic solutes and corona of a micelle. Therefore, it is always beneficial to consider the interaction parameter between entire block copolymer and the drugs of interest. It is worth noting that χ calculated from the above MD approaches is between drugs and entire copolymer, not between drugs and the PCL block only. As a result, the effect of the PEO block on χ can be evaluated. According to the Flory-Huggins theory, the critical χ value above which a polymer and a low molecular weight compound (e.g., drug) become immiscible is 0.5 (Refer Section 2.6.2.1). In other words, if χ for drug/block copolymer pair is lower than 0.5 or negative, they are soluble into each other.



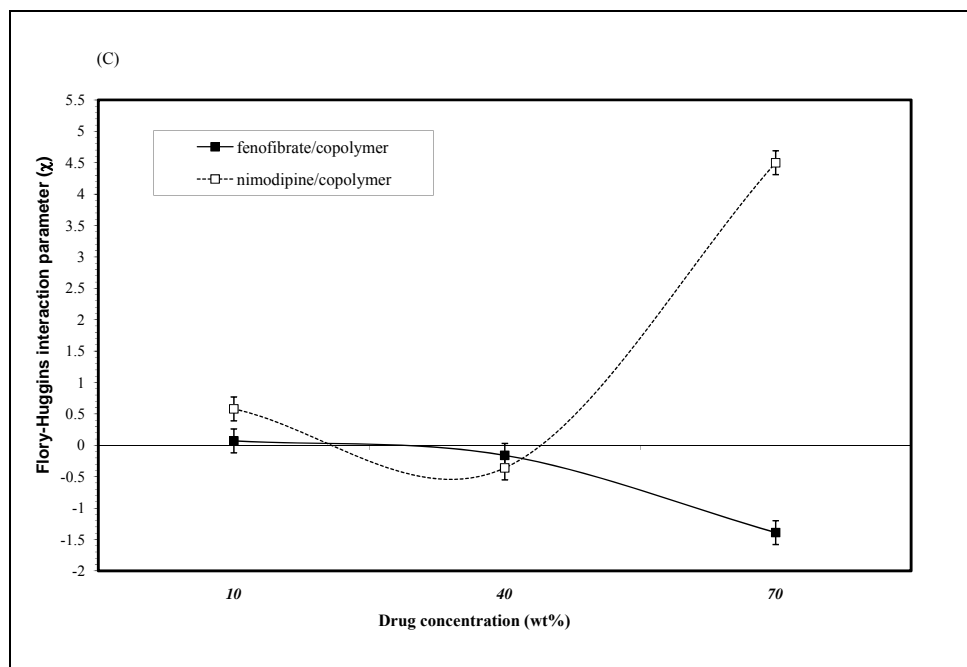
**[Lines are drawn to guide the eye]*

Figure 4.6(A) Concentration dependence of the χ parameters for drugs/PEO(1250)-*b*-PCL(2500) pairs.



**[Lines are drawn to guide the eye]*

Figure 4.6(B) Concentration dependence of the χ parameters for drugs/PEO(2500)-*b*-PCL(2500) pairs.



**[Lines are drawn to guide the eye]*

Figure 4.6(C) Concentration dependence of the χ parameters for drugs/PEO(2500)-*b*-PCL(1250) pairs.

However, as the theory was developed mainly for solvent and polymer that interact mainly through non-polar dispersion forces, use of 0.5 for our systems, which involves both Coulombic and hydrogen bonding interactions, is not suitable. Therefore, we judge whether compatibility prediction is successful or not by comparing the trend of the computed interaction parameters, either from MD or GCM, with the observed experimental solubility trend.

It can be seen from Figures 4.6(A), (B), and (C) that the computed χ increases (miscibility decreases) as the hydrophilicity of the block copolymer increases. These results on decreasing compatibility with increasing PEO chain length are consistent with the observation of Aliabadi *et al.* [85] that an increase in the percentage of PEO in PEO-*b*-PCL micelles results in a decrease in the loading capacity of the micelles and encapsulation efficiency of model drug cyclosporine A (CyA). Nevertheless, at low drug loading (i.e., 10 wt% drug), we can observe that χ for nimodipine-copolymer pair is always greater than χ for fenofibrate-copolymer pair regardless of the molecular weight of the block copolymer, which is in agreement with the experimental solubility data shown in Table 4.1 and with the results obtained from the first approach (Table 4.7). However, the numerical values are quite different from those obtained from the first approach. This is reasonable as the first approach does not include the effect of geometry fittings of the drug molecules and the block copolymers. The interesting observation is that the trend of the 10 wt% drug was not followed when the concentration of the drug was 40 wt% or higher except the case with 70 wt% drug in PEO(2500)-*b*-PCL(1250). It should be noted that the drug loading used in practice is around 10

– 15 wt% of drug. [79, 80]. At higher drug loadings, drugs tend to precipitate as reported by Kahori *et al.*[86] and Leroux *et al.*[87]. Therefore, one can consider that the data of 10 wt% drug is most relevant to the practical situations. However, it is worth pointing out that the χ values reported in the present work were computed based on a randomly mixed mixture of the block copolymer and drug while drug loadings reported in the literature correspond to the situation in which drug molecules are more or less surrounded by the copolymer in the form of micelle. In other words, spatial arrangement of the copolymer molecules in the experimental system is not the same as that in our simulation system even though both systems share the same concentration.

Nevertheless, to understand the miscibility behaviour at low block copolymer concentrations (i.e., high drug loadings), we examined the radial distribution functions (i.e., RDF or $g(r)$), which signify the local molecular packing of molecules of the mixtures. Since we observe completely reverse trends for 70 wt% drug in the cases of PEO(1250)-*b*-PCL(2500) and PEO(2500)-*b*-PCL(1250), we calculated the RDFs of those two cases for the pairs of atoms consisting of oxygen atoms of drug molecules and hydrogen atoms of PEO and PCL blocks. In total, eight RDF plots (Figure 4.7) were generated for the two drugs with two copolymers having different molecular weights (PEO(1250)-*b*-PCL(2500) and PEO(2500)-*b*-PCL(1250)). Here, the continuous dark line in the plots corresponds to the intermolecular association between the oxygen atoms of the drug molecules and hydrogen atoms of either PEO or PCL blocks of PEO-*b*-PCL,

while the broken line in the plots signifies the intra-molecular association among the oxygen and hydrogen atoms of drug molecules themselves.

In general, comparing the RDF plots, we found that inter-RDF values of nimodipine molecules is much higher in the vicinity of PCL block only, while those of the fenofibrate molecules are comparable for both PEO and PCL blocks. These results lead us to conclude that fenofibrate molecules exhibit comparable tendency to associate themselves with both the PEO and PCL blocks, while nimodipine molecules show strong association with the PCL block but not the PEO block. This leads to the situation that fenofibrate would exhibit higher compatibility (i.e., lower χ) than nimodipine with PEO(2500)-*b*-PCL(1250) as the PEO block in such a block copolymer is longer than the PCL block. On the other hand, when the PEO block is shorter than the PCL block, the opposite compatibility trend would be observed (see Figures 4.6(A) and 4.6(C)). These results show that when the concentration of PEO-*b*-PCL is low (i.e., system contains more drug molecules), local molecular packing between the drug molecules and segments of both the PEO and PCL blocks should be considered in the determination of their compatibility. In other words, the inclusion of the PEO block in the calculation of χ is needed at high drug loadings when PEO-*b*-PCL concentration is low.

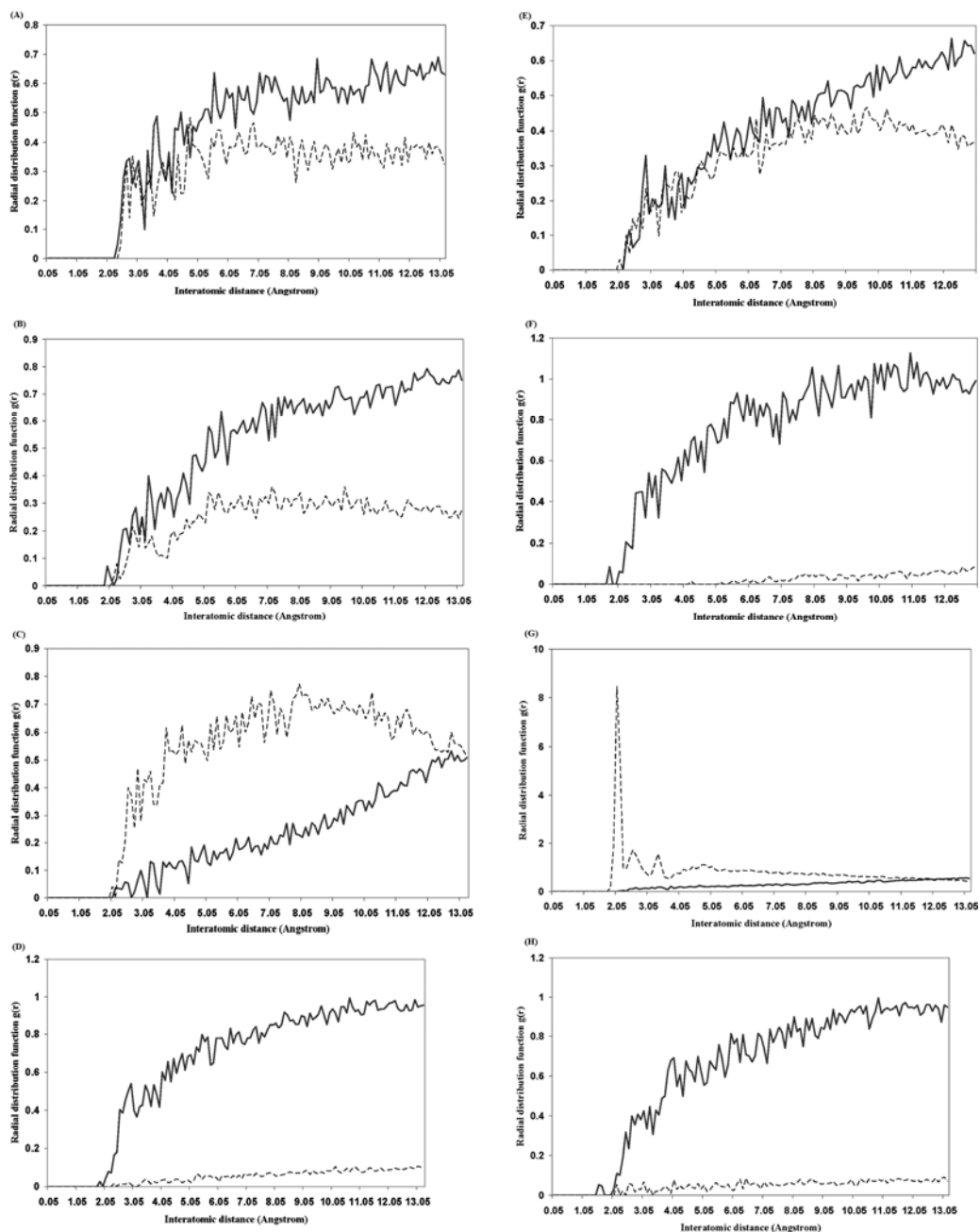


Figure 4.7 RDF plots for 70 wt% drug in (I) PEO(1250)-*b*-PCL(2500) for (A) O atoms of fenofibrate and H atoms of PEO block; (B) O atoms of fenofibrate and H atoms of PCL block; (C) O atoms of nimodipine and H atoms of PEO block; (D) O atoms of nimodipine and H atoms of PCL block and in (II) PEO(2500)-*b*-PCL(1250) for (E) O atoms of fenofibrate and H atoms of PEO block; (F) O atoms of fenofibrate and H atoms of PCL block; (G) O atoms of nimodipine and H atoms of PEO block; (H) O atoms of nimodipine and H atoms of PCL block. *Key*: solid line, intermolecular association; dashed line, intra-molecular association

4.4 Summary

Flory-Huggins interaction parameters between two water-insoluble drugs, fenofibrate and nimodipine, and three PEO-*b*-PCL block copolymers with varying PEO and PCL block lengths were calculated using two MD simulation approaches. In one approach, we calculated χ values by using δ values derived from MD simulations of drugs and PEO-*b*-PCL in their pure component forms. The results are consistent with the observed solubility of fenofibrate and nimodipine in liquid caprolactone, which indicates that the inclusion of the PEO block in the calculation of δ , and thereby that of χ , yields a better compatibility prediction than the GCM. Paradoxically, the results of this approach also indicate that the computed χ is insensitive to the PEO chain length but depends strongly on the PCL chain length, which supports the conventional compatibility studies that are focused on the interaction between the hydrophobic block of a block copolymer and the drug of interest.

To further investigate the role of PEO block, we used a second approach in which heats of mixing were computed from MD data of binary mixtures of drugs and block copolymers at three different concentrations. We found that at a concentration of 10 wt% drug, the computed χ values between fenofibrate and nimodipine and the block copolymers are consistent with their experimental solubility results. Nevertheless, the numerical χ values are different from those obtained from the first approach. This is attributed to the fact that the local packing of drug molecules and segments of the block copolymers in a mixture environment is taken into account in the latter approach. At low block copolymer

concentrations, the nimodipine exhibits lower χ values (i.e., higher solubility in caprolactone) than does the fenofibrate with the block copolymers when the molecular weight of PCL block is 2500. This is due to the fact that fenofibrate more-or-less exhibits the same tendencies to cluster around PEO and PCL blocks, whereas nimodipine mostly clusters around the PCL block, as illustrated by the computed intermolecular radial distribution functions. The observation of the effect of local packing on compatibility may explain why the inclusion of the PEO block in the calculation of δ is needed in the first approach. Our results confirm that both the interaction energy potential and the local molecular arrangement play vital roles in the correct prediction of solubility parameters and Flory-Huggins interaction parameters.

Chapter 5

Improvement of the Drug Loading Capacity of PEO-*b*-PCL with Increasing PCL Content for Two Hydrophobic Cucurbitacin Drugs: Roles of Non-Polar and Polar Intermolecular Interactions²

5.1 Introduction

In the previous chapter, we demonstrated the superiority of MD simulation over the existing group contribution method in the prediction of the solubility of two hydrophobic drugs, fenofibrate and nimodipine, in PEO-*b*-PCL di-block copolymer based nano-carriers. It was found that in addition to the interaction energy potential (i.e., $u(r)$), the local molecular arrangement characterized by the radial distribution function (i.e., $g(r)$) plays an important role in determining the drug solubility. In the present chapter, our aim is to determine whether MD simulation can provide insights into the involvement and relative contribution of

² A version of this chapter has been published. Patel, S.K.; Lavasanifar, A.; Choi, P. (2009). *Biomacromolecules*. 10, 2584-91.

different possible inter/intra molecular interactions of drug/di-block copolymer pairs (e.g., dispersive interactions, electrostatic interactions and hydrogen bonding interactions) in the drug solubilisation of di-block copolymer carriers. For this purpose, two hydrophobic drugs bearing several hydrogen bonding moieties in their structure, Cucurbitacin-B (CuB) and Cucurbitacin-I (CuI) (see Figure 5.1) were chosen and the role of non-polar and polar intermolecular interactions on their solubilisation in PEO-*b*-PCL based carriers with increasing PCL content was evaluated by MD simulation.

Cucurbitacins are complex compounds found primarily in plants belonging to the cucumber family (Cucurbitaceae). This family of plants tend to contain a group of substances classified as triterpenoid that are well-known for their bitterness and toxicity. Cucurbitacins are structurally characterized by tetracyclic cucurbitane nucleus skeleton, with a variety of oxygenation functionalities at different positions [88]. Cucurbitacins have shown cytotoxic, anti-inflammatory and hepatoprotective effects [89-91]. Among the twelve different categories of Cucurbitacins, CuB and CuI are noted for their cytotoxic and anticancer activity and have been shown to be effective inhibitors of signal transducer and activator of transcription 3 (STAT3) pathways. [92-94]. Despite the potency of CuB and CuI as effective anticancer agents, their clinical application has been hindered mainly due to their non-specific cytotoxicity and low water solubility.

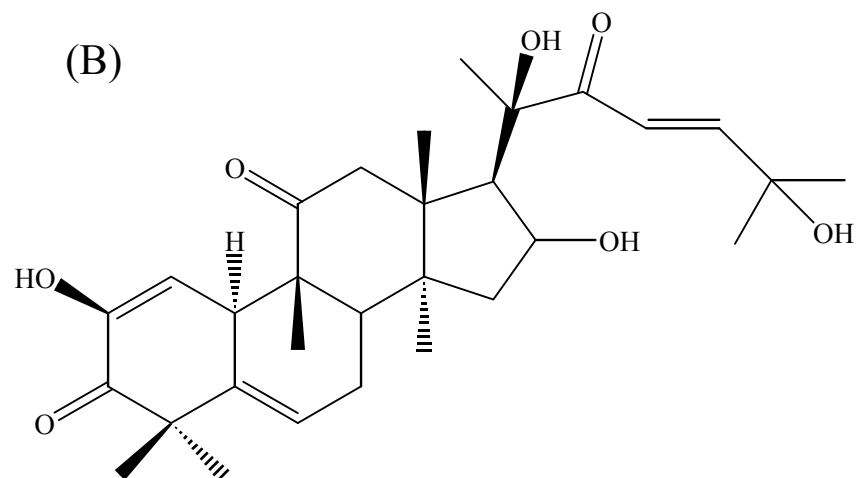
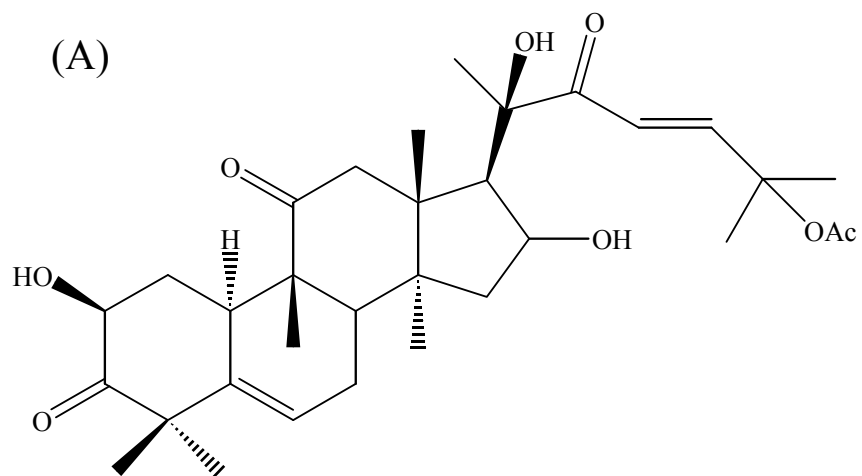


Figure 5.1 Chemical structures of (A) Cucurbitacin B; and (B) Cucurbitacin I

To overcome such limitations, development of nanometre scale polymeric formulations that increase the solubilisation levels of CuB and CuI and also limit their premature release in systemic circulation and restrict the distribution of these toxic drugs to tumour tissue has been pursued by our research group. [95, 96].

Consistent with our experimental observations, MD simulation predicted an increase in the level of encapsulated drug for both CuB and CuI as a result of an increase in PCL/PEO (w/w) ratio on the basis of molecular weights of the corresponding blocks. The predictions, from MD simulation, were based on the calculations of χ parameters using random binary mixture models containing 10 – 12 wt% drug and remaining PEO-*b*-PCL. As demonstrated in the present work, the increased drug solubilisation, however, was attributed to the enhanced polar interactions and to the hydrogen bonds formed between single hydrogen bond sites on the drugs and multiple hydrogen bond sites on the PCL block at high PCL/PEO ratio rather than to the increase in the hydrophobic characteristics of the di-block copolymer. The implications of the presence of additional hydrogen bonds on comparative release rates of these drugs were also studied. The information on the nature of intermolecular interactions contributing to drug solubilisation in di-block copolymer based carriers provided by the MD simulation, is expected to allow for the better prediction of drug solubility levels as well as the rate of drug release from di-block copolymers of different hydrophobic/hydrophilic block ratios.

5.2 Simulation Details

The simulation procedures are very similar to those described in the Chapter 4. In particular, the method of Theodorou and Suter [73] was employed to build the amorphous unit cells of pure di-block copolymers, drugs and their mixtures subjected to the density constraint. Such amorphous structures were constructed using the amorphous builder module available in Cerius². Three PEO-*b*-PCL block copolymers with different hydrophilic (PEO) and hydrophobic (PCL) block lengths were used. They were PEO(1250)-*b*-PCL(2500), PEO(2500)-*b*-PCL(2500) and PEO(2500)-*b*-PCL(1250), where the number in the bracket signifies the molecular weight of the particular block and the corresponding PCL/PEO (w/w) ratios are 2, 1 and 0.5, respectively.

Since experimental density values of the drugs and their binary mixtures with aforementioned di-block copolymers at 200 °C (i.e., 473 K) were not available, we carried out NPT MD simulation (P = 1 atm; T = 473 K) using density values from the GCM as the initial values to determine the density values of pure substances. Here, the temperature was chosen to ensure that both the drug molecules and the di-block copolymers are in the liquid state. Nose thermostat [69] and Andersen barostat [72] methods were employed to control the temperature and pressure of the systems, respectively. It is worth noting that we only used NPT MD simulation to determine the density of pure substances. The resultant values were then used to calculate the density values of mixtures by assuming that the volume change on mixing is negligible. The mixture density values were used in the subsequent canonical MD simulations to determine the χ

values. NVT MD simulation requires much less computational time than NPT MD for the same system (saving of 1 day of CPU time) as only one intensive variable (i.e., T) is required to be controlled.

The distribution of torsion angles of skeletal bonds in di-block copolymers were determined using the RIS theory.[81, 82]. The Boltzmann weighting factor was applied to the energies of the RIS minima to determine this distribution. The detailed method for describing the initial distribution of torsion angles for PEO-*b*-PCL di-block copolymer is given in the Section 4.2.2. The initial conformations of the di-block copolymers used in the NPT MD simulations were also subjected to the RIS constraints.

All the initial structures were energy-minimized using the conjugate gradient method in order to remove strong van der Waals overlaps. The COMPASS force field [62] was used to describe inter-atomic potentials. The partial atomic charges were assigned by the COMPASS force field using the method described in Section 3.3. NVT MD simulations were carried out at 473 K using the Nose thermostat.[69] The velocity Verlet method, with a time step of 1 fs, was used as an integrator in all simulations. The non-bonded dispersive interactions were evaluated using atom based cut-off distance of 9.50 Å with a spline width of 1 Å, while the long-range electrostatic interactions especially important in polymeric and 3D periodic systems were evaluated using the well-known Ewald summation method [67]. Long-range tail corrections were applied to the non-bonded interactions during MD simulations. Simulations were carried out until the total energy of the system was stabilized. Each simulation was carried out for a total of

2000 ps. The properties of interest (e.g., the total energy, radial distribution function, etc.) were calculated by averaging over the last five hundred ps of the corresponding trajectory file. As discussed in the previous chapter, owing to the several drawbacks associated with the use of the Hildebrand solubility parameters of pure substances to calculate the χ values for drug/di-block copolymer pairs, we adopted the MD simulation approach in which the internal energy changes on mixing were calculated and then used to obtain the χ values for drug/di-block copolymer pairs. [21]

5.3 Results and Discussion

5.3.1 MD Simulation

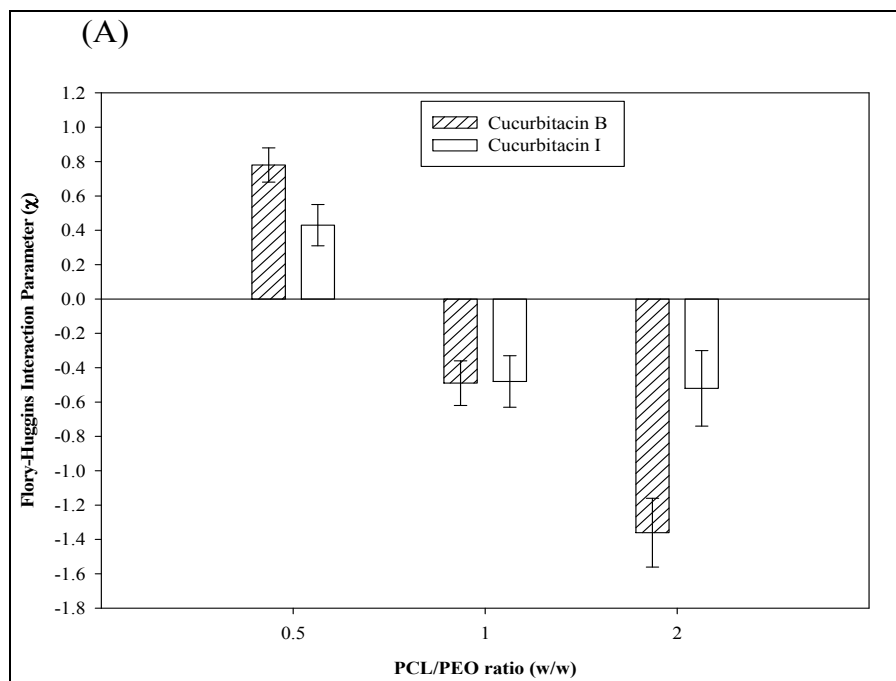
Table 5.1 summarizes the computed density values for di-block copolymers, drugs and their mixtures (10 – 12 wt% drug) at a pressure of 1 atm and a temperature of 473 K. It should be noted that the density values of mixtures were calculated using those of the pure components obtained from MD simulation, not directly from the MD simulation of the mixture. Nevertheless, we have carried out additional NPT MD simulations on two drug/PEO(2500)-*b*-PCL(2500) mixtures to determine their density values and found that such results and those calculated based upon the density values of pure components are in good agreement, indicating that the assumption of negligible volume change on mixing is valid. Therefore, we feel justified to use the canonical MD to calculate the internal energy change on mixing (i.e., ΔE_m ($\approx \Delta H_m$)), thereby the χ parameters (Equations (4.5) and (4.6)).

Table 5.1 Computed density values of CuB, CuI, PEO-*b*-PCL and their mixtures (10 – 12 wt% drug) at 1 atm and 473 K along with the number of drug molecules involved.

Drug/Block Copolymer/Mixture	Density (g/cm³)	No. of Drug Molecules	No. of Block Copolymer Chains	Drug Concentration (wt%)
Cucurbitacin B (CuB)	1.15	-	-	-
Cucurbitacin I (CuI)	1.12	-	-	-
PEO(1250)- <i>b</i> -PCL(2500) (P ₁)	1.14	-	1	-
CuB & P ₁	1.14	1	1	12
CuI & P ₁	1.14	1	1	12
PEO(2500)- <i>b</i> -PCL(2500) (P ₂)	1.13	-	1	-
CuB & P ₂	1.13	1	1	10
CuI & P ₂	1.13	1	1	10
PEO(2500)- <i>b</i> -PCL(1250) (P ₃)	1.18	-	1	-
CuB & P ₃	1.17	1	1	12
CuI & P ₃	1.17	1	1	12

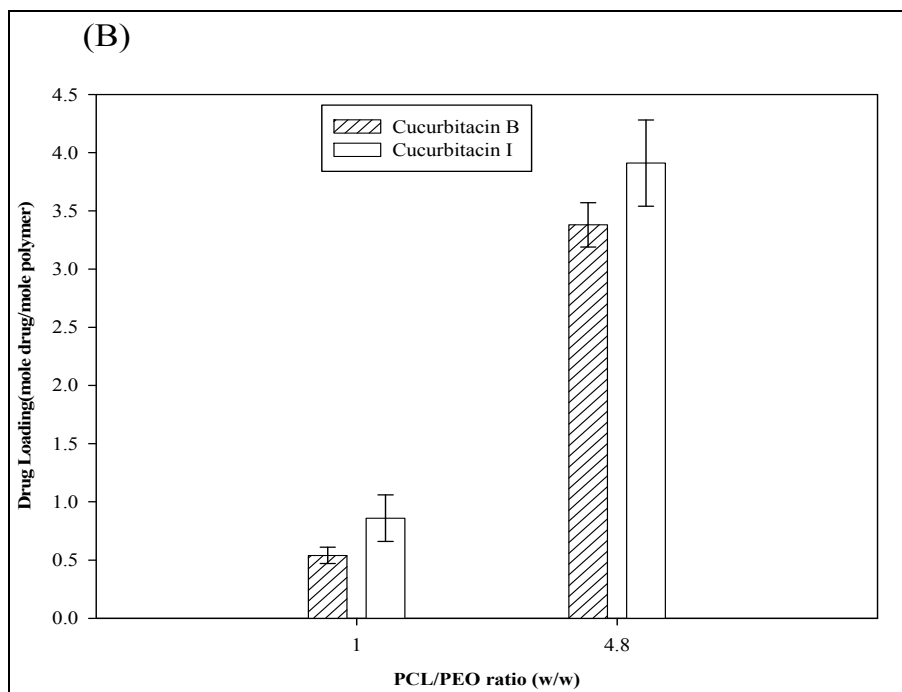
In regard with the reliability of the computed density of pure substances, we have demonstrated in our previous work (Chapter 4) that the COMPASS force field was able to reproduce the density values for PEO-*b*-PCL and two other water insoluble drugs. [21]. The mean potential energies of the bulk states of pure di-block copolymers, drugs and mixtures of them were calculated by using time average of the potential energy over the last five hundred ps of the corresponding trajectory of 2000 ps at equal interval of 2 ps. Note that the velocity autocorrelation functions of the drug molecules de-correlated in less than 2 ps. The analysis of mean values and standard errors were performed using the Sigma Plot version 11.0 (Systat Software, Inc.).

The computed χ values are plotted in the Figure 5.2(A). We note that the error bars shown in the figure are ensemble fluctuations and were determined using the data of last 500 ps of the corresponding MD trajectories. According to the Flory-Huggins solution theory, lower χ values indicate higher affinity between the components and hence better solubility of one component into the other. We can see that for PCL/PEO ratio of 1, the χ values of CuB and CuI/di-block copolymer pairs are very close, indicating that both drugs have similar affinity for PEO-*b*-PCL. Comparing this observation with the experimental drug loading data (mole drug/mole di-block copolymer) (Figure 5.2(B)) of CuB and CuI in PEO(5000)-*b*-PCL(5000), i.e., PCL/PEO ratio of 1, our MD results are consistent with the experiment.



*Data are means. Bars are standard errors

Figure 5.2(A) Plot of the computed χ values of binary mixtures of two cucurbitacins and three model PEO-*b*-PCL with different PCL/PEO ratio (w/w).



*Data are means. Bars are standard deviations

Figure 5.2(B) Plot of experimentally measured drug loading capacity of PEO-*b*-PCL micelles with two different PCL/PEO ratio (w/w) for cucurbitacins as reported by Molavi *et al.*

Another important observation from Figure 5.2(A) is that when the PCL/PEO ratio increases from 0.5 to 2 (4 times increase), χ decreases for both drugs, from positive to negative values which indicate that increasing the PCL/PEO ratio increases the solubility of both drugs. Similar to the experimental observation, increasing the PCL/PEO ratio from 1 to 4.8 leads to a significant change in the solubility of both drugs (Figure 5.2(B)). In short, the trend of the computed χ values reflects very well the experimental trend in the solubility of these drugs. The question is what is the molecular origin for such an observation.

5.3.2 Non-bond Energy Analysis

To answer the above question, we first examined the non-bonded energy of model mixture systems with PCL/PEO ratios of 0.5 and 2.0 [i.e., PEO(2500)-*b*-PCL(1250) and PEO(1250)-*b*-PCL(2500)]. The total non-bonded energy data of the two mixtures along with its dispersive energy and electrostatic energy contributions, which were calculated by using the time average of the non-bonded energy over the last 500 ps of the corresponding trajectory of 2000 ps, are shown in the Table 5.2. It is obvious that as the PCL/PEO ratio is increased from 0.5 to 2.0, the total non-bonded energy decreases considerably indicating that the latter system is more stable than the former one. However, such decrease in the non-bonded energy is not due to the decrease in the dispersive energy (i.e., increase in hydrophobicity of PEO-*b*-PCL) with increasing PCL content. In fact, the dispersive energy increases slightly. And it is due to the substantial decrease in electrostatic energy contribution that led to negative χ .

Table 5.2 Contributions of dispersive and electrostatic energy to non-bonded energy of mixtures of both drugs with PEO(2500)-*b*-PCL(1250) and PEO(1250)-*b*-PCL(2500).

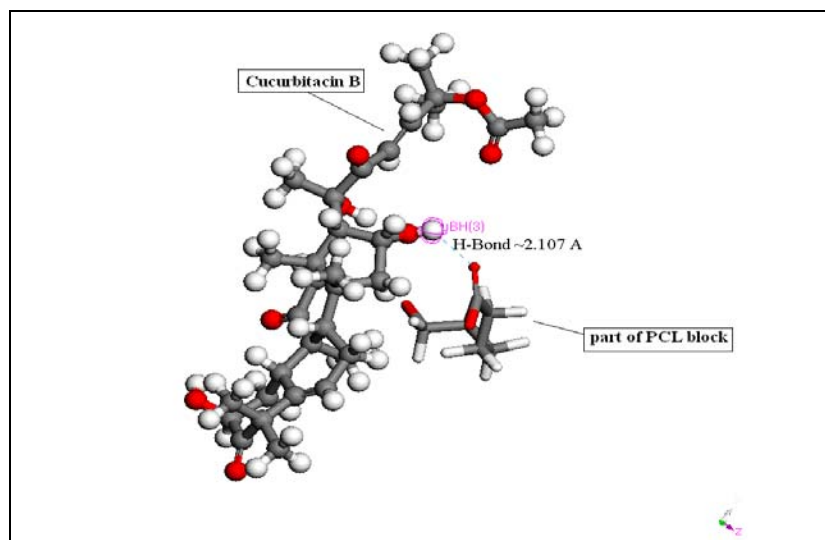
Block Copolymer	Drug	Total non-bonded energy* (Kcal/mol)	Dispersive Energy* (Kcal/mol)	Electrostatic Energy* (Kcal/mol)
PEO(2500)-<i>b</i>-PCL(1250)	CuB	-4.45 ± 5.81	-197.15 ± 10.49	192.99 ± 2.23
	CuI	-21.65 ± 2.25	-208.01 ± 5.08	186.7 ± 2.08
PEO(1250)-<i>b</i>-PCL(2500)	CuB	-162.70 ± 2.94	-182.31 ± 7.10	19.55 ± 1.83
	CuI	-148.36 ± 4.31	-170.17 ± 7.82	21.79 ± 2.85

*Data are Means ± Standard Errors

This clearly indicates that increasing PCL/PEO ratio increases the attractive interactions between drugs and the PCL block that lead to stronger affinity. Such an increase in attractive interactions can be attributed to the increase in the attractive forces due to more atoms carrying opposite charges and the number of hydrogen bonds formed. Here, it should be pointed out that the electrostatic energy contribution originates from both Columbic interactions and hydrogen bonds formed between cucurbitacins and di-block copolymers. To determine the contribution from hydrogen bonds (H-bonds), we determined the average number of H-bonds formed between two drugs and three PEO-*b*-PCL di-block copolymers based on the definition discussed below. This is because a considerable amount of hydroxyl and carbonyl groups are present on the drug molecules and the PCL block, respectively. Figures 5.3 and 5.4 show that H-bonds could form between drug molecules and two respective blocks of PEO-*b*-PCL.

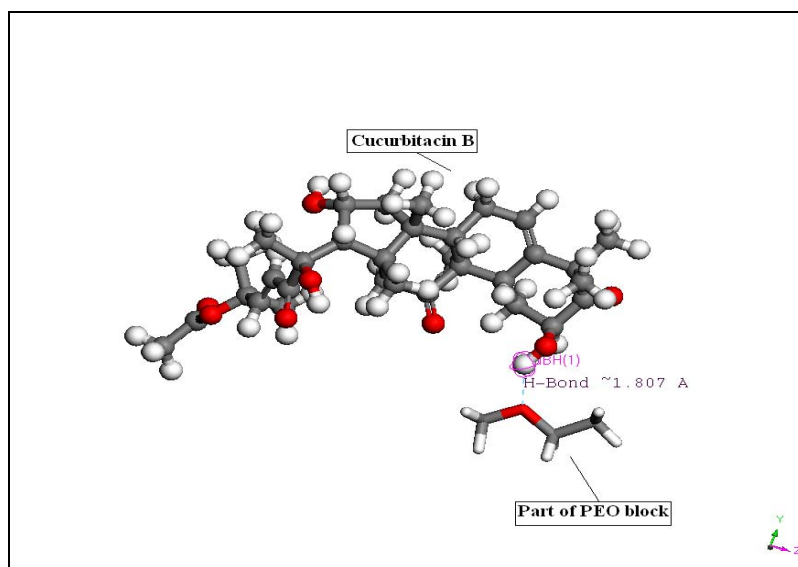
5.3.3 Hydrogen Bond Definition

The commonly used H-bond definitions are either based on energetic criteria or geometric criteria.[97, 98] In MD simulation, the intermolecular energy of the system is depicted by a continuous interaction potential and hence it is difficult to distinguish with accuracy whether two molecules are H-bonded or not.



**For clarity purpose, only a single monomer of PCL block is shown. (Red: O atom; White: H atom; Gray: C atom)*

Figure 5.3 Snapshot of H-bond formed between H atom of one of the –OH groups of CuB with O atom of carbonyl group of PCL block of PEO(1250)-*b*-PCL(2500).



**For clarity purpose, only a single monomer of PEO block is shown. (Red: O atom; White: H atom; Gray: C atom)*

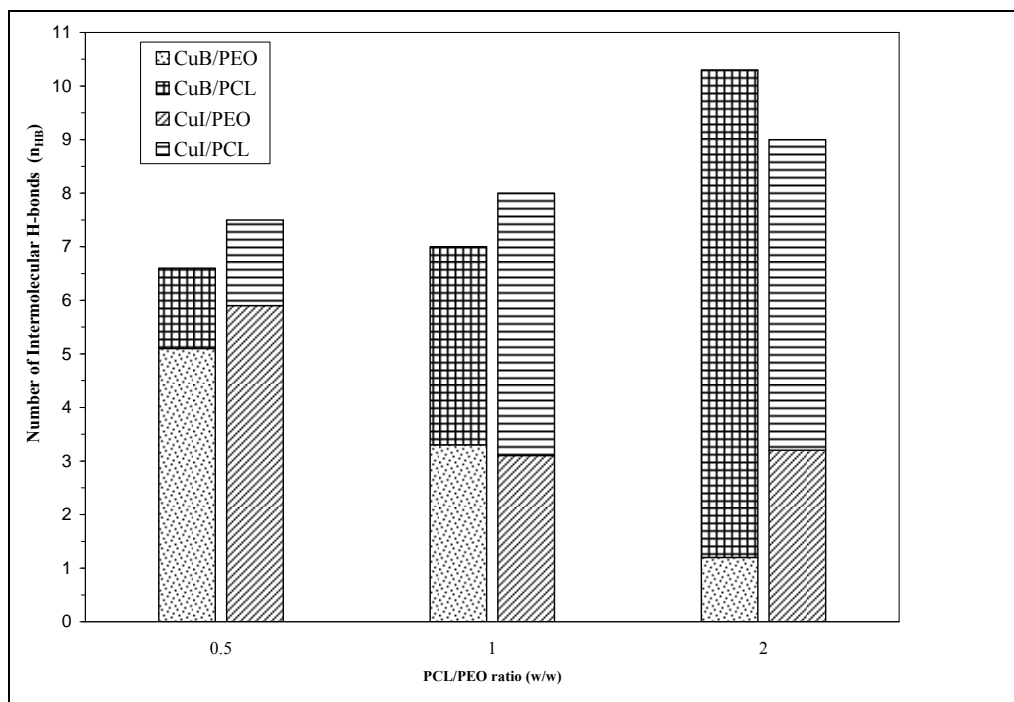
Figure 5.4 Snapshot of H-bond formed between H atom of one of the –OH groups of CuB with the O atom of PEO block of PEO(2500)-*b*-PCL(1250).

Therefore, we adopted a geometric definition, i.e., we assume that H-bond exists between hydrogen bond donor and acceptor atoms of two different molecules if following conditions are fulfilled:

1. The distance between hydrogen atom and the acceptor atom (R_{HA}) is less than or equal to R_{HA}^c .
2. The angle between the donor, hydrogen and acceptor atom (θ) is greater than or equal to 90 degrees.

The positions of the first minima of the radial distribution functions $g_{OH}(r)$ gave us an indication of the cut-off value R_{HA}^c . In the present work, we used $R_{HA}^c = 2.6 \text{ \AA}$ as the cut-off value.

The major advantage of using the geometric definition is that we can identify which atoms are participating in each H-bond. The list of probable hydrogen bond donors includes nitrogen, oxygen, sulphur and carbon atoms. Feeding this definition into the MD simulation trajectory files, we could then calculate the average number of intermolecular H-bonds formed between drug molecules and the entire di-block copolymer, which is shown in the form of stacked bar graph in Figure 5.5. The average values and errors associated with the number of H-bonds were also calculated based on the time average of last 200 ps of the trajectory files. In order to check the reproducibility of the results of Figure 5.5, we repeated the MD simulations with three different initial structures and counted the total number of intermolecular H-bonds in the systems containing PEO(2500)-*b*-PCL(2500) for both drugs. Results were found to be highly reproducible (data not shown).



*Standard errors are in the range of 0.47 to 0.75 with the maximum error (i.e, 0.75) associated with the bar of PCL/PEO ratio (w/w)=2/CuI

Figure 5.5 Plot showing the total number of intermolecular H-bonds formed by CuB and CuI with the block copolymers shown in the form of sum of contribution from H-bond with PEO and PCL blocks.

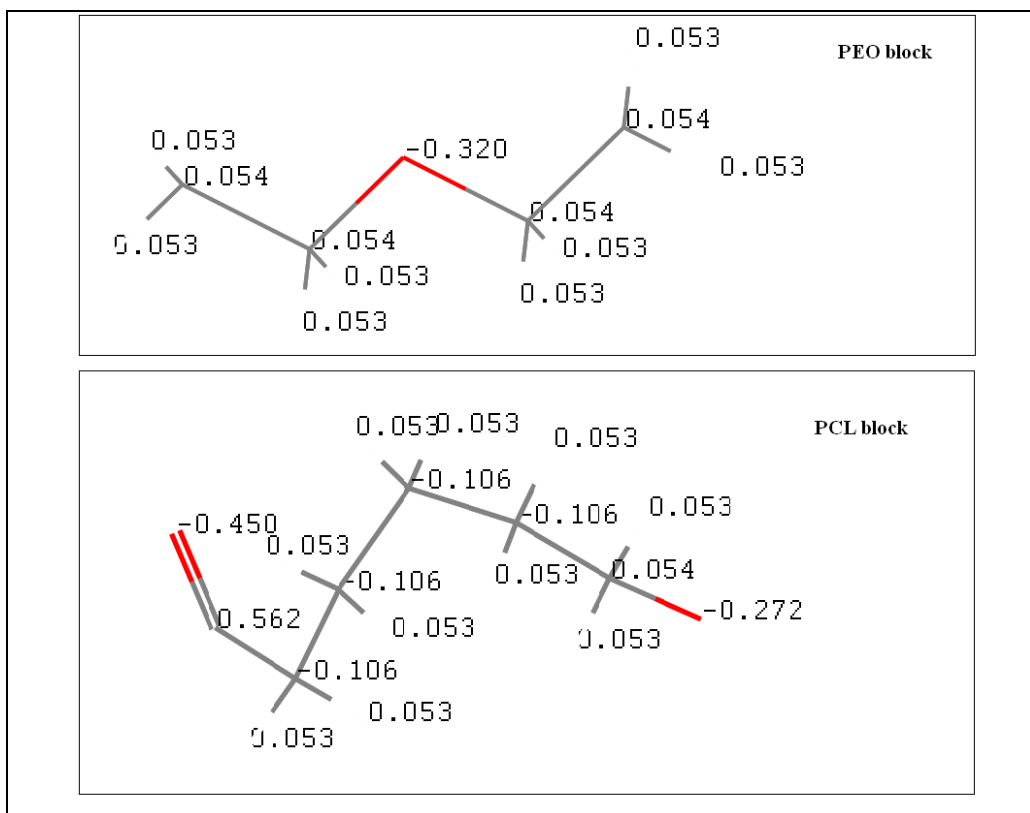
It is clear from Figure 5.5 that there is an increase in average total number of H-bonds as the PCL/PEO ratio is increased from 0.5 to 2. This indicates that the decrease in electrostatic energy is at least partly attributed to the formation of additional H-bonds as H-bonds would lower the electrostatic energy of the system. However, it is impossible to determine the respective contributions of Coulombic interactions and H-bonds to the non-bonded electrostatic energy. It is also clear that the average number of H-bonds formed between drugs and the PCL block increases while this number decreases for the PEO block with increasing PCL/PEO ratio suggesting that H-bonds formed between two drugs and the PCL block favour encapsulation.

It is worth pointing out that in our solution models, which were subjected to three-dimensional periodic boundary conditions, intra- and inter-chain hydrogen bonds could form between the PEO-*b*-PCL molecule in the primary cell and its periodic images. And such interactions were included in the calculations of the interaction parameter and the number of intermolecular H-bonds formed between the di-block copolymer and the drugs. Considering the fact that there are only a small number of hydrogen bond donors and acceptors present in the backbone of PEO-*b*-PCL that could form intra- and inter-chain hydrogen bonds, we believe that the effect should be minor. However, it is unlikely that such inter-chain H-bonds could be formed between two PEO-*b*-PCL chains in the micelle environment.

5.3.4 Radial Distribution Functions

To examine the nature of the H-bonds, we also calculate the radial distribution functions between various pairs of interacting hydrogen and oxygen atoms (i.e., $g_{OH}(r)$) present in two drugs and PEO-*b*-PCL with PCL/PEO ratios of 0.5 and 2. In the context of the present work, the radial distribution function (RDF) is defined as the ratio of the local density of the intermolecular O-H pairs to their average density of the entire simulation system at various inter-atomic distances. To compute $g_{OH}(r)$, we have considered the interactions between the hydrogen atoms of hydroxyl groups of CuB and CuI with the oxygen atoms of carbonyl groups of the PCL block and the oxygen atoms of the PEO block as well as the interactions between the oxygen atoms of carbonyl groups of CuB and CuI with the hydrogen atoms of the PCL block. The reasons for including the hydrogen atoms of the PCL block as hydrogen bond donors are explained below. Generally, hydrogen bonds formed between the hydrogen atoms of methylene and/or methine groups and the oxygen atoms (C-H \cdots O) is observed in proteins especially when the C-H group is present close to electron withdrawing groups like carbonyl and amide groups. As a result, the carbon atom of C-H group becomes electronegative and is generally termed as '*activated carbon*'. The hydrogen atom attached to such activated carbon shows tendency to form hydrogen bond with other electronegative atoms like oxygen atom. [99]. In PEO-*b*-PCL, carbonyl groups (-C=O) are present in the PCL block and hence activated carbons (carbon atoms of methylene group) are present in the PCL block. However, such activated carbon atoms are not present in the PEO block due to the

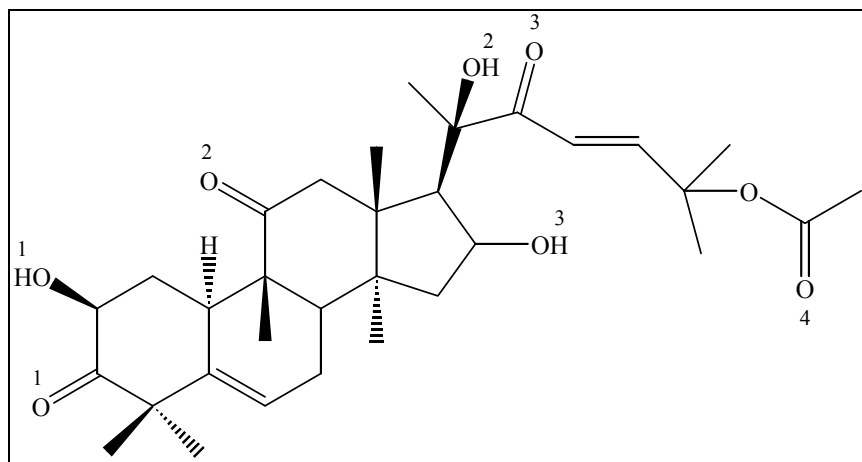
absence of strongly electron withdrawing groups. The other way of confirming this is to examine the partial atomic charges on the carbon atoms of the PCL and PEO blocks. Figure 5.6 shows partial atomic charges present on the various atoms of PEO and PCL monomers. It is obvious that the majority of carbon atoms have 0.054 and -0.106 partial atomic charges on PEO and PCL blocks, respectively. Due to the presence of negative partial atomic charges on the carbon atoms of PCL block, they can be considered as activated and consequently hydrogen atoms attached to them will have greater tendency to attract oxygen atoms from drug molecules. Since there are several carbonyl and hydroxyl groups on both drugs, we adopt a numbering scheme as shown in Figures 5.7 (A) and (B) to designate the oxygen and hydrogen atoms of the two moieties. Table 5.3 shows the first peak locations of $g_{OH}(r)$ values in terms of the inter-atomic distance from the corresponding RDF plots of the drug/di-block copolymer mixtures. For clarity, we do not show the original RDF plots here. The positions of peaks in a RDF plot signify the preferred inter-atomic distances between the atoms of interest (intermolecular O and H in this case). The position of the first peak in the $g_{OH}(r)$ plot denotes the maximum probability of finding O-H pair at that inter-atomic distance. According to generally accepted geometric definition of H-bond, close proximity of H-bond donor/acceptor pair atoms (O-H pair) at distances less than or equal to 2.6 Å may possibly lead to H-bond formation. [97, 98] This can be further reinforced by an observed decrease in electrostatic energy.



*Red : O atom; Gray: C atom

Figure 5.6 Partial atomic charges on the atoms of PEO and PCL block monomers.

(A)



(B)

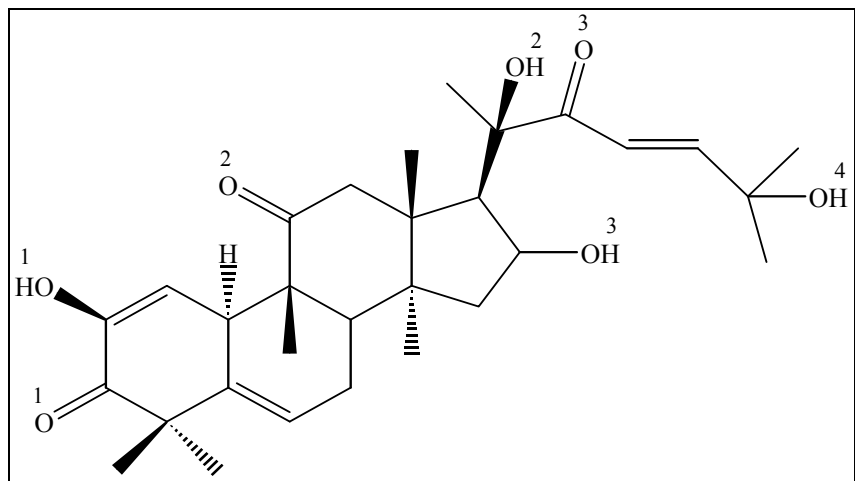


Figure 5.7 Numbering scheme of H and O atoms of Hydroxyl and Carbonyl groups in (A) CuB; and (B) CuI.

Table 5.3 Locations of the first intermolecular OH peaks obtained from $g_{OH}(r)$ of mixtures containing 12 wt% drug (CuB and CuI) and remaining di-block copolymer with PCL/PEO (w/w) ratio of 0.5 and 2.0.

Drug	Potential intermolecular hydrogen bonds	Position of first peak (Å) for PCL/PEO (w/w) = 0.5	Position of first peak (Å) for PCL/PEO (w/w) = 2
CuB	(CuB)C=O(1)---H(PCL)	~ 2.45	~ 2.55
	(CuB)C=O(2)---H(PCL)	~ 5.45	~ 1.95
	(CuB)C=O(3)---H(PCL)	~ 2.65	~ 2.35
	(CuB)C=O(4)---H(PCL)	~ 2.55	~ 3.20
	(CuB)H(1)---O=C(PCL)	~ 5.95	~ 4.10
	(CuB)H(2)---O=C(PCL)	~ 2.95	~ 4.55
	(CuB)H(3)---O=C(PCL)	~ 4.95	~ 2.15
	(CuB)H(1)---O(PEO)	~ 1.65	~ 3.85
	(CuB)H(2)---O(PEO)	~ 3.65	~ 6.15
(CuB)H(3)---O(PEO)	~ 1.55	~ 5.25	
CuI	(CuI)C=O(1)---H(PCL)	~ 4.85	~ 3.05
	(CuI)C=O(2)---H(PCL)	~ 2.35	~ 2.45
	(CuI)C=O(3)---H(PCL)	~ 2.25	~ 2.55
	(CuI)H(1)---O=C(PCL)	~ 6.25	~ 1.75
	(CuI)H(2)---O=C(PCL)	~ 5.85	~ 3.65
	(CuI)H(3)---O=C(PCL)	~ 7.25	~ 1.65
	(CuI)H(4)---O=C(PCL)	~ 1.95	~ 4.65
	(CuI)H(1)---O(PEO)	~ 1.75	~ 1.95
	(CuI)H(2)---O(PEO)	~ 1.85	~ 4.65
	(CuI)H(3)---O(PEO)	~ 1.95	~ 4.65
	(CuI)H(4)---O(PEO)	~ 1.55	~ 3.25

Note: O: Oxygen atom; H: Hydrogen atom. The bold figures in dark boxes represent inter-atomic distance capable of forming H-bond.

The bold figures in Table 5.3 represent the inter-O-H distances of the first peak locations that fall under the above mentioned category. In other words, these pairs can be considered as probable H-bond sites. This indirectly allows us to count the approximate number of available H-bond sites between drugs and di-block copolymers. Accordingly, it can be seen from Table 5.3 that in the case of PCL/PEO ratio of 0.5, there are approximately 6 (CuB) to 7 (CuI) H-bond sites while in the case of ratio of 2.0, there are only approximately 4 (CuB) to 5 (CuI) H-bond sites. It is expected that a higher number of available H-bond sites would indicate higher chance for forming more H-bonds and that the di-block copolymer with PCL/PEO ratio of 0.5 would yield lower χ value. However, this is not the case (see Figures 5.2(A) and 5.5). Instead, on average, there are about 6 to 7 H-bonds and about 9 to 10 H-bonds formed in the cases of PCL/PEO ratio of 0.5 and 2.0, respectively. These results suggest that multiple H-bonds are formed per available site on the drug molecules (about two per site) in the higher PCL/PEO ratio case but single H-bonds in the other case. In fact, it was observed that multiple H-bond sites on the PCL block, mainly in the form of hydrogen atoms attached to '*activated carbon*' formed H-bonds with single carbonyl groups on the drug molecules. In the case of low PCL/PEO ratio, more single H-bonds formed between the H-bonds of the drugs and the PEO block. The result suggests that H-bond sites (hydrogen atoms attached to the *activated carbons*) on the PCL block is much more useful than those of the PEO block on inducing drug/di-block copolymer affinity. In the next chapter, we will be focusing on studying the effect

of varying the chemical architecture of the PCL block on drug/PEO-*b*-PCL compatibility.

5.3.5 Implications on *in vitro* Drug Release Profiles

The release profiles of both drugs (CuB and CuI) encapsulated by PEO-*b*-PCL micelles with two different PCL/PEO ratios of 1 and 4.8 corresponding to PEO(5000)-*b*-PCL(5000) and PEO(5000)-*b*-PCL(24000), respectively, were measured by Molavi *et al.*[95] and were analyzed here with the aforementioned findings. In brief, it was found experimentally that the accumulative release within 8 h, expressed in terms of percentage of encapsulated drugs, decreases for both drugs when PCL/PEO ratio increases from 1 to 4.8. In particular, CuB shows a drastic 37.5% decrease (from 64% to 40% of encapsulated drugs) in accumulative release within 8 h, while in the case of CuI, there is only 11.1% decrease (from 90% to 80% of encapsulated drugs) in the accumulative release. Thus, CuB, as compared to CuI, shows substantial decrease in the release rates when PCL/PEO ratio increases by 4.8 times. In the literature, several studies have demonstrated that the presence of specific interactions like H-bonding between probe/drug and polymer molecules significantly affects the diffusion characteristics of probe/drug molecules through polymer matrix. Lee *et al.*[100, 101] reported that the retarded diffusion of methyl red (MR) in the presence of poly(vinyl acetate) (PVAc)/toluene solutions and poly(methyl methacrylate) (PMMA)/toluene as compared to the polystyrene (PS)/toluene solutions was ascribed to the H-bonding between MR and carbonyl groups present in PVAc and

PMMA polymers. Another study of Lee *et al.*[102] reported retarded release of Papaverine drug from carboxylic acid group substituted PEO-*b*-PLA micelles. Again, the presence of H-bonds between carboxylic groups of the di-block copolymer and the drug slows down the drug release from such micelles.

H-bond analysis (Figure 5.5) shows that when PCL/PEO ratio is increased from 0.5 to 2 (4 times increase), there is a substantial increase of ~ 6 times in the number of H-bonds formed between CuB and the PCL block. On the other hand, there is only about 3.6 times increase in the number of H-bonds formed between CuI and the PCL block. It seems that this result may explain the experimental result that the release rate of CuB is drastically reduced compared to that of CuI.

5.4 Summary

Two hydrophobic anti cancer drugs, CuB and CuI show similar solubility trends in PEO-*b*-PCL di-block copolymer micelles experimentally, where with an increase in PCL/PEO (w/w) ratio, both drugs show an increase in solubility. We computed the χ parameters between two drugs and di-block copolymers at three different PCL/PEO ratios using the MD approach in order to assess the power of this approach in predicting the experimental solubility trends. The MD approach predicted the experimental solubility trends very well. Our results confirm that besides the local molecular packing and non-polar intermolecular interactions like short-range dispersive interactions which are generally believed to be dominant forces in the system of hydrophobic drugs, the electrostatic intermolecular interactions also play a vital role in inducing the compatibility in drug/di-block

copolymer systems. In fact, in the present set of hydrophobic drugs, we found that the dispersive interactions did not contribute positively in inducing compatibility while the electrostatic interactions, in the form of H-bonding, contributed positively, leading to lower χ values for drug/PEO-*b*-PCL systems with high PCL/PEO ratios.

The average number of H-bonds and $g_{OH}(r)$ computed from the MD trajectories show that H-bonding is the key feature of specific interactions/favourable interactions in this kind of drugs with multiple H-bond donors and acceptors. It was also apparent that multiple H-bond sites on the PCL block of the di-block copolymer formed H-bonds with single H-bond sites on drug molecules inducing compatibility of them. This type of information can surely help us tailor-make the di-block copolymers to induce favourable interactions with the groups present on drugs.

In addition, the effect of PCL/PEO ratio on *in vitro* drug release rate can be explained by the number of H-bonds formed between drugs and the PCL block of di-block copolymer. MD simulation proves to be a valuable tool for predicting binary interactions between di-block copolymer and hydrophobic drug and provides useful atomistic details related to forces contributing to thermodynamic compatibility.

Chapter 6

Molecular Origin of Solubility of Water Insoluble Drugs in PEO-*b*-Poly(α -Benzyl Carboxylate ϵ -Caprolactone) with Different Tacticities³

6.1 Introduction

One key concept used by many researchers to increase the loading capacity of a self-associating block copolymer for a given hydrophobic drug is to introduce certain chemical moieties into the backbone of the block copolymer that are capable of interacting with the drug, with specific interactions of the types leading to negative heat of mixing [102-104]. In such studies, the block copolymer structure suitable for the solubilization of a given drug is usually selected based on the predictions of χ parameters calculated by the GCM [6, 78, 96, 105]. However, the stereochemistry and tacticity of polymer are not taken into account in predicting the solubility of drugs in block copolymers this way. The objective of this study was to assess whether the application of MD simulation for the

³ A version of this chapter has been published. Patel, S.K.; Lavasanifar, A.; Choi, P. (2010). *Biomaterials*. 31, 345-57.

determination of drug/block copolymer interaction parameter can address the shortcoming of GCM in this aspect and provide a reliable means to predict the solubilisation of drugs in block copolymers having different tacticities.

Recently, Mahmud *et al.* [106] have reported successful synthesis of self-associating tailor-made carriers having pendant aromatic and/or other reactive functional groups on the PCL block of PEO-*b*-PCL block copolymers. These core-functionalized micelles especially PEO-*b*-poly(α -benzyl carboxylate ϵ -caprolactone) (PEO-*b*-PBCL) (Figure 6.1) have shown great potential in improving the loading capacity of two anti-cancer drugs CuB and CuI [95]. The presence of pendant benzyl carboxylate groups on the PCL block may induce the formation of additional inter or intra-molecular specific interactions (e.g., π - π interactions, hydrogen bonds, etc.) which would eventually lead to the improvement of drug loading capacity of the di-block copolymer.

PEO-*b*-PBCL di-block copolymers are synthesized by ring opening polymerization of α -benzyl carboxylate- ϵ -caprolactone using methoxy-PEO as an initiator and stannous octoate as a catalyst [106]. It is worth noting that benzyl carboxylate- ϵ -caprolactone monomer possesses one asymmetric carbon and is used in the polymerization reaction as a racemic mixture. Upon polymerization, the hydrophobic block of the di-block copolymer can potentially contain similar or different stereo isomers leading to different tacticities, viz., isotactic, syndiotactic and atactic forms. The site labelled C* in Figure 6.1, is termed pseudo-asymmetric or chiral carbon atom center in the PBCL repeating unit.

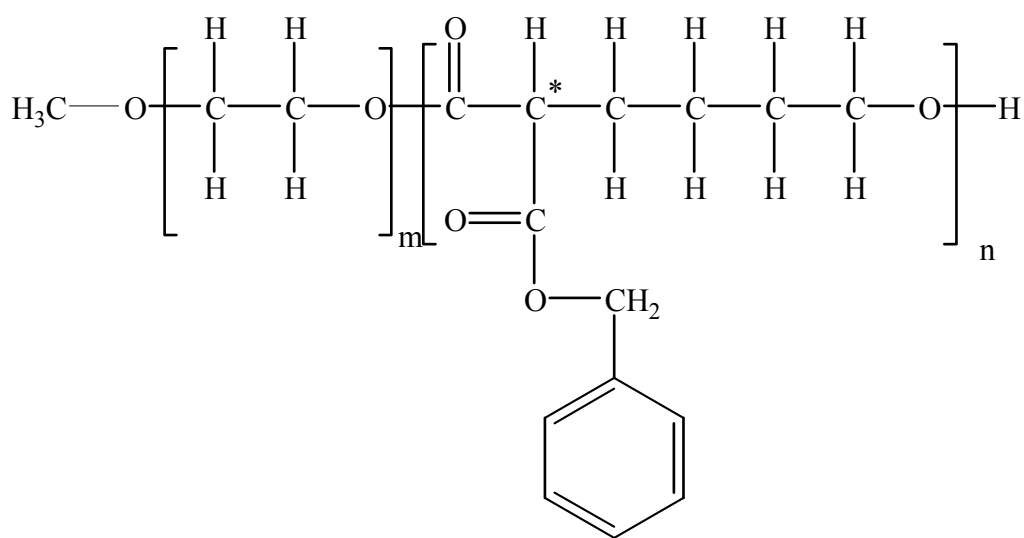


Figure 6.1 Chemical Structure of PEO-*b*-PBCL.

The stereo chemical configurations of successive chiral carbon atoms in the backbone of di-block copolymer will define its tacticity. Figure 6.2 shows a schematic diagram of three possible stereo isomers of the PBCL block. If configurations of all the successive chiral carbon atoms are same (i.e., the substituent branches lie on the same side of the reference plane), the PBCL block is termed *isotactic* (Figure 6.2(A)). If configurations of successive chiral carbon atoms differ (i.e., the substituent branches appear alternatively above and below the reference plane), the PBCL block is termed *syndiotactic* (Figure 6.2(B)). Alternatively, when configurations at the chiral centers are more or less random then the PBCL block is termed *atactic* (Figure 6.2(C)). Since specific interactions depend on tacticity of a polymer [74], tacticity of the di-block copolymer is expected to affect the solubility of drug in the micelle formed by such di-block copolymers. And it is expected that the differences in intermolecular interactions between the drug and the di-block copolymer could be captured by the corresponding χ values. Therefore, in this work, we applied the technique of MD simulation to determine the compatibility between two hydrophobic drugs (Set-I (CuB and CuI)) used by Molavi *et al.* [95] and PEO-*b*-PBCL with different tacticities. This set of drugs are ideal for studying intermolecular interactions between drugs and functionalized block copolymers since they contain multiple H-bond donors and acceptors evenly distributed on their molecules. To this end, the stereo configuration of PEO-*b*-PBCL that would yield higher solubility can be determined.

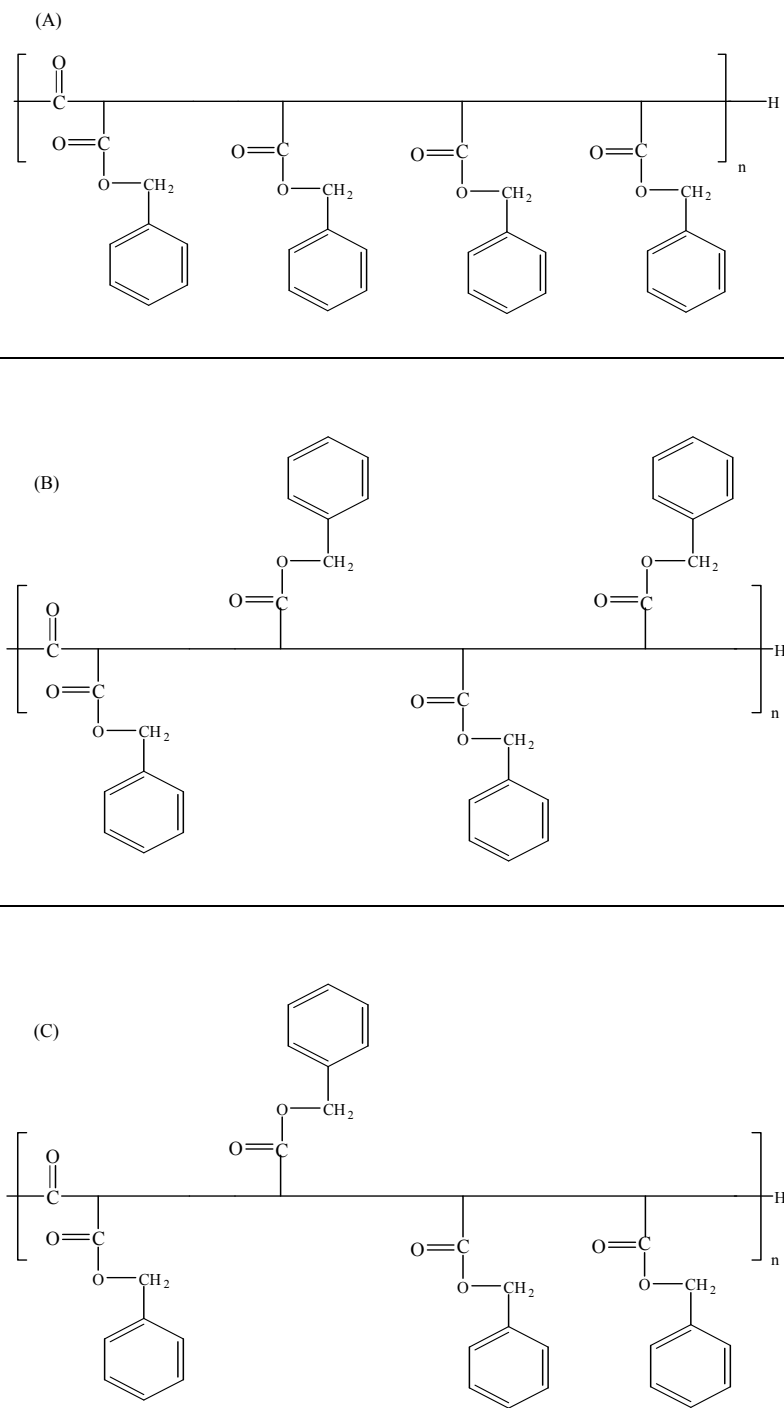


Figure 6.2 Schematics of the PBCL block with different tacticities. (A) Isotactic; (B) Syndiotactic; and (C) Atactic.

Such molecular level understanding can also aid in the process of chemical tailoring of the di-block copolymer to obtain drug carriers with optimized functional properties. Later in Section 6.3.2, we will apply the MD simulation strategy developed above to examine the potential of PEO-*b*-PBCL to encapsulate another set of drugs (Set-II (fenofibrate and nimodipine)) that contain only clustered hydrogen bond acceptors (Figure 4.1 (B) and (C)), in their structures.

6.2 Simulation Details

All MD simulations reported here were performed using the Materials Studio (MS Modeling version 4.2, Accelrys) run on a SGI workstation cluster. The initial liquid state models of all di-block copolymers were generated based on the RIS theory using the amorphous builder module available in another commercial software Cerius². The inter-atomic interactions were modeled with the COMPASS force field [62] (Section 3.3).

Three tactic forms (i.e., isotactic, syndiotactic and atactic) of PEO-*b*-PBCL (Figure 6.2) with a molecular weight of 2500 for each block, were built. The amorphous builder module in Cerius² defines the tacticity of a polymer using meso-diad ratio, which is generally defined as the relative proportion of isotactic monomer pairs in a given polymer. Thus, a polymer with a meso-diad ratio of 0.0 is a syndiotactic polymer and a polymer with a ratio of 1.0 is an isotactic polymer. A meso-diad ratio of 0.5 was used to build an atactic polymer. Throughout the chapter, the di-block copolymers with isotactic, syndiotactic, and atactic stereo configurations of PBCL repeating unit will be denoted as PEO-*b*-*i*PBCL, PEO-*b*-

*s*PBCL, and PEO-*b*-*a*PBCL, respectively. The method of Theodorou and Suter [73] was employed in the amorphous builder module of Cerius² to build the bulk amorphous states of pure di-block copolymers, drugs and their mixtures subjected to periodic boundary conditions and density constraint. The detailed procedure for constructing such initial structures has been described in Section 4.2.2.

In order to acquire the density values of the pure di-block copolymers and drugs at simulation temperatures of 413 K and 473 K, we carried out MD simulation in NPT statistical ensemble ($P = 1 \text{ atm}$; $T = 413 \text{ K} \ \& \ 473 \text{ K}$). In order to be consistent with the studies performed in Chapters 4 and 5, the simulation temperature of 413 K was chosen for studying the binary mixtures containing fenofibrate and nimodipine drugs, while simulation temperature of 473 K was chosen for studying the binary mixtures containing CuB and CuI drugs. The pressure and temperature of the systems were controlled using the Andersen barostat [72] and the Nose thermostat [69] algorithms, respectively.

During the model construction, the distribution of torsion angles of the skeletal bonds in the di-block copolymers was determined using the RIS theory [81, 82]. The distribution of torsion angles was determined by applying the Boltzmann weighting factor to the energies of the RIS minima to determine the distribution of torsion angles. The initial distribution of torsion angles for the PEO block of PEO-*b*-PBCL di-block copolymer remains the same as it was in PEO-*b*-PCL di-block copolymer. The detailed method can be found in Section 4.2.2. We identified a total of nine torsion angles for PEO-*b*-PBCL and they are depicted in Figure 6.3.

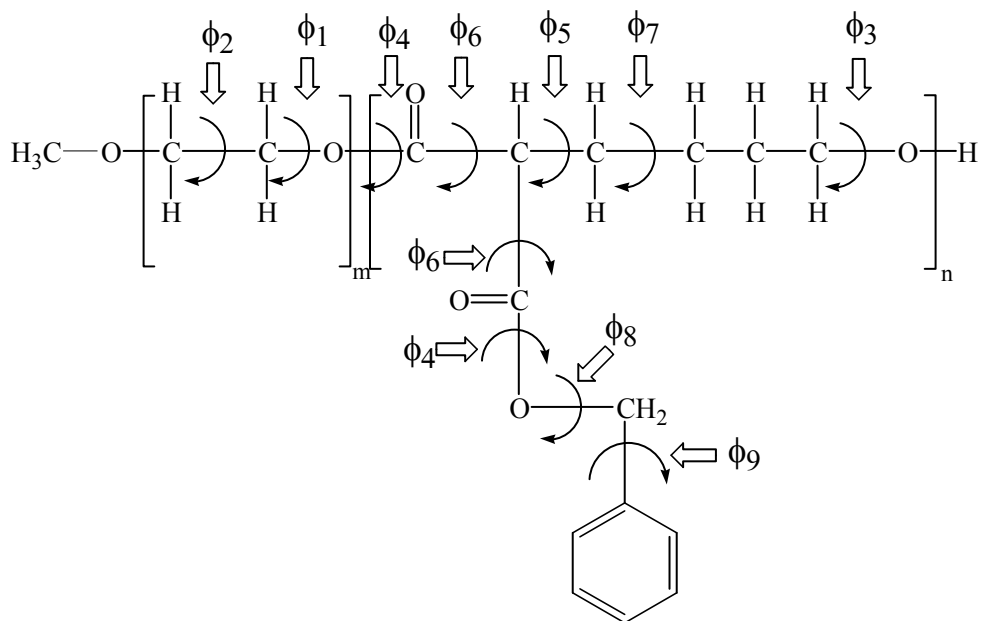


Figure 6.3 Schematics of all torsion angles identified in PEO-*b*-PBCL.

In Table 6.1, we list the values of RIS minima and respective tolerances for all nine torsion angles that have significant influence on the conformation of di-block copolymer. Once the RIS state distribution was determined, the RIS states were populated allowing for angle tolerances stated in Table 6.1.

All the initial amorphous structures are in relatively high energy state and hence before performing MD simulations, they were subjected to energy minimization step using the conjugate gradient method. NVT MD simulations were carried out at required simulation temperature using the Nose thermostat [69]. The velocity Verlet method, with a time step of 0.001 ps, was used as an integrator in all simulations. The non-bonded dispersive interactions were evaluated using the atom based cut-off distance of 9.50 Å with a spline width of 1 Å, while the long-range electrostatic interactions especially important in 3D periodic systems were evaluated using the well-known Ewald summation method [67]. Each simulation was carried out for a total of 2000 ps. The properties of interest (e.g., the total energy, radial distribution function, etc.) were calculated by averaging over the last five hundred ps of the corresponding trajectory file. Here, we adopted the MD simulation approach in which the internal energy changes on mixing were calculated and then used to obtain χ parameters for the drug/di-block copolymer pairs. [21]

Table 6.1 Rotational isomeric states for all torsion angles of PEO-*b*-PBCL.

Skeletal Bond	State 1*	State 2*	State 3*	State 4*
Φ_1	170 ± 20	300 ± 10	330 ± 10	N/A
Φ_2	40 ± 10	60 ± 10	280 ± 10	350 ± 10
Φ_3	270 ± 10	290 ± 10	330 ± 10	N/A
Φ_4	130 ± 10	300 ± 10	N/A	N/A
Φ_5	50 ± 10	90 ± 10	120 ± 10	N/A
Φ_6	110 ± 10	N/A	N/A	N/A
Φ_7	70 ± 15	180 ± 10	230 ± 5	N/A
Φ_8	70 ± 10	N/A	N/A	N/A
Φ_9	140 ± 10	160 ± 10	330 ± 10	N/A

*Data are Torsion angle \pm Tolerance

6.3 Results and Discussion

6.3.1 PEO-*b*-PBCL/Cucurbitacin Drugs

6.3.1.1 MD Simulation

Table 6.2 summarizes the computed density values for di-block copolymers, cucurbitacin drugs and their mixtures (10 wt% drug) at a pressure of 1 atm and a temperature of 473 K. It is worth noting that density values for all three tactic forms, viz., PEO-*b-i*PBCL, PEO-*b-s*PBCL and PEO-*b-a*PBCL were assumed to be the same. Therefore, only the density of PEO-*b-i*PBCL was calculated. Generally, density values of stereo isomers of polymers differ only in the crystalline state due to their different packing characteristics while their density values are essentially the same in the amorphous state. For example, the densities of *i*-Polypropylene (*i*-PP) and *s*-Polypropylene (*s*-PP) are identical in the liquid (amorphous) state while differ significantly in their solid state [107]. In the present work, since the amorphous state of the di-block copolymer was of interest, we feel justified to use the same density value for all three tactic forms of PEO-*b*-PBCL. We have demonstrated in our previous work [21] that the density values for di-block copolymers and hydrophobic drugs computed using the COMPASS force field are reproducible and reliable. The mean potential energies of the bulk states of the pure di-block copolymers, drugs and their mixtures were calculated by using the time average of the potential energy over the last 500 ps of the corresponding trajectories of 2000 ps at equal interval of 2 ps.

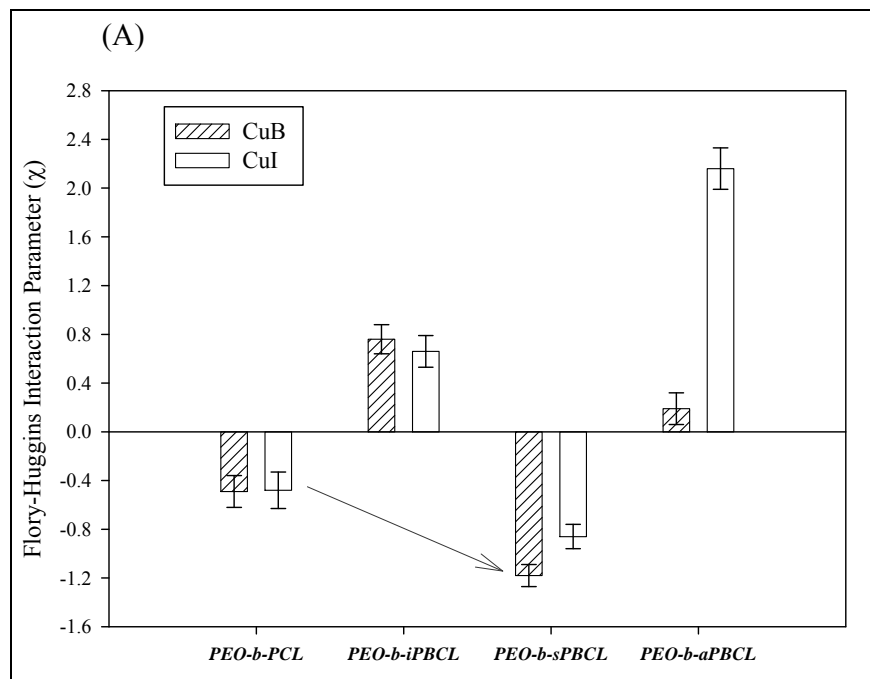
Table 6.2 Computed densities of CuB, CuI, all tactic forms of PEO(2500)-*b*-PBCL(2500) and their mixtures (10 wt% drug) at 1 atm and 473 K along with the number of drug molecules involved.

Drug/Block Copolymer/Mixture	Density (g/cm³)	No. of Drug Molecules	No. of Block Copolymer Chains
Cucurbitacin B (CuB)	1.15	-	-
Cucurbitacin I (CuI)	1.12	-	-
PEO- <i>b</i> - <i>i</i> PBCL (P ₁) PEO- <i>b</i> - <i>s</i> PBCL (P ₂) PEO- <i>b</i> - <i>a</i> PBCL (P ₃)	1.18	-	1
CuB & P ₁ CuB & P ₂ CuB & P ₃	1.18	1	1
CuI & P ₁ CuI & P ₂ CuI & P ₃	1.18	1	1

The velocity autocorrelation functions of the drug molecules, not shown here, indicated that the drug molecules de-correlated in less than 2 ps. The analysis of mean values and standard errors were performed using the Sigma Plot version 11.0 (Systat Software, Inc.).

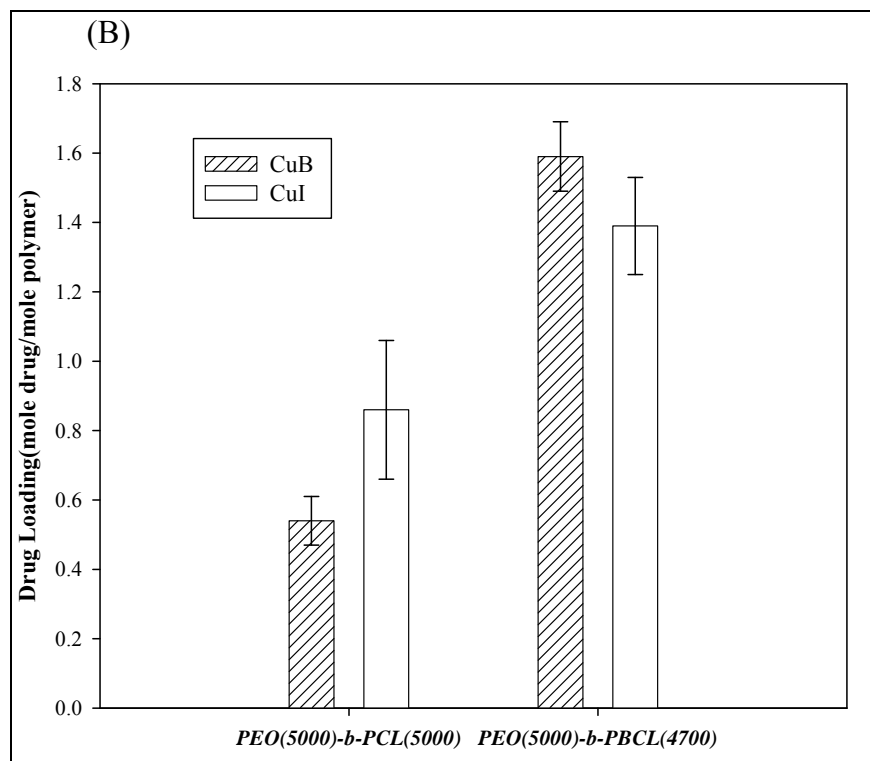
The computed χ values are plotted in the Figure 6.4(A). We note that the error bars shown in the figure are ensemble fluctuations and were determined using the data of last 500 ps of the corresponding MD trajectories. Since the solubility prediction from simulation is solely based on the qualitative trend in χ values of different systems, we have compared the χ values of the current systems, viz., PEO(2500)-*b*-PBCL(2500) with those of PEO(2500)-*b*-PCL(2500) (Chapter 5).

Figure 6.4(A) shows negative χ values only for binary mixtures containing syndiotactic version of di-block copolymer (i.e., PEO-*b-s*PBCL). Comparing these χ values with those of non-functionalized mixture systems containing PEO-*b*-PCL, these χ values decreased by about three times. Comparing this observation with the experimental drug loading data (mole drug/mole di-block copolymer) (Figure 6.4(B)) of CuB and CuI in PEO(5000)-*b*-PCL(5000) and PEO(5000)-*b*-PBCL(4700), our MD results on PEO-*b-s*PBCL are consistent with the experiment. It should be pointed out that the tacticity of PEO-*b*-PBCL was unknown in the experimental case. However, the simulation data strongly suggest that the tacticity of the experimentally synthesized PEO-*b*-PBCL should be syndiotactic.



*Data are means. Bars are standard errors (Note: the red arrow indicates decrease in χ values)

Figure 6.4(A) Plot of the computed χ values of binary mixtures of two cucurbitacins and three tactic forms of PEO-*b*-PBCL compared with the data for PEO-*b*-PCL.



*Data are means. Bars are standard errors

Figure 6.4(B) Comparison plot of experimentally measured drug loading capacity of PEO-*b*-PCL and PEO-*b*-PBCL micelles for cucurbitacins as reported by Molavi *et al.*

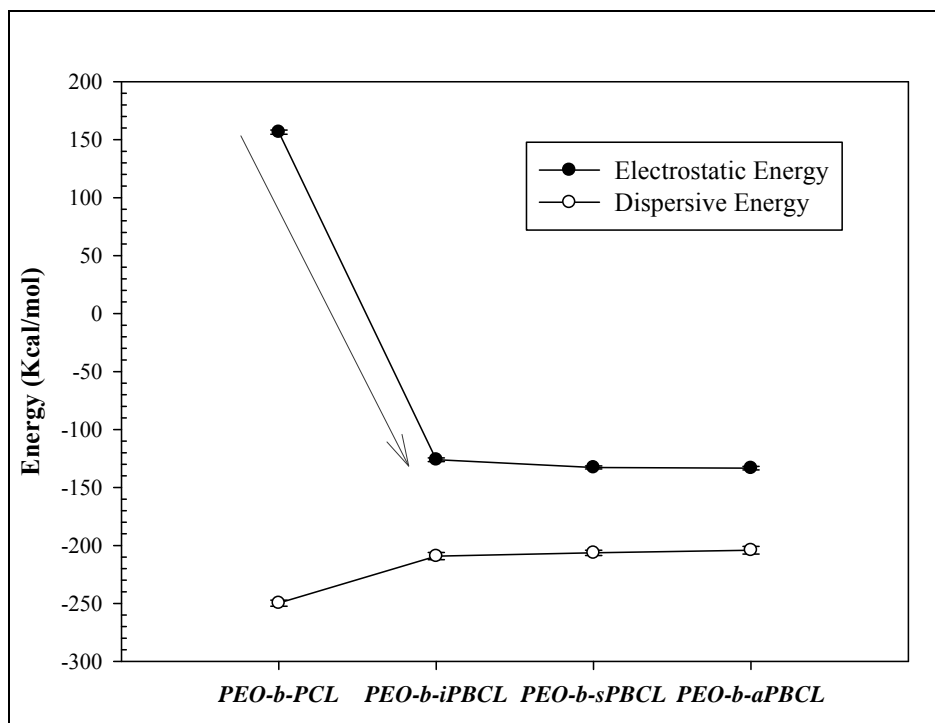
Various mechanistic and NMR studies along with predictions from Monte Carlo calculations performed by Kricheldorf *et al.*[108, 109] and Thakur *et al.*[110, 111] demonstrate that stannous octoate, an achiral catalyst, commonly used in the ring opening polymerization of lactides shows a clear preference for syndiotactic addition. Since our synthesis process of PEO-*b*-PBCL uses stannous octoate catalyst for the ring opening polymerization of α -benzyl carboxylate- ϵ -caprolactone, it is likely that stereo form of the di-block copolymer is syndiotactic. However, further NMR experiment is needed to verify the tacticity of di-block copolymer.

The next step is to identify the factors that contribute to the favourable interactions in the mixture containing PEO-*b*-sPBCL and the drugs. Functionalization of the PCL core of PEO-*b*-PCL with aromatic benzyl carboxylate group is expected to affect the intra-molecular interactions to a certain extent in pure polymer state due to the presence of aromatic rings in the di-block copolymer structure. The strength of these intra-molecular interactions indirectly affects the strength of intermolecular interactions between the di-block copolymer and drug molecules in the mixture environment because these intermolecular associations would have to overcome existing intra-molecular associations in the pure polymer.

6.3.1.2 Intra-molecular Non-bonded Energy

In order to assess the intra-molecular specific interactions, a preliminary study on the electrostatic and dispersive contributions to the intra-molecular non-bonded

energy values for pure PBCL was carried out and compared with the values for pure PCL. Figure 6.5 shows the time average values of electrostatic and dispersive energy values for pure states of PEO-*b-i*PBCL, PEO-*b-s*PBCL, and PEO-*b-a*PBCL along with the values for pure state PEO-*b*-PCL for the sake of comparison. The energy values were averaged over the last 500 ps of the corresponding trajectory of 2000 ps. It is clear from Figure 6.5 that the dispersive energy became unfavourable in PBCL while the electrostatic energy became favourable. In fact, due to the functionalization, the electrostatic energy decreased substantially from positive to negative values, indicating stronger intra-molecular interactions in the cases of PEO-*b*-PBCL as compared to the case of PEO-*b*-PCL. This is also consistent with our experimental observation showing a higher rigidity of the PBCL compared to the PCL core structures estimated by a fluorescence probe study [96]. An increase in the attractive interactions can be attributed to the increase in attractive forces due to more atoms carrying opposite charges and the number of hydrogen bonds formed. Here, it should be pointed out that the electrostatic energy contribution originates from Columbic interactions and specific interactions like intra-molecular hydrogen bonds, $\pi - \pi$ interactions, etc. Since the commercial software package Materials Studio was unable to display the hydrogen bonds formed with aromatic rings, we could not carry out the counting of hydrogen bonds in this case. Instead, we examined the radial distribution functions (RDF) among different intra-molecular and intermolecular segments in the pure and mixture states of the systems.



**Note: The red arrow indicates the drastic decrease in electrostatic energy value*

Figure 6.5 Comparison of electrostatic and dispersive energy values for PEO-*b*-PCL and all the tactic forms of PEO-*b*-PBCL in their pure state.

Hence, we will be defining a particular pair to be interacting only based on RDF plots showing the proximity of different segments. But before discussing RDF calculations, we briefly describe different types of specific interactions probable between the different segments of di-block copolymers and between those with the drug molecules in the following section.

6.3.1.3 Specific Interactions

In systems involving long chain di-block copolymers, specific interactions play a vital role in inducing miscibility by achieving negative heats of mixing. Figure 6.6 shows all probable intra-molecular and intermolecular specific interactions between di-block copolymers and drug molecules. The numbering of all these interactions is listed in Table 6.3.

Aromatic --- aromatic / π - π interactions: Benzene rings are generally considered to be non-polar but their electron distribution is a complex multi-pole with no net dipole moment. This multi-polar distribution makes benzene have electron rich faces and partial positive charges on hydrogen atoms around the edges. Hence, when benzene rings centroid comes between 4.5 and 7.0 Å separation distance [112], the positively charged edge interacts with negatively charged faces. Such type of interaction is termed as π - π interactions. In a study by Barlow *et al.* [113], this type of interaction between aromatic rings of Polystyrene (PS) and Tetramethyl bisphenol-A polycarbonate (TMPC) polymers were found to be responsible for inducing miscibility in their corresponding blends.

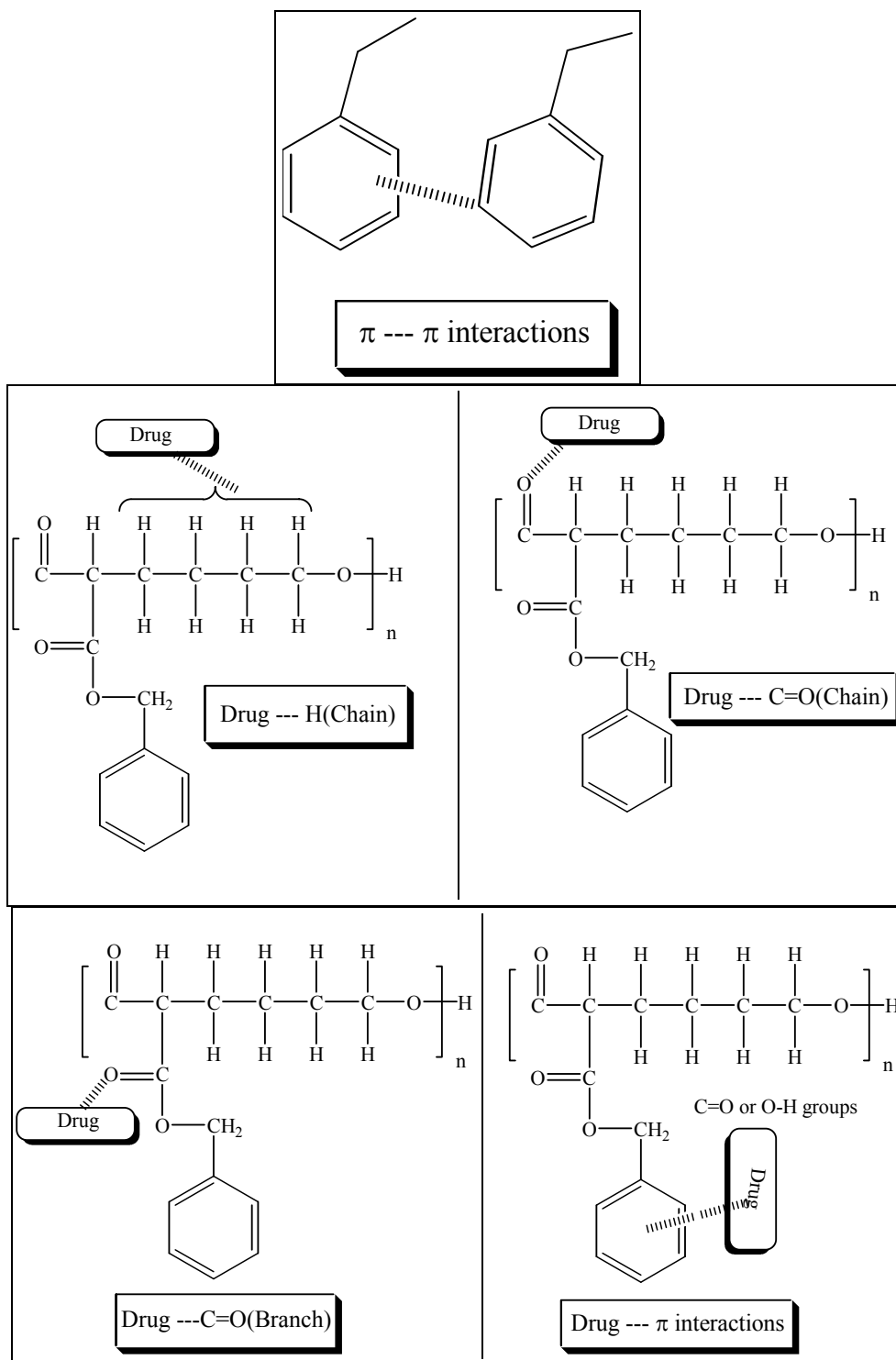


Figure 6.6 Different types of intra-molecular and intermolecular interactions probable in the binary mixtures of PEO-*b*-PBCL and cucurbitacin drug molecules.

Table 6.3 Numbering of intra-molecular and intermolecular interactions shown in Figure 6.6.

Interaction Number	Interacting Pair	Type of Interaction
1	Aromatic --- Aromatic / π --- π	Intra-molecular
2	Drug --- H(Chain)	Intermolecular
3	Drug --- C=O(Chain)	Intermolecular
4	Drug --- C=O(Branch)	Intermolecular
5	Drug --- π (C=O or -OH groups of drug)	Intermolecular

In the present work, we have aromatic rings on substituent branches of di-block copolymers and hence intra-molecular $\pi - \pi$ interactions would be important.

Drug --- H(Chain): The H(Chain) are hydrogen atoms attached to *activated carbons* on the backbone of di-block copolymer. The carbonyl groups on drug molecules favourably interact and form multiple hydrogen bonds with these hydrogen atoms. This type of conventional hydrogen bonding has already been discussed in our previous work (Chapter 5).

Drug --- C=O(Chain): The hydroxyl (-OH) groups present in drug molecules interact and form hydrogen bonds with the carbonyl (-C=O) groups present in the backbone of di-block copolymer. For details, refer Chapter 5.

Drug --- C=O (Branch): This type of interaction is similar to the previous one except that the drug molecules interact with the carbonyl (-C=O) groups present in the substituent branches.

Drug --- π interactions: Drug molecules contain various carbonyl and hydroxyl groups. These groups could interact with aromatic rings either by $n \text{ --- } \pi / \text{C=O} \text{ --- } \pi$ or $\pi \text{ --- } \pi$ hydrogen bonding interactions (i.e., OH --- π interactions). The miscibility is induced in polyester/PC blend through the formation of $n \text{ --- } \pi$ complex between ester carbonyl and PC aromatic rings [114]. In another example, $\pi \text{ --- } \pi$ hydrogen bonding interactions between π electrons of PC aromatic

groups and –OH groups of styrene-co-4-vinyl phenol copolymer was responsible for inducing the miscibility in their corresponding polymer blends [115].

6.3.1.4 Radial Distribution Function

The spatial correlation between any two molecules or segments of molecules can be described using radial distribution function (RDF). The value of RDF is a relative measure rather than an absolute one. The RDF $g_{AB}(r)$ between two selected groups A and B can be calculated using following general expression:

$$g_{AB} = \frac{N_{AB}(r) \times V}{(N_A N_B - N_{AB}) 4\pi r^2 dr} \quad (6.1)$$

where N_A and N_B are number of atoms in groups A and B, respectively, N_{AB} is number of atoms common to both groups A and B, and V is unit cell volume.

Intra-molecular π - π interactions

Figure 6.7 (A) and (B) shows RDF plots for intra-molecular π - π interactions in PEO-*b*-PBCL and binary mixtures formed by the di-block copolymer and drugs, respectively. It is worth noting that throughout the plots of RDF analysis, the *i*PBCL is used interchangeably for PEO-*b*-*i*PBCL and similarly *s*PBCL for PEO-*b*-*s*PBCL and *a*PBCL for PEO-*b*-*a*PBCL.

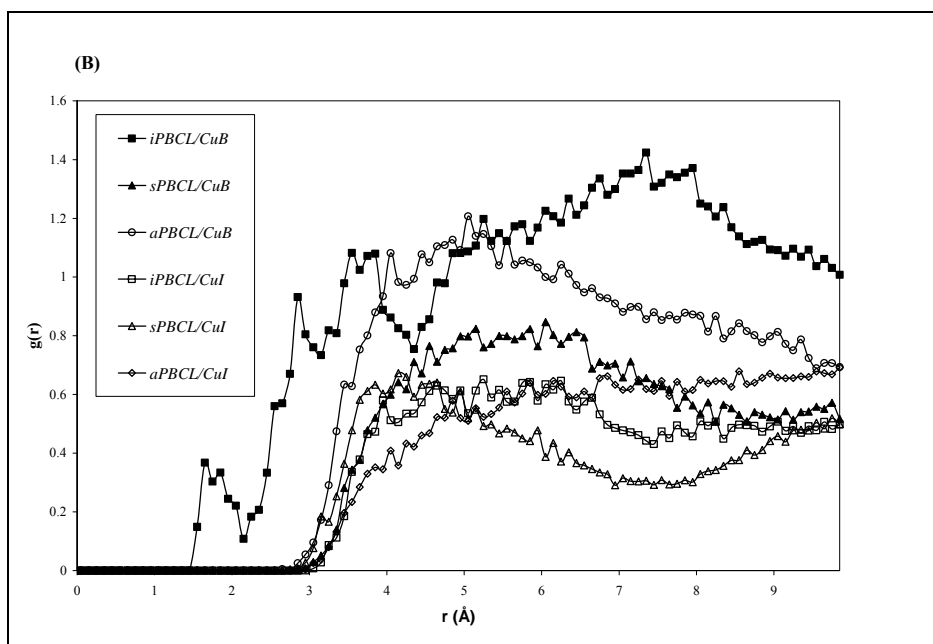
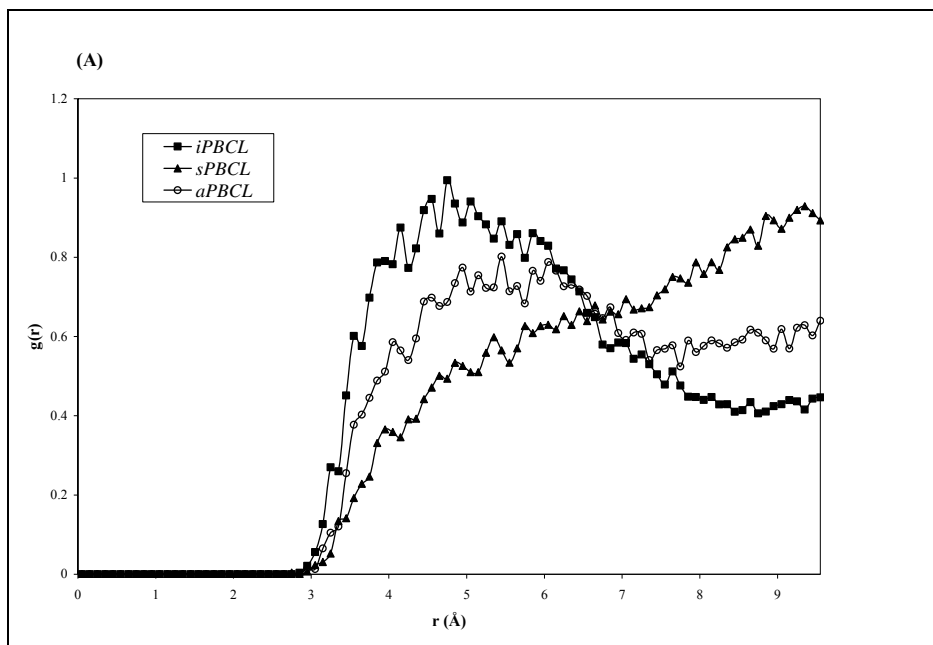


Figure 6.7 RDF plots for Interaction No. 1 (listed in Table 6.3) in (A) pure di-block copolymer system; and (B) mixture system of drug/di-block copolymer.

It is obvious from Figure 6.7(A) that $\pi - \pi$ correlation is highest in the case of *i*PBCL while lowest in the case of *s*PBCL indicating favourable $\pi - \pi$ interactions in the case of *i*PBCL. In order to establish favourable intermolecular interactions/contacts between di-block copolymer and drug molecules, the existing intra-molecular interactions in the di-block copolymer needs to be overcome. Thus, due to lowest $\pi - \pi$ correlation in the case of *s*PBCL, we expect to observe maximum intermolecular associations between this di-block copolymer and drug molecules. In Figure 6.7(B) we compare $\pi - \pi$ correlation of different di-block copolymers in a mixture environment of both drugs. In the PEO-*b*-PBCL/CuB mixtures, the intra-molecular $\pi - \pi$ correlation is still strong in the isotactic form of the copolymer while in the mixture containing CuI, the intra-molecular $\pi - \pi$ correlation decreases drastically for all tactic forms, which we believe is due to strong correlation of CuI drug with aromatic rings. In a later section (Refer OH--- π interactions), we will show that the intermolecular OH --- π interactions between the CuI drug and the aromatic ring has weakened the intra-molecular $\pi - \pi$ interactions. It is obvious that the local packing of substituent branches will be different in different stereo isomers and the effect of this local packing is visible on the strength of $\pi - \pi$ interactions.

Intermolecular Specific Interactions for CuB

RDF plots showing correlations for interaction no. 2, 3, 4, and 5 listed in Table 6.3 are shown in Figures 6.8 (A), (B), (C), and (D), respectively, for all the tactic forms of di-block copolymer and CuB mixture.

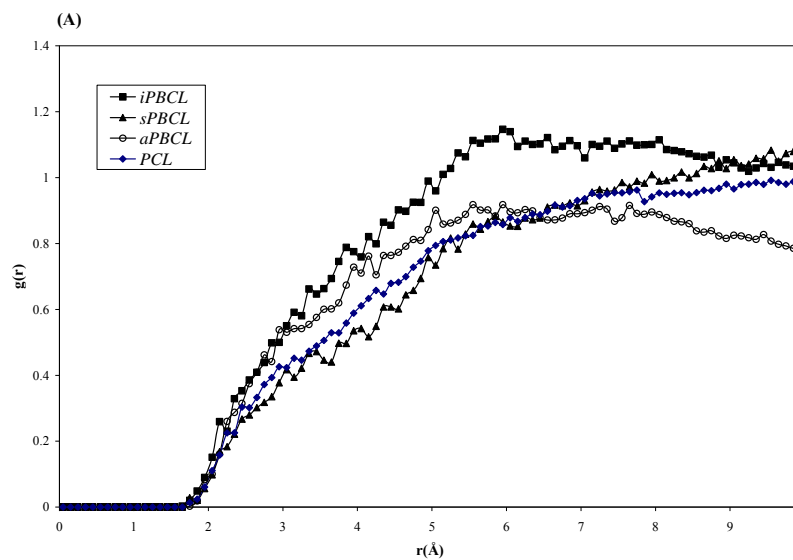


Figure 6.8(A) RDF plot of CuB drug in PEO-*b*-PBCL for Interaction No. 2.

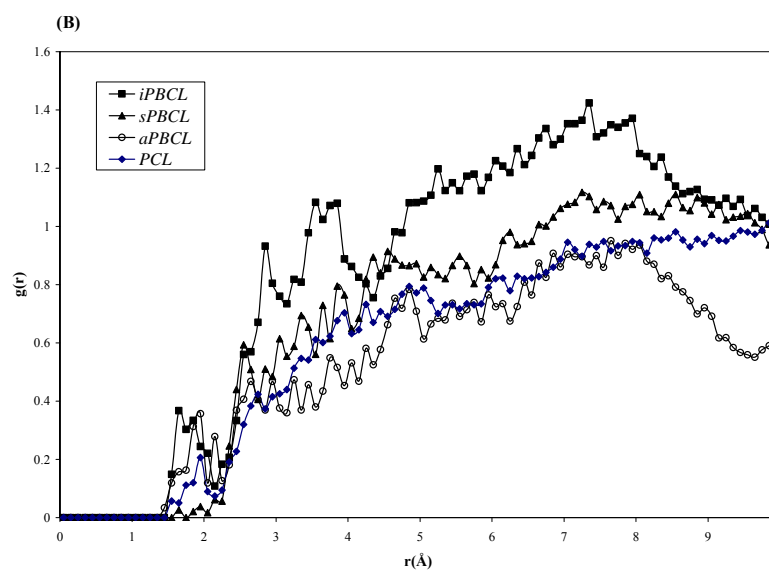


Figure 6.8(B) RDF plot of CuB drug in PEO-*b*-PBCL for Interaction No. 3.

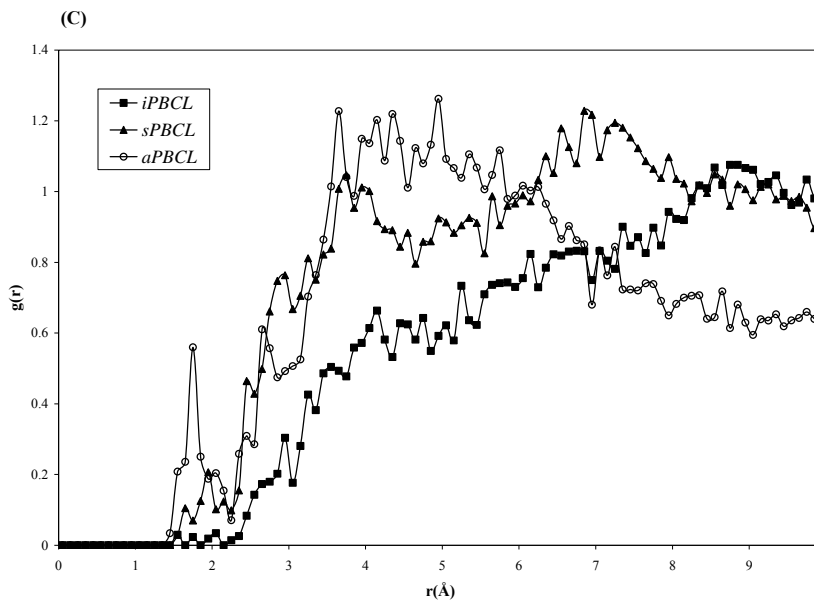


Figure 6.8(C) RDF plot of CuB drug in PEO-*b*-PBCL for Interaction No. 4.

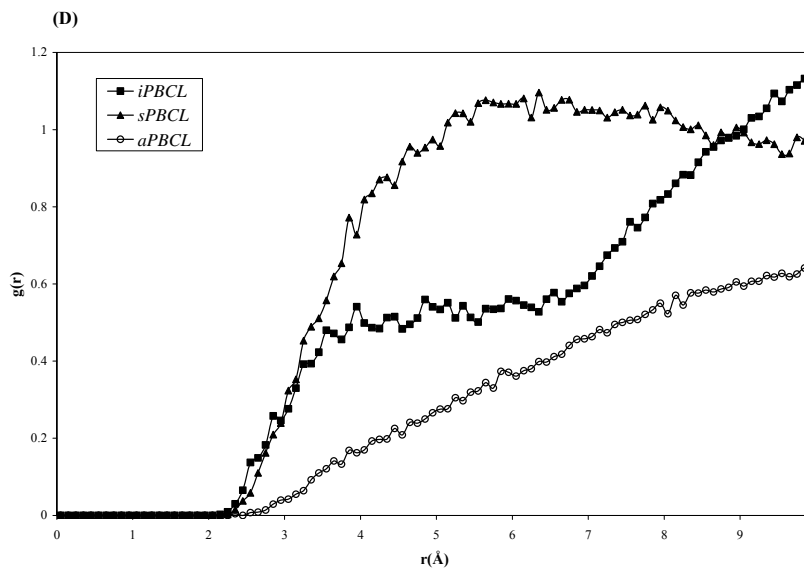


Figure 6.8(D) RDF plot of CuB drug in PEO-*b*-PBCL for Interaction No. 5.

Since the χ values of PEO-*b-s*PBCL has decreased (almost three times) as compared to that of PEO-*b*-PCL, we try to compare the correlations for interactions no. 2 and 3 between PEO-*b*-PBCL and PEO-*b*-PCL. From Figures 6.8 (A) and (B), it is clear that the correlation of CuB with H(Chain) and C=O(Chain) in PEO-*b*-PBCL is similar to those in PEO-*b*-PCL. While the correlation for the isotactic form is found to be slightly higher than the other forms of di-block copolymer. Figure 6.8 (C) shows higher correlation between CuB and C=O(Branch) for PEO-*b-s*PBCL and PEO-*b-a*PBCL. The probable reason behind this observation is more free space available for interaction with the carbonyl groups of the substituent branches in such copolymers. From Figure 6.8 (D), it is clear that for PEO-*b-s*PBCL, the correlation of CuB with the aromatic ring is a lot higher than other di-block copolymers. There are two probable reasons: (i) due to the alternating arrangement of branches in the syndiotactic version of di-block copolymer, the exposure of CuB drug is more with aromatic rings; and (ii) CuB drug is not able to pierce through the strong intra-molecular π - π interactions present in isotactic and atactic forms of the di-block copolymer. Here, π - π interactions are strong in the mixtures with CuB as compared to with CuI, as shown in Figure 6.7(B).

Comparison between CuB and CuI

Since the difference between χ values of CuB and CuI is negligible in the case of PEO-*b-i*PBCL as compared to PEO-*b-s*PBCL and PEO-*b-a*PBCL, we compare correlations for CuB and CuI drugs for the latter two cases only.

(a) PEO-*b*-sPBCL

Figures 6.9 (A) – (D) show RDF plots comparing correlations for CuB and CuI in PEO-*b*-sPBCL. Compared to CuI, CuB shows more correlations with the backbone atoms like H(Chain) and C=O(Chain) indicating its favourable interactions with them. Since the carbonyl groups present on drug molecules are responsible for favourable interactions (through hydrogen bonding) with the H atoms attached to the *activated carbon* atoms, CuB with more carbonyl groups, shows more correlation with backbone H atoms. Both drugs show almost similar correlations/interactions with the carbonyl group and aromatic rings of substituent branches (Figures 6.9 (C) and (D)).

(b) PEO-*b*-aPBCL

Figures 6.10 (A) – (D) compare RDF plots for CuB and CuI in PEO-*b*-aPBCL. In this case, both drugs show almost similar correlations with the H(Chain), while for the correlation with C=O(Chain) (Figure 6.10 (B)), the first coordination shell signified by the first peak (at ~ 1.96 Å in the present case) for CuB is absent in CuI. This first coordination shell is an indication of favourable interactions (mainly specific interactions like hydrogen bonding). Thus, Figure 6.10 (B) implies that CuB has strong favourable interactions with C=O(Chain) but not CuI. The correlations of drug molecules with C=O(Branch) is similar for both drugs (Figure 6.10 (C)). The surprising result was found for the correlation between drug molecules and aromatic rings for the present atactic form of copolymer.

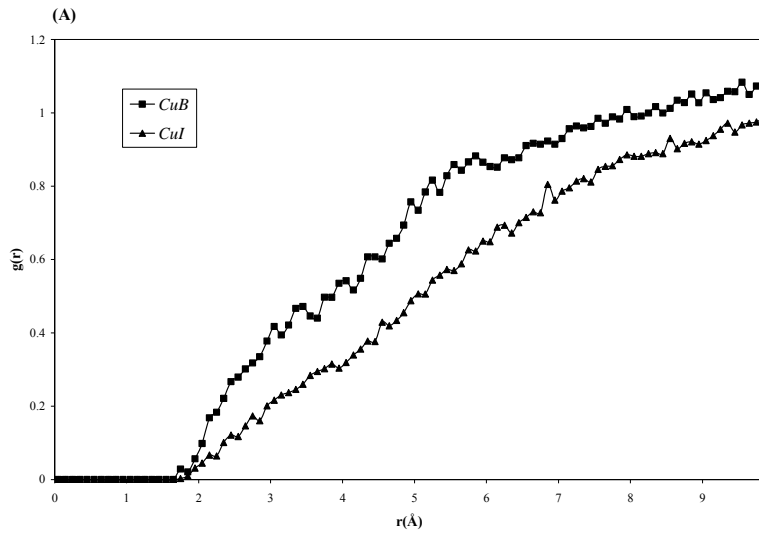


Figure 6.9(A) RDF plot of comparison of CuB and CuI drugs in PEO-*b*-sPBCL for Interaction No. 2.

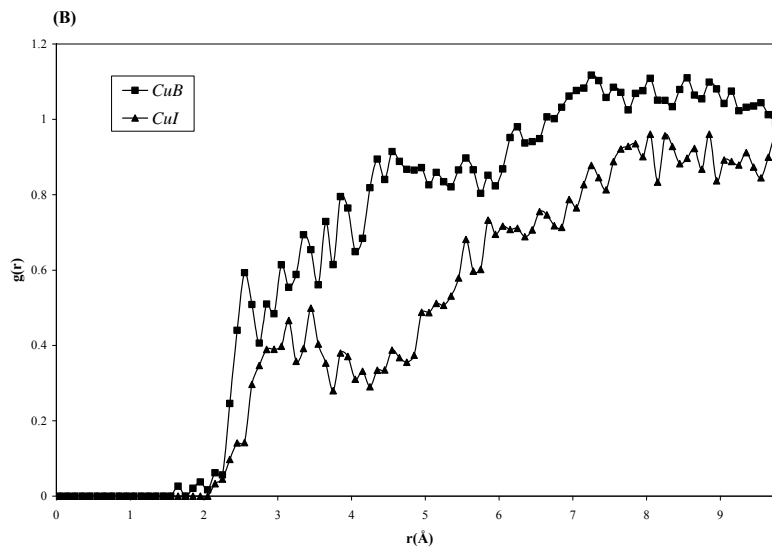


Figure 6.9(B) RDF plot of comparison of CuB and CuI drugs in PEO-*b*-sPBCL for Interaction No. 3.

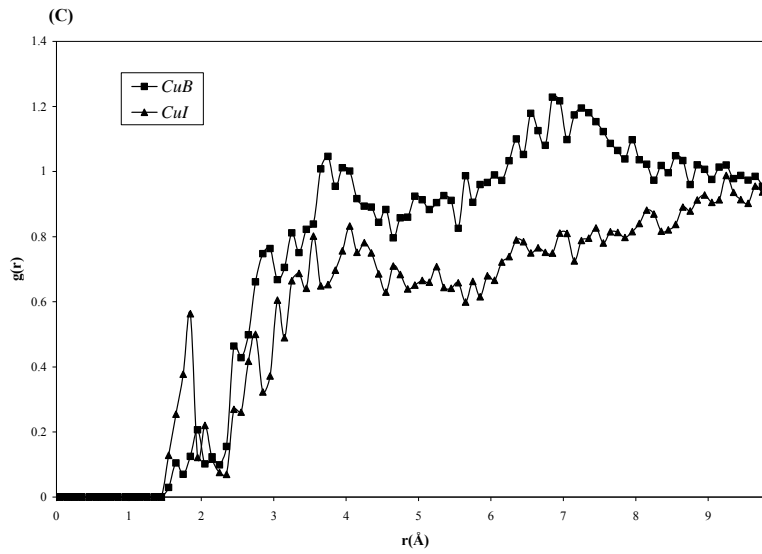


Figure 6.9(C) RDF plot of comparison of CuB and CuI drugs in PEO-*b*-sPBCL for Interaction No. 4.

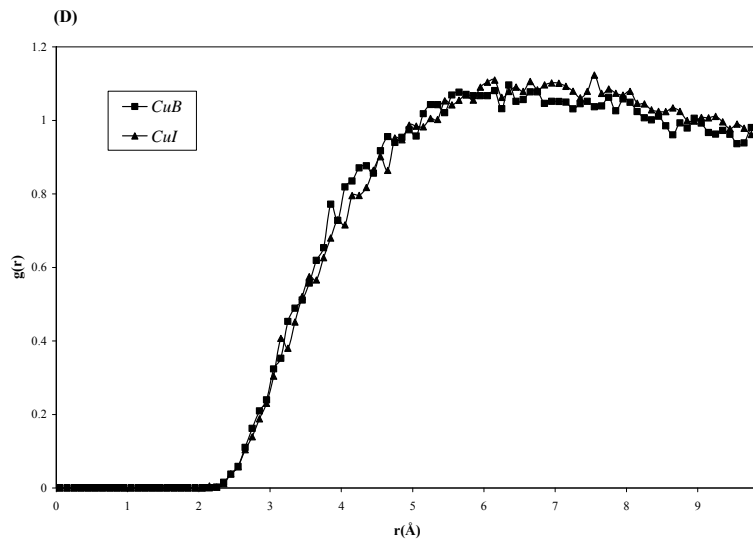


Figure 6.9(D) RDF plot of comparison of CuB and CuI drugs in PEO-*b*-sPBCL for Interaction No. 5.

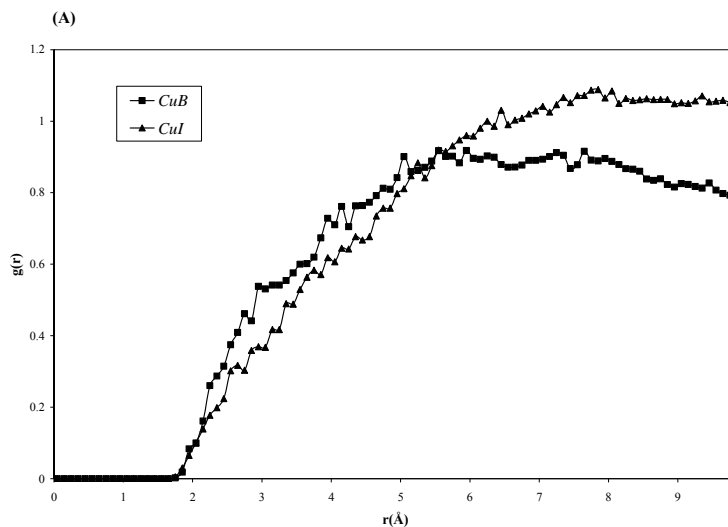


Figure 6.10(A) RDF plot of comparison of CuB and CuI drugs in PEO-*b*-*a*PBCL for Interaction No. 2.

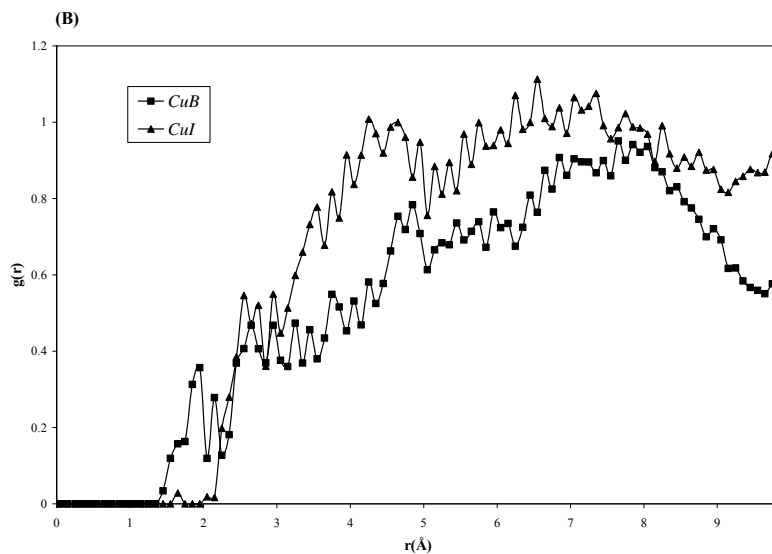


Figure 6.10(B) RDF plot of comparison of CuB and CuI drugs in PEO-*b*-*a*PBCL for Interaction No. 3.

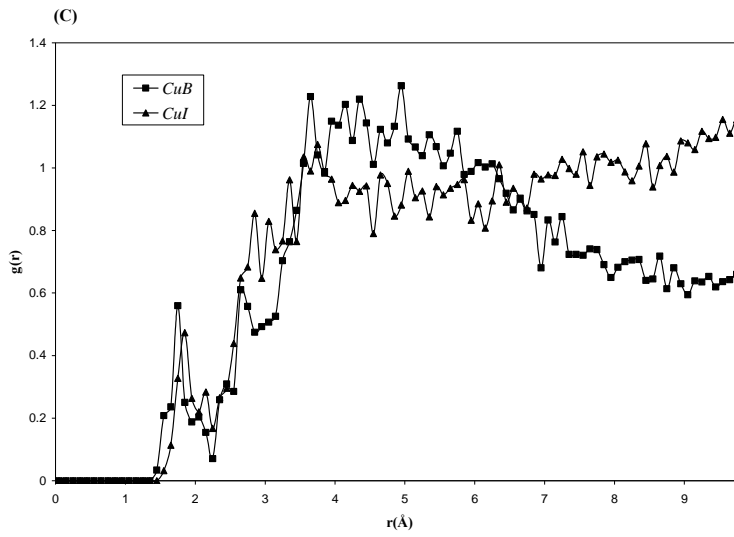


Figure 6.10(C) RDF plot of comparison of CuB and CuI drugs in PEO-*b*-*a*PBCL for Interaction No. 4.

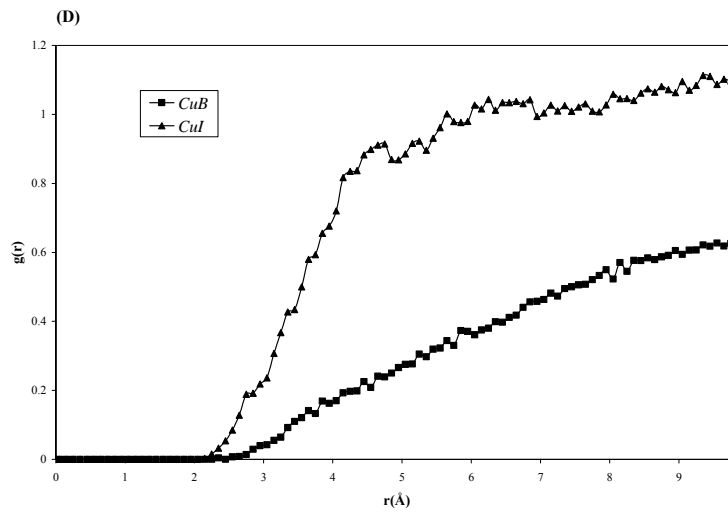


Figure 6.10(D) RDF plot of comparison of CuB and CuI drugs in PEO-*b*-*a*PBCL for Interaction No. 5.

The correlation of CuI with aromatic rings was much higher than that found in the CuB case (Figure 6.10 (D)). The probable reasons behind this surprising result will be discussed later.

The above comparison can be summarized as follows: for the PEO-*b*-*s*PBCL/drug binary mixture case, there are almost equal correlations/interactions between drugs and functional groups of substituent branches, i.e., carbonyl groups and aromatic rings. CuB shows more interactions with the backbone atoms (H(chain) and C=O(Chain)), while CuI interacts mainly with the substituent branch atoms (C=O(Branch) and aromatic rings). This is because CuI has 4 hydroxyl groups as compared to 3 in the CuB case.

For the PEO-*b*-*a*PBCL/drug binary mixture case, the intra-molecular $\pi - \pi$ interactions between aromatic rings are strong compared to the previous case and hence both drugs show almost equal and reduced interactions with the backbone atoms and carbonyl groups of branches. As stated earlier, the only surprising part was the large difference between the correlations/interactions of the drugs with the aromatic rings. CuI has much higher correlation as compared to CuB. It is evident in $\pi - \pi$ interactions graph for binary mixtures of di-block copolymers and drugs (Figure 6.7(B)) that CuI reduces intra-molecular $\pi - \pi$ interactions drastically. To find the possible reasons behind these two inter-related observations, we further examined the correlation functions of specific groups (especially hydroxyl groups) on drug molecules with aromatic rings. Here, the drug molecules could interact with the aromatic ring either by OH --- π interactions or C=O --- π interactions. Since the focus was particularly on the

intermolecular interactions between drug molecules and aromatic rings of di-block copolymer, we examined the PEO-*b*-sPBCL case, which has minimal intramolecular π - π interactions.

OH --- π interactions

Figure 6.11 shows RDF plot for the correlation between all hydroxyl ($-OH$) groups of each drug and aromatic rings of the di-block copolymer. The hydroxyl groups of CuI, having higher correlation, are in fact closer to the aromatic rings as compared to CuB. We also examined such correlations of individual $-OH$ groups on the drug molecules. Here, we adopted a numbering scheme shown in Figure 6.12 (A) and (B) to identify different groups present on drug molecules. Figure 6.13 shows RDF plots for the correlations of individual hydroxyl groups of CuI and compared them with the $-OH$ group (1) of CuB. CuIH(1) and CuIH(4) are closer to aromatic rings as compared to the other $-OH$ groups. CuIH(4), being attached to the free end of the molecule, is relatively flexible compared to other hydroxyl groups and hence it can easily adjust itself to have maximum interactions with the aromatic ring. This particular $-OH$ group is absent in CuB. The maximum correlation was observed for CuIH(1). This correlation was much higher compared to that of CuBH(1). This observation was very surprising. However, it may be attributed to the differences in the partial atomic charges on the drug molecules. Figure 6.14 (A) and (B) show structures of CuB and CuI, respectively, along with the partial atomic charges displayed on $-OH$ groups of interest.

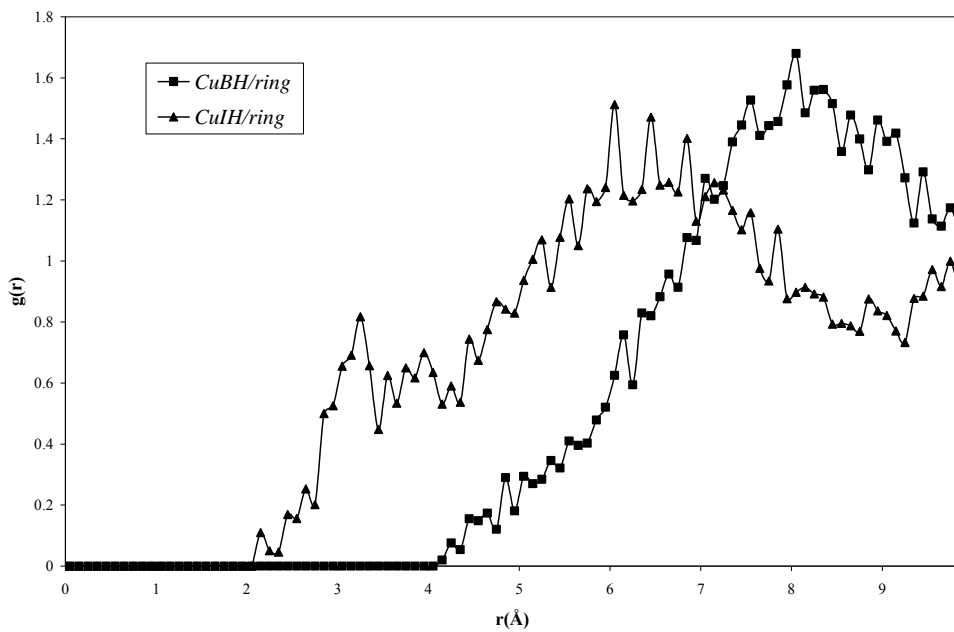
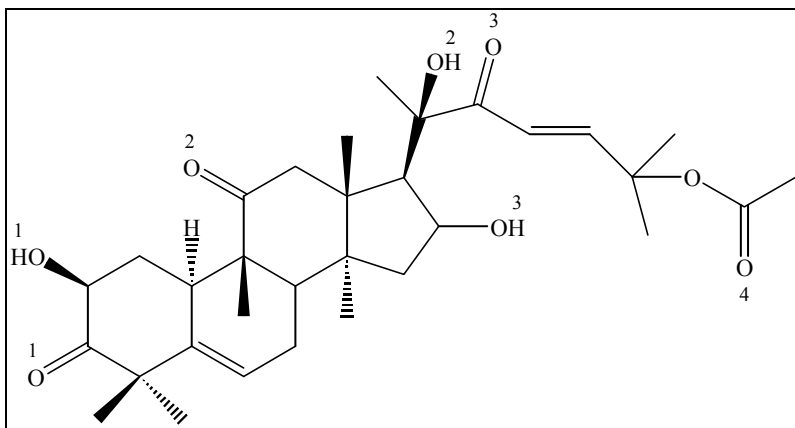


Figure 6.11 RDF plot showing the comparison of correlation between -OH groups of CuB and CuI and aromatic rings of the di-block copolymer.

(A)



(B)

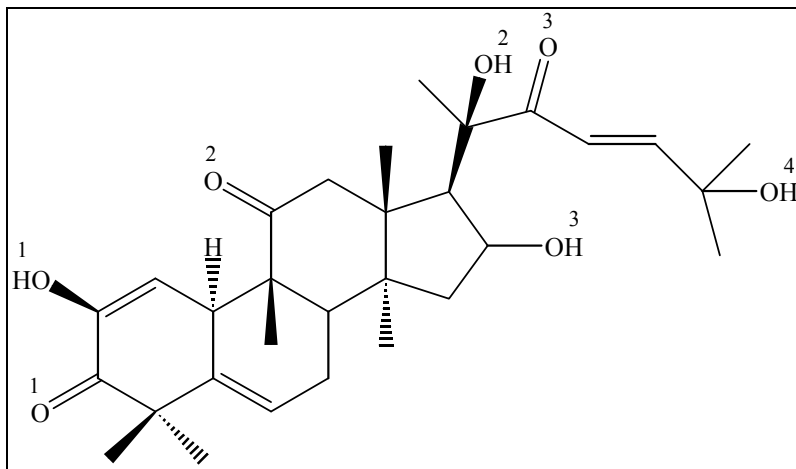


Figure 6.12 Numbering scheme of H and O atoms of Hydroxyl and Carbonyl groups in (A) CuB; and (B) CuI.

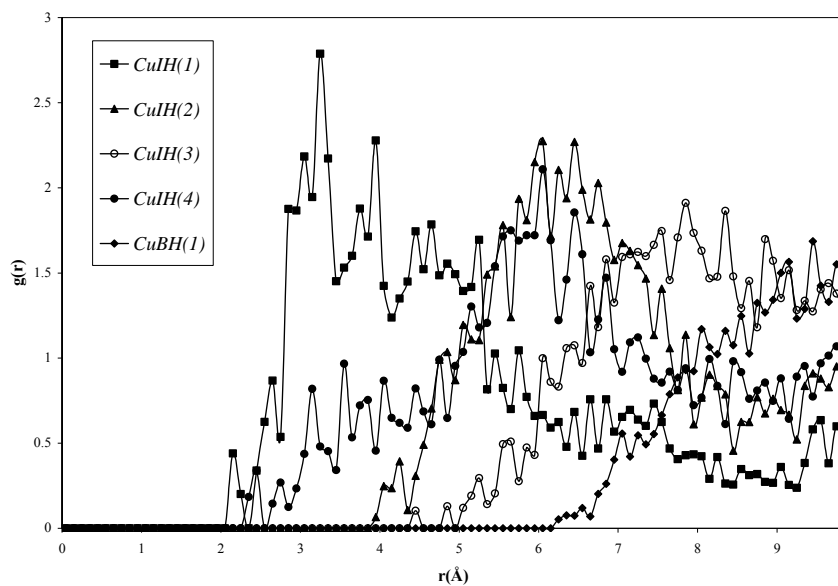


Figure 6.13 RDF plot showing correlations between all the -OH groups of CuI, the -OH(1) group of CuB and aromatic rings of the di-block copolymer.

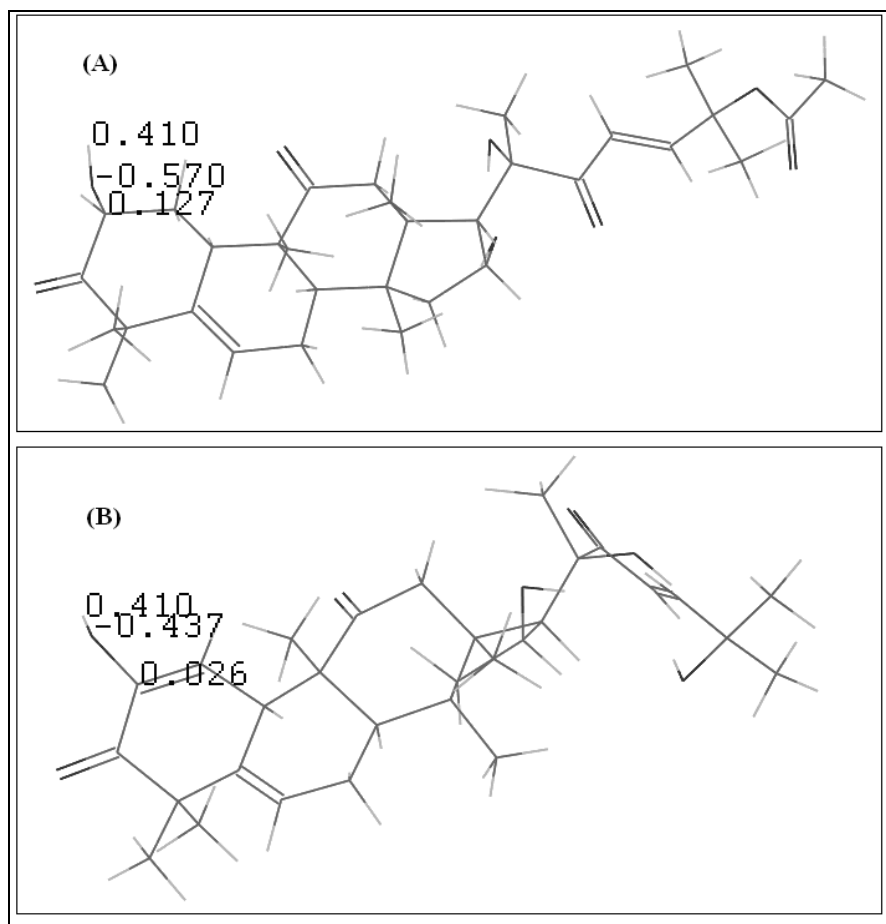


Figure 6.14 Partial atomic charges of -OH(1) group on (A) CuB; and (B) CuI.

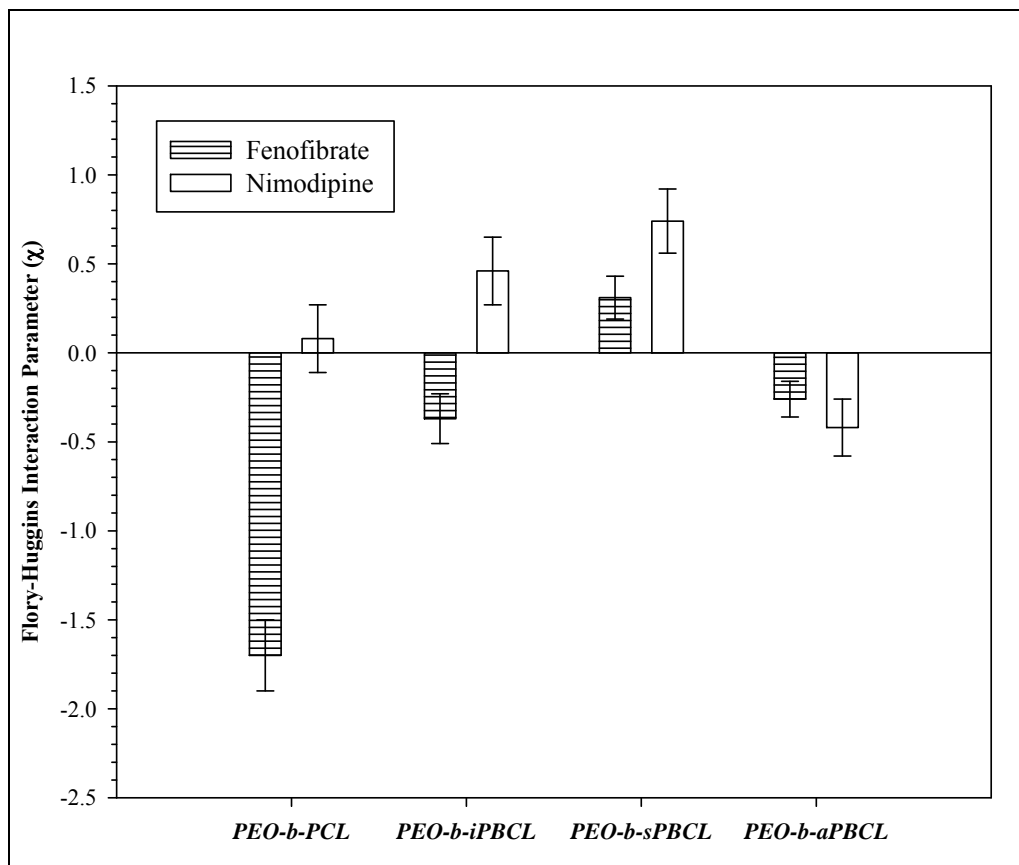
Owing to the presence of double bond near the –OH(1) group in CuI, the partial atomic charge of oxygen atom in this –OH group is less negative than that of CuB. Due to this, the electro negativity disparity of -OH(1) is different in both cases as seen in the Figure 6.14. The –OH (1) group is more polar in CuB as compared to the one in CuI. The more polar –OH bond forms strong dipole and has tendency to get attracted to other strong dipoles like carbonyl groups (-C=O) rather than engaging themselves with relatively weak OH --- π interactions. Thus, the less polar OH(1) group of CuI will have favourable interactions with the aromatic ring while OH(1) group of CuB will have favourable interactions with the carbonyl groups. All the above factors contribute towards higher correlation of CuIH with the aromatic ring. Moreover, CuI interacts mostly through –OH groups with π electrons of the aromatic ring while CuB interacts through carbonyl groups –C=O with the edges (-CH) of aromatic ring.

In general, from the above RDF plots, we found that for drugs like CuB and CuI, with multitude of hydroxyl and carbonyl groups, to be miscible in functionalized block copolymers, the drugs need to interact not only with the substituent branches but also with the backbone atoms (in the form of multiple hydrogen bonding with backbone atoms). These intermolecular associations in the mixture of drug/copolymer largely depends on the strength of intra-molecular π - π interactions between aromatic rings of pure di-block copolymer. MD simulation is a powerful tool to predict this interplay of intra and inter molecular interactions.

6.3.2 PEO-*b*-PBCL/Fenofibrate & Nimodipine Drugs

The simulation procedures were similar to the one described earlier in the Section 6.3.1.1, except that the simulation temperature was 413 K. The computed χ values are plotted in Figure 6.15. Again, we have compared the χ values of the current systems, viz., PEO(2500)-*b*-PBCL(2500) with those of PEO(2500)-*b*-PCL(2500) (Chapter 4).

It is clear from Figure 6.15 that none of the tactic forms of PEO-*b*-PBCL shows a significant decrease in χ values when compared to the case of unfunctionalized block copolymer (PEO-*b*-PCL). In other words, the presence of substituent branches of α -benzyl carboxylate groups on the hydrophobic block does not favour the process of encapsulation for fenofibrate and nimodipine drugs. On the other hand, the syndiotactic version of PEO-*b*-PBCL was more compatible with cucurbitacin drugs compared to PEO-*b*-PCL (Section 6.3.1). We believe that differences in molecular characteristics of both sets of drugs are responsible for such an observation. In particular, cucurbitacin drugs contain multiple H-bond donors and acceptors while fenofibrate and nimodipine drugs contain only H-bond acceptors. As discussed previously in the Section 6.3.1, the substituent branches containing only H-bond acceptors (i.e., -C=O(Chain) and Aromatic rings) were able to interact favourably with H-bond donors (e.g., -OH groups) present on drug molecules (i.e., through Interaction No. 4 and 5 listed in Table 6.3).



*Data are means. Bars are standard errors

Figure 6.15 Plot of the computed χ values of binary mixtures of fenofibrate and nimodipine and three tactic forms of PEO-*b*-PBCL compared with the data for PEO-*b*-PCL.

Owing to the absence of H-bond donors on Set-II drug molecules, they are not able to establish favourable interactions like Interaction No. 3, 4, and 5 (Table 6.3) with the di-block copolymer which were found to be important in enhancing the solubility of cucurbitacin drugs. The only intermolecular interaction that can be established between drugs and di-block copolymers is Interaction No. 2 (i.e., Drug---H(Chain)). But, before establishing this interaction, the drug molecules need to overcome the existing intra-molecular interactions (e.g., π - π and π - H(Chain) interactions) by establishing Interaction No. 4 and 5 with the substituent branches which are essentially absent in this set of drugs. Due to this, we also expect to see less interaction of these drugs with the hydrogen atoms of PCL block (H(Chain)). To confirm this, we perform RDF analysis between drug molecules and H(Chain) atoms of hydrophobic block and H-atoms of PEO block. Figures 6.16 and 6.17 compare such correlations with that in the system of PEO-*b*-PCL. It is clearly evident from this RDF analysis that the correlations of fenofibrate and nimodipine drugs has decreased with the H-atoms of PBCL block and increased with the H atoms of PEO block when compared with the case of PEO-*b*-PCL. Hence, owing to the unfavourable interactions with the substituent branches, we observe less correlation of these drugs with PBCL block which, in turn, is responsible for higher χ values for such systems.

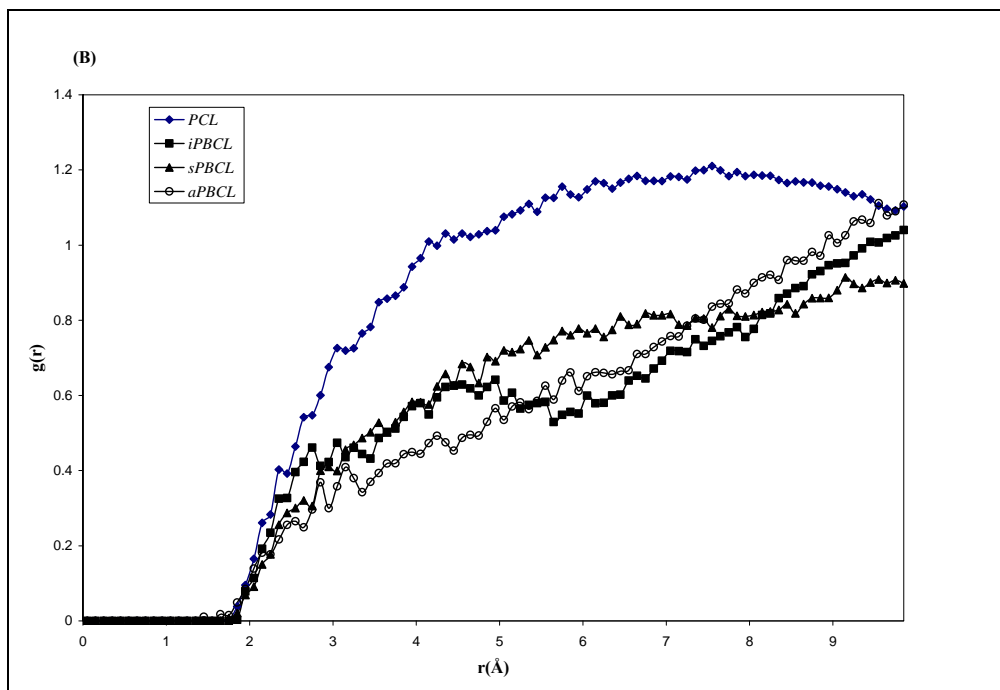
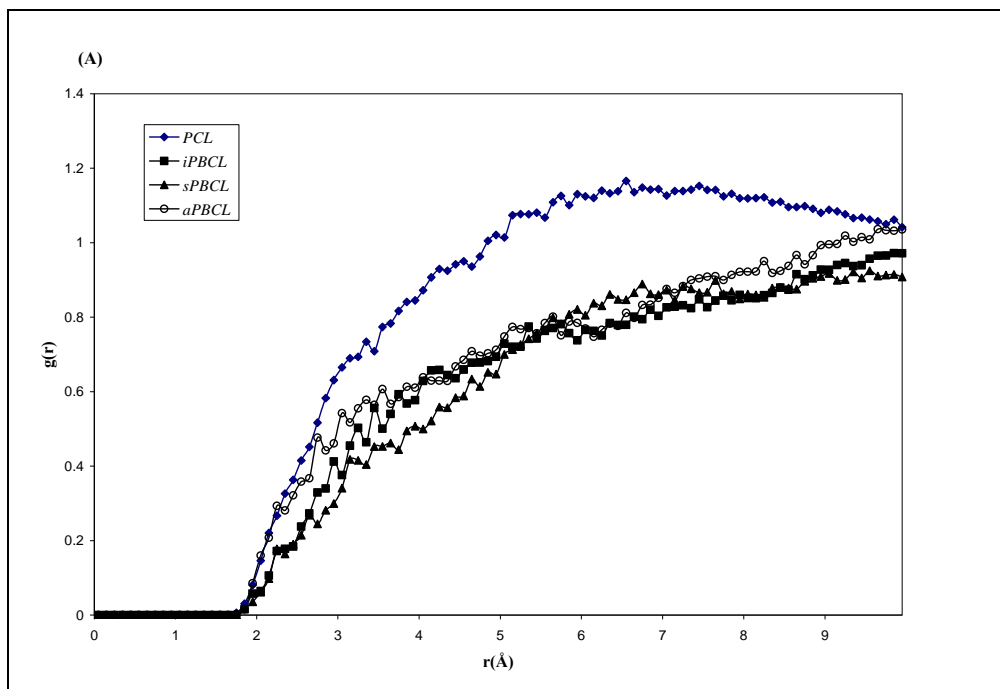


Figure 6.16 RDF plot showing correlation of H(Chain) atoms with (A) Fenofibrate; and (B) Nimodipine.

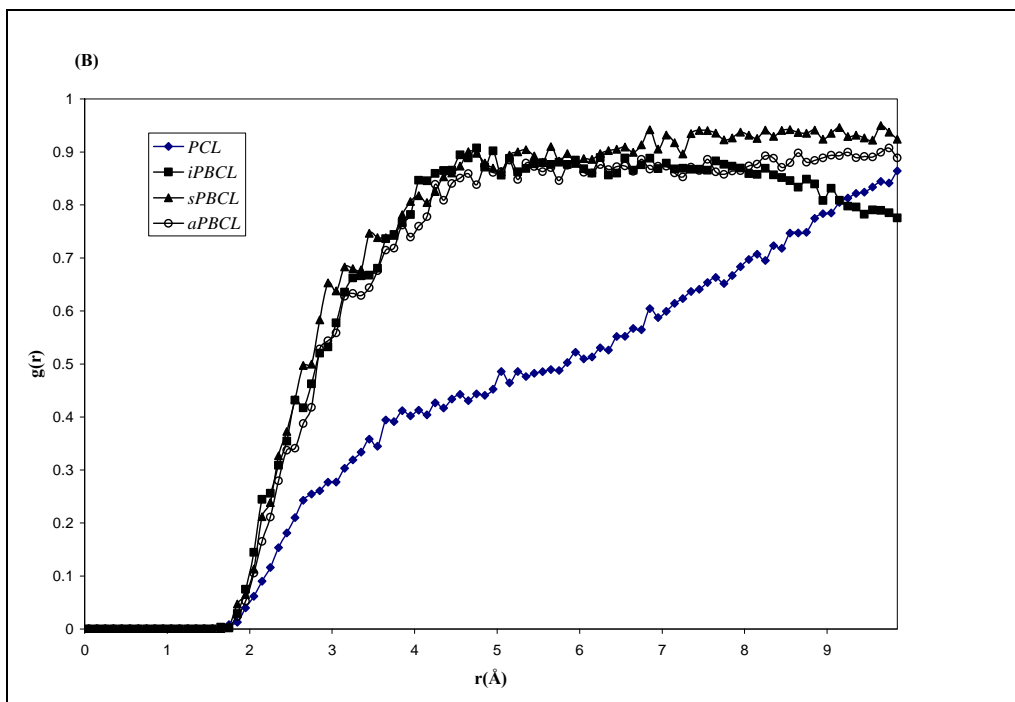
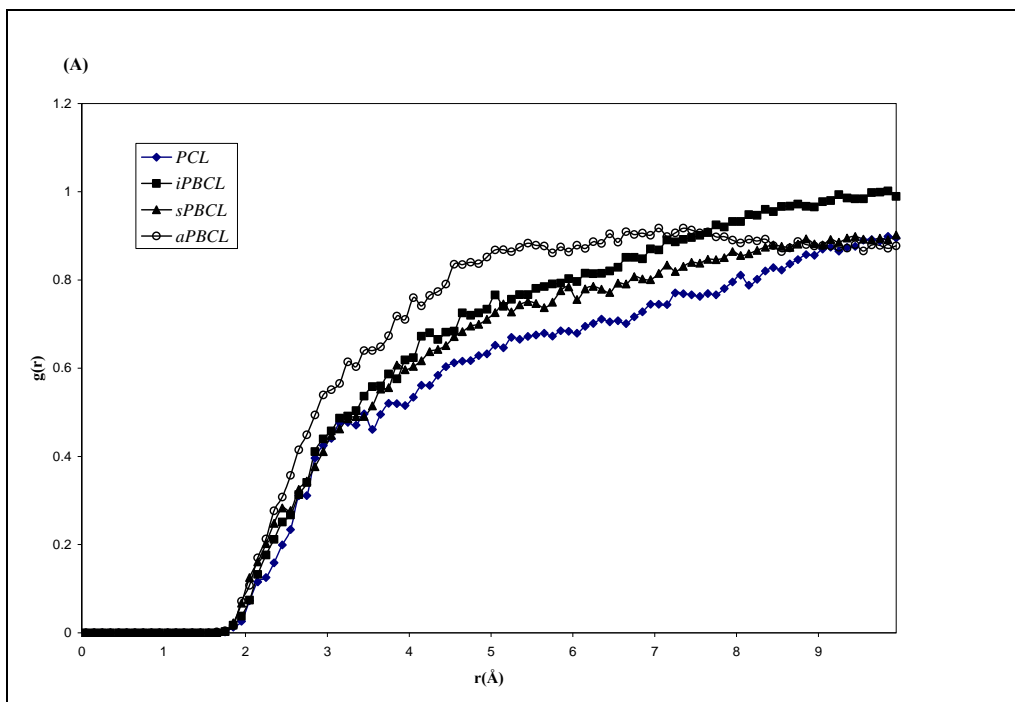


Figure 6.17 RDF plot showing correlation of H atoms of PEO block with (A) Fenofibrate; and (B) Nimodipine.

6.4 Summary

Finally, we shall conclude this study with the following comments. MD simulation approach was used to compute the χ parameters for the binary di-block copolymer/drug mixtures formed by two sets of hydrophobic drugs (Set-I (CuB and CuI) and Set-II (fenofibrate and nimodipine)) and PEO-*b*-PBCL with three different tacticities viz. PEO-*b-i*PBCL, PEO-*b-s*PBCL, and PEO-*b-a*PBCL. For comparing our simulation results, the experimental data were only available for the system of binary mixtures of PEO-*b*-PBCL/Set-I drugs. Hence, we validated and established the current method firstly on this system and then later extended it to another system of binary mixtures of PEO-*b*-PBCL/Set-II drugs.

Based on the study performed on cucurbitacin drugs, it was found that only the χ values for binary mixtures containing PEO-*b-s*PBCL agree with the experiment. In particular, the χ values of two other stereo isomers of PEO-*b*-PBCL are even much higher than those of the mixtures containing PEO-*b*-PCL. The results suggest that the syndiotactic configuration is the ideal stereo isomer for inducing the miscibility between these drugs and the PEO-*b*-PBCL. The strength of the intra-molecular π - π interactions was found to be dependent on stereo configurations of di-block copolymers. In order to induce the miscibility in drug/copolymer mixture, intermolecular associations/interactions need to be established through specific interactions which aid in achieving negative values of heats of mixing and hence negative χ values. The formation of such intermolecular specific interactions is largely hindered by the presence of intra-molecular π - π interactions. Hence, the syndiotactic version of the di-block

copolymer which exhibits minimal $\pi - \pi$ interactions succeeds in establishing favourable intermolecular specific interactions between the drug molecules and the di-block copolymer.

On the other hand, none of the tactic forms of PEO-*b*-PBCL showed a potential in encapsulating Set-II drugs consisting of fenofibrate and nimodipine drugs which contain only clustered H-bond acceptors. It is believed that the absence of H-bond donors on these drugs restricted their interaction with the substituent branches of the hydrophobic block. Consequently, the strong intramolecular interactions existing in pure di-block copolymers could not be overcome which, in turn, led to increased χ values in such binary mixture systems.

Chapter 7

Encapsulation Capability of a Multi-block Copolymer Containing Three PCL Blocks Connected to One End of a PEO Block⁴

7.1 Introduction

It was evident from the study described in Chapter 5 that polar interactions between drug and the entire block copolymer play important roles in enhancing the drug loading capacity in a given polymeric carrier. In addition, the extent of drug solubilisation by a block copolymer based carrier was found to be dependent on the intra- as well as intermolecular interactions of the copolymer chains (Chapter 6). The purpose of the present study was to apply the MD simulation strategy developed so far to examine the potential of using a multi-block copolymer with three PCL blocks connected to one end of a PEO block (designated as PEO-*b*-3PCL, see Figure 7.1) in encapsulating two sets of hydrophobic drugs with distinctively different molecular structures.

⁴ A version of this chapter has been accepted for publication. Patel, S.K.; Lavasanifar, A.; Choi, P. (2009). *Biomaterials*. **Article in Press**, doi:10.1016/j.biomaterials.2009.11.060.

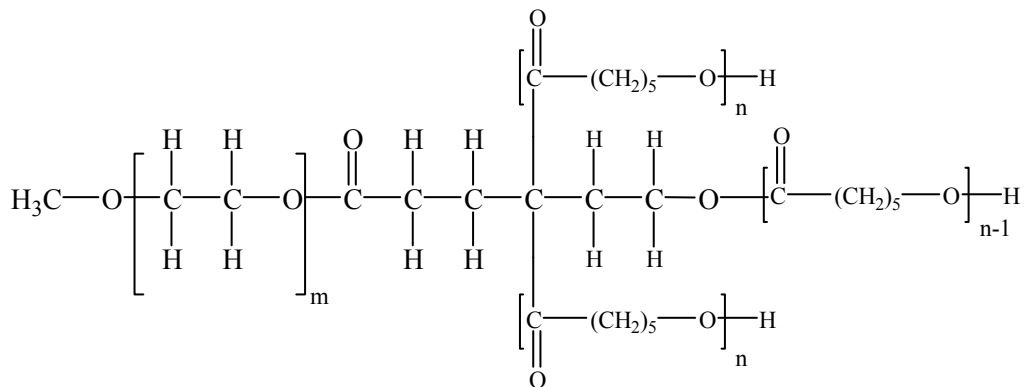


Figure 7.1 Chemical Structure of PEO-*b*-3PCL.

The reason for choosing the multi-hydrophobic block architecture is that such architecture is expected to contain a higher concentration of H-bond donors because the radius of gyration of three PCL blocks would be lower than that of a linear PCL with equivalent molecular weight. It is worth noting that as demonstrated in Chapter 5, increase in the drug loading capacity of PEO-*b*-PCL with higher PCL/PEO (w/w) ratios is attributed to the presence of multiple hydrogen bond donors on the PCL block (hydrogen atoms connected to the *activated carbons*).

The Set-I drugs used in the present work consisted of cucurbitacin drugs (CuB and CuI (Figure 5.1(A) and (B))) that contain multiple H-bond donors and acceptors in their structures, while the Set-II drugs, fenofibrate and nimodipine (Figure 4.1(B) and (C)), contain only clustered hydrogen bond acceptors. The results of PEO-*b*-3PCL will then be compared with results of the linear di-block copolymer PEO-*b*-PCL with the same PCL/PEO (w/w) ratio of 1 reported in Chapters 4 and 5. Binary liquid mixtures containing a drug and PEO-*b*-3PCL at 10 wt% of drug were used to determine their corresponding χ parameters, which will in turn help to infer the drug solubility. The present study also serves as the first attempt to provide an atomistic understanding of the differences in the drug encapsulation mechanisms of the multi-block copolymer-based carriers compared to those of the linear di-block copolymers with comparable molecular weights.

7.2 Model Building and Simulation Methodology

The model multi-block copolymer was generated by connecting three PCL blocks, each having a molecular weight of 800 g/mol, to one end of a PEO block having molecular weight of 2500 g/mol as shown in Figure 7.1. We designate this block copolymer as PEO(2500)-*b*-3PCL(2400), where the number in bracket signifies the molecular weights of the corresponding block(s). The initial liquid state structure of PEO-*b*-3PCL was generated based on the rotational isomeric state (RIS) theory [81, 82] using the amorphous builder module in commercially available software Cerius² from Accelrys. All MD simulations reported here were performed using another commercially available software package Materials Studio (MS Modeling version 4.2, Accelrys) run on a Silicon Graphics (SGI) workstation cluster. The COMPASS force field [62] was used to model the intra- and intermolecular interactions. Detailed description of this force field can be found in Section 3.3. The procedures of constructing initial liquid state models are very similar to those described in the Chapter 4.

The density values of the pure multi-block copolymer and drugs at two simulation temperatures (413 K and 473 K) were determined by performing isobaric-isothermal (NPT) MD simulations ($P = 1 \text{ atm}$; $T = 413 \text{ K} \ \& \ 473 \text{ K}$). Owing to the differences in the melting temperatures of the drugs of interest, 413 K was used for the binary mixtures containing fenofibrate and nimodipine drugs, while 473 K was chosen for those containing CuB and CuI drugs. These temperatures were selected so that results can be compared directly to our previous studies (Chapters 4 and 5). The pressure and temperature of the systems

are controlled using Andersen barostat [72] and Nose Thermostat [69] algorithms, respectively. The densities of binary mixtures of multi-block copolymer and drugs (10 wt% drug concentration) were calculated based on the densities of the pure components with the assumption of no volume changes on mixing. These mixture and pure substance density values were used in the subsequent canonical (NVT) MD simulations to determine the χ parameters.

Due to the fact that the simulation times normally is insufficient for systems such as polymers in the amorphous state to undergo very drastic reorientation and relaxation, it is crucial that the initial state of system of the multi-block copolymer to be as close to the equilibrated state as possible. This was why the RIS theory was used. The distribution of torsion angles was determined by applying the Boltzmann weighting factor to the energies of the RIS minima. The initial distribution of torsion angles for the PEO block of PEO-*b*-3PCL is the same as that of the PEO block in the PEO-*b*-PCL di-block copolymer, but in the case of the three PCL blocks, they are different from that of the corresponding di-block copolymer. Here, we identified a total of nine torsion angles for PEO-*b*-3PCL and they are depicted in Figure 7.2. In Table 7.1, we list the values of RIS minima and the respective tolerances for all nine torsion angles that have significant influence on the conformation of the multi-block copolymer. Once the RIS state distribution was determined, the RIS states were populated allowing for the angle tolerances stated in Table 7.1.

All initial amorphous structures were subjected to energy minimization step using the conjugate gradient method, before performing MD simulations.

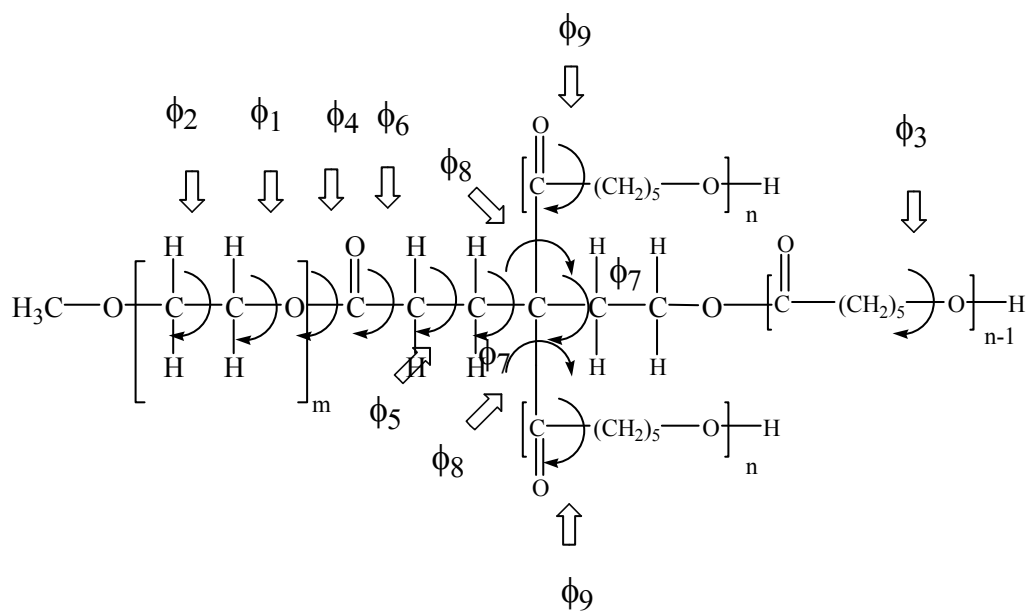


Figure 7.2 Schematics of all torsion angles identified in PEO-*b*-3PCL.

Table 7.1 Rotational isomeric states for all torsion angles of PEO-*b*-3PCL.

Skeletal Bond	State 1*	State 2*	State 3*	State 4*
Φ_1	170 ± 20	300 ± 10	330 ± 10	N/A
Φ_2	40 ± 10	60 ± 10	280 ± 10	350 ± 10
Φ_3	270 ± 10	290 ± 10	330 ± 10	N/A
Φ_4	130 ± 10	300 ± 10	N/A	N/A
Φ_5	70 ± 15	180 ± 10	230 ± 5	N/A
Φ_6	60 ± 10	240 ± 15	N/A	N/A
Φ_7	200 ± 5	N/A	N/A	N/A
Φ_8	140 ± 5	N/A	N/A	N/A
Φ_9	60 ± 5	170 ± 5	N/A	N/A

*Data are Torsion angle \pm Tolerance

NVT MD simulations were carried out at 473 K and 413 K for Set-I and Set-II drugs, respectively. The velocity Verlet method, with a time step of 0.001 ps, was used as an integrator in all simulations. The non-bonded dispersive interactions were evaluated using atom based cut-off distance of 9.50 Å with a spline width of 1 Å, while the long-range electrostatic interactions especially important in three-dimensional periodic systems were evaluated using the well-known Ewald summation method [67]. Long-range tail corrections were applied to the non-bonded interactions during MD simulations. Each simulation was carried out for a total of 2000 ps. The properties of interest (e.g., the total energy) were calculated by averaging over the last five hundred ps of the corresponding trajectory file. Here, we adopted the MD simulation approach in which the internal energy changes on mixing were calculated and then used to obtain χ parameters for the drug/multi-block copolymer pairs of interest (Equations (4.5) and (4.6)).

7.3 Results and Discussion

Table 7.2 summarizes the computed density values for PEO(2500)-*b*-3PCL(2400), CuB, CuI, fenofibrate, nimodipine and their binary mixtures (10 wt% drug) at a pressure of 1 atm and two simulation temperatures (413 K and 473 K). The density values of the binary mixtures were calculated using those of the pure components obtained from the corresponding MD simulations. Here, it is assumed that the volume change of mixing is negligible.

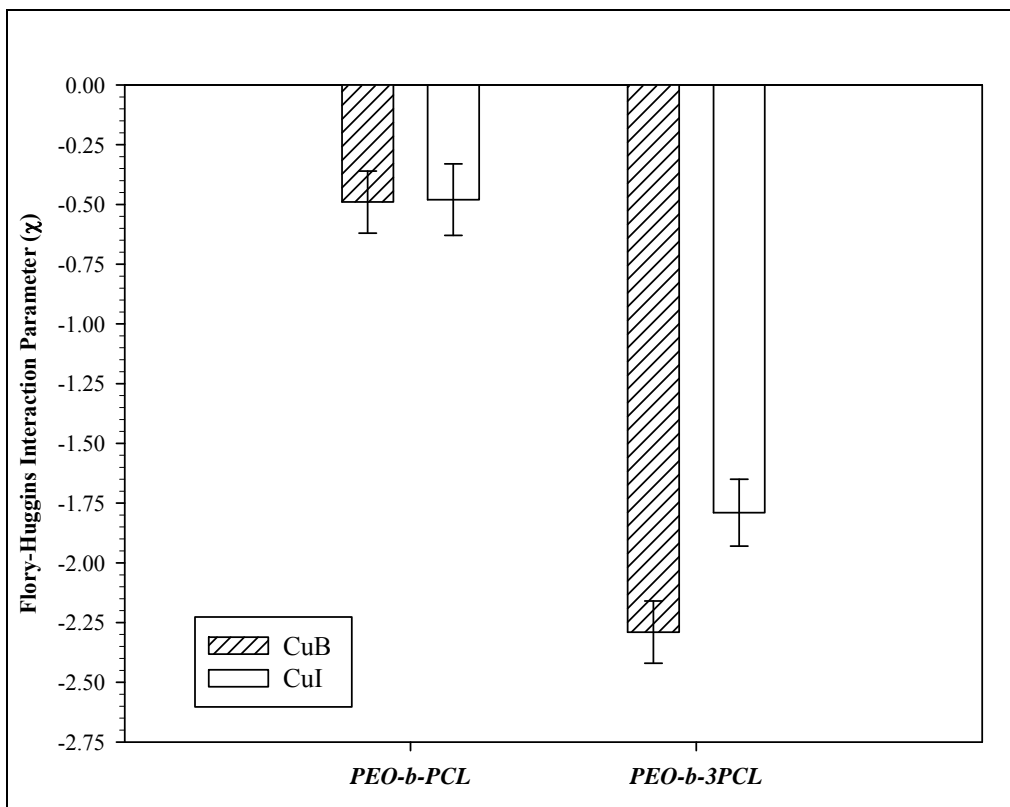
Table 7.2 Liquid density values of CuB, CuI, Fenofibrate, Nimodipine, PEO(2500)-*b*-3PCL(2400) and of their binary mixtures (10 wt% drug) computed at 1 atm and two temperatures (473 K and 413 K).

Temperature (K)	Drug/Block Copolymer/Mixture	Density (g/cm³)	No. of Drug Molecules	No. of Block Copolymer Chains
473	Cucurbitacin B (CuB)	1.15	-	-
	Cucurbitacin I (CuI)	1.12	-	-
	PEO- <i>b</i> -3PCL (P)	1.08	-	1
	CuB & P	1.10	1	1
	CuI & P	1.09	1	1
413	Fenofibrate (F)	1.12	-	-
	Nimodipine (N)	1.07	-	-
	PEO- <i>b</i> -3PCL (P)	1.10	-	1
	F & P	1.10	2	1
	N & P	1.09	1	1

χ parameters of all the aforementioned binary mixtures were then computed using the MD simulation strategy described in previous chapters. In particular, the mean potential energies of the bulk liquid states of the pure multi-block copolymer, of the pure drugs and of their binary mixtures were calculated by time averaging the potential energy of the corresponding trajectories over the last 500 ps at an equal interval of 2 ps.

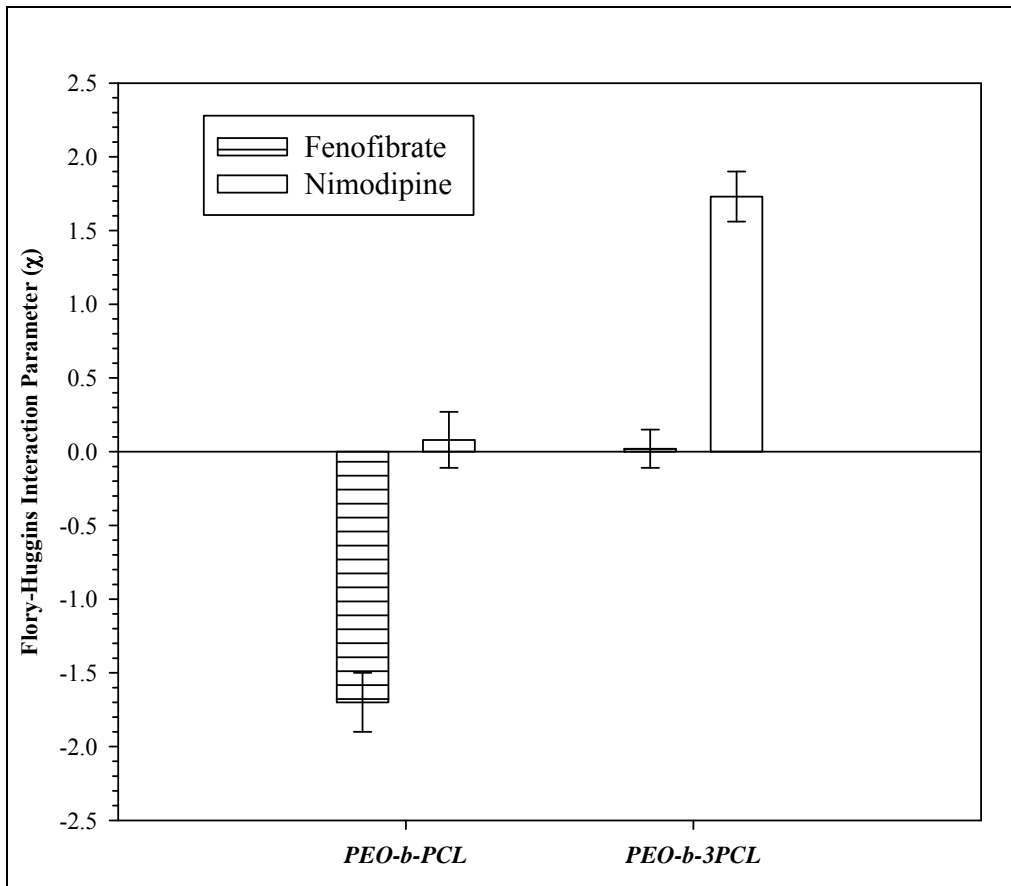
The computed χ values are plotted in Figures 7.3 and 7.4. The error bars shown in the figures are ensemble fluctuations and were also determined using the data of the last 500 ps of the corresponding MD trajectories. According to the Flory-Huggins solution theory, the lower the χ , the higher the affinity between the components, thereby better solubility of one component into the other. Since the solubility prediction from simulation is based on the qualitative trend of the computed χ values of different systems, we have compared the four χ values of the current systems containing PEO(2500)-*b*-3PCL(2400) with those of previously reported for PEO(2500)-*b*-PCL(2500) (Chapters 4 and 5).

Figure 7.3 clearly shows that the χ values of the mixtures composed of cucurbitacin drugs and PEO-*b*-3PCL are approximately four times more negative than those containing PEO-*b*-PCL with roughly the same PCL/PEO (w/w) ratio of 1.0. On the other hand, χ values of the binary mixtures containing other set of drugs (i.e., fenofibrate and nimodipine) and the multi-block copolymer are about two times more positive than those containing the linear di-block copolymer (Figure 7.4).



*Data are means. Bars are standard errors

Figure 7.3 Plot of the computed χ values of binary mixtures of cucurbitacin (Set-I) drugs and PEO-*b*-3PCL along with the data for PEO-*b*-PCL.

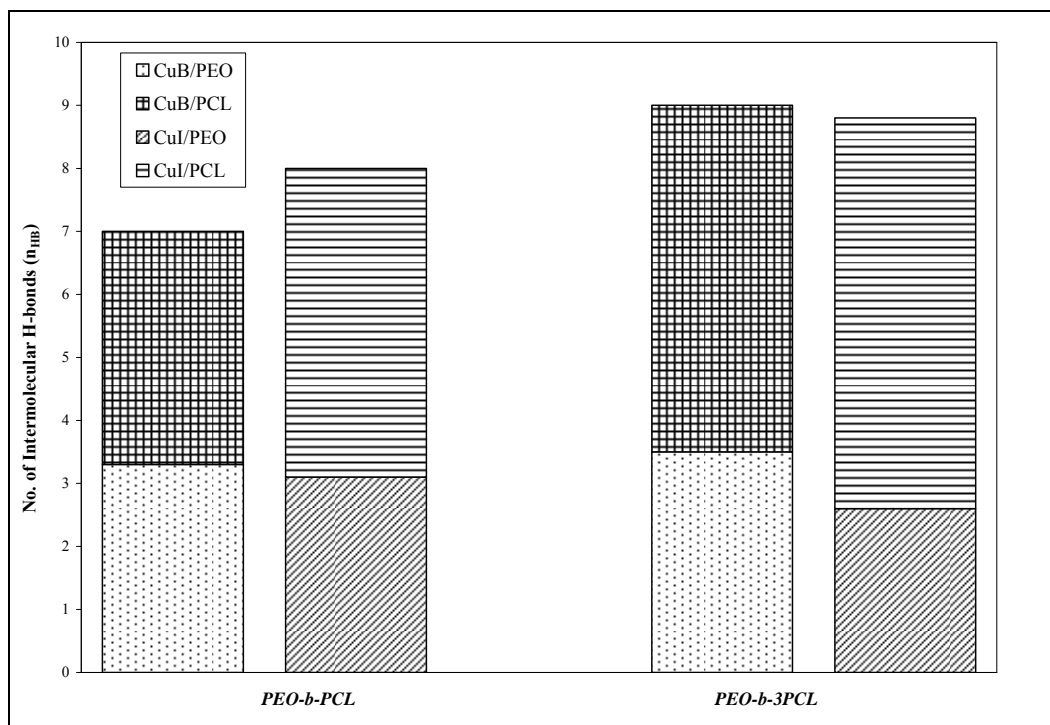


*Data are means. Bars are standard errors

Figure 7.4 Plot of the computed χ values of binary mixtures containing PEO-*b*-3PCL and fenofibrate and nimodipine (Set-II) drugs along with the data for PEO-*b*-PCL.

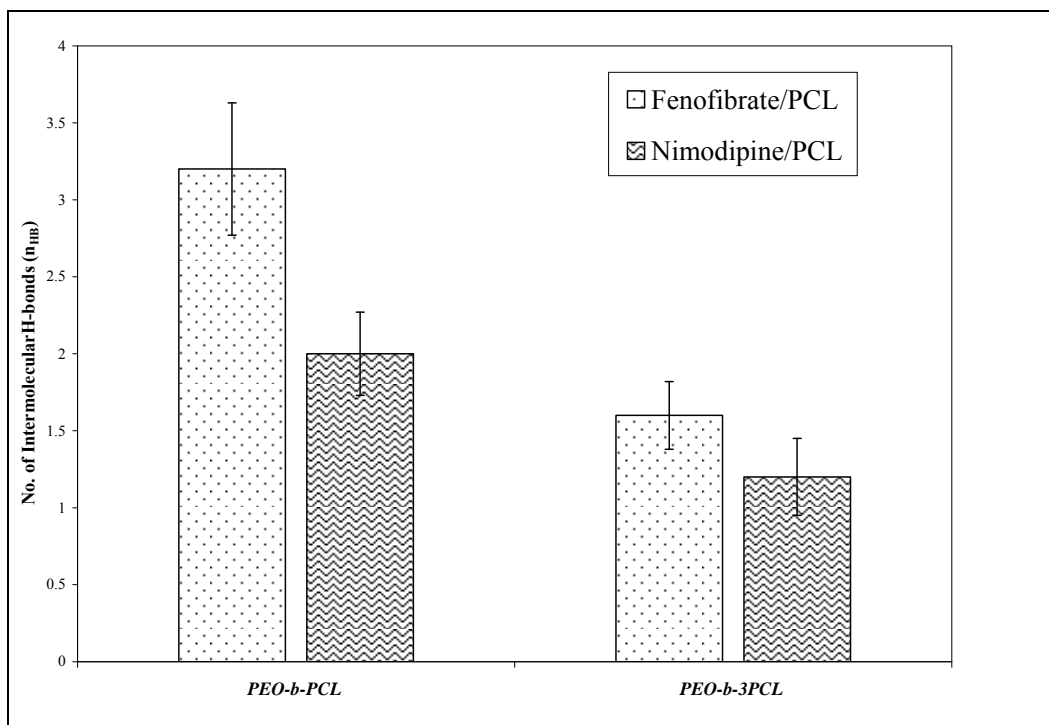
This suggests that PEO-*b*-3PCL is much more compatible with the first set of drugs compared to its linear counterpart, but it is not the case for fenofibrate and nimodipine. Hence, depending on the set of hydrophobic drugs, we may observe increase or decrease in the encapsulation capability of the multi-hydrophobic block architecture when compared to that in the linear architecture. The following data analysis addresses the above observation.

It has been shown in our previous work (Chapter 5) that the formation of more H-bonds between drugs and the H-bond donors (hydrogen atoms connected to the *activated carbons*) on the PCL block is responsible for the increase in the drug loading capacity of PEO-*b*-PCL with higher PCL/PEO (w/w) ratios. In the present case, the multi-hydrophobic block architecture would contain a higher concentration of H-bond donors because the radius of gyration of three PCL blocks is lower than that of a linear PCL with equivalent molecular weight. Since both sets of drug molecules contain comparable numbers of H-bond acceptors (See Figures 4.1(B), (C) and 5.1 (A), (B)), it is expected that additional intermolecular H-bonds would form between both sets of drugs and PEO-*b*-3PCL. To determine whether this is the case, we determined the average number of intermolecular H-bonds formed for all four binary mixtures based on the geometric definition of H-bond of Bertolini *et al.* and Geiger *et al.* [97, 98] described in Section 5.3.3. Figure 7.5 shows the results for cucurbitacin drugs along with the previous reported data for linear di-block PEO-*b*-PCL while Figure 7.6 shows the same quantities for fenofibrate and nimodipine drugs.



*Standard errors are in the range of 0.37 to 0.75 with the maximum error(i.e, 0.75) associated with the bar of PEO-b-3PCL/CuI

Figure 7.5 Plot showing the total number of intermolecular H-bonds formed by CuB and CuI with the PEO-*b*-3PCL in the form of sum of contributions from H-bond with PEO and PCL blocks.



*Note: No H-bonds were formed between drug molecules and PEO blocks of the block copolymers.

Figure 7.6 Plot showing the total number of intermolecular H-bonds formed by fenofibrate and nimodipine drugs with the PCL blocks of the PEO-*b*-PCL and PEO-*b*-3PCL.

Here, the average values and errors associated with the number of H-bonds were calculated based on the time averages of the last 200 ps of the trajectory files. It is clear from Figure 7.5 that the increase in the average total number of H-bonds from PEO-*b*-PCL to PEO-*b*-3PCL is attributed to the additional H-bonds formed between cucurbitacin drugs and the PCL blocks in PEO-*b*-3PCL. Here, the number of H-bonds formed between the drugs and the PEO block remains unchanged. On the other hand, fenofibrate and nimodipine exhibit a completely opposite trend as depicted in Figure 7.6. One of the reasons is the absence of H-bond donors on the molecules of such drugs (nimodipine contains a very weak H-bond donor) which makes them not able to interact with H-bond acceptors (e.g., carbonyl groups) present on the PCL blocks that was found to be important in enhancing solubility of cucurbitacin drugs (Chapter 5). Nevertheless, as discussed above, the concentration of H-bond donors on the multi-hydrophobic block architecture is higher than that of the linear architecture with equivalent molecular weight; the decrease in the number of H-bonds in the cases of fenofibrate and nimodipine was somewhat unexpected. Thus, a further investigation on the H-bonds formed between them and the PCL blocks was carried out.

To examine the H-bonds formed between the H-bond acceptors on drug molecules (O atoms) and the H-bond acceptors on the PCL blocks (H atoms attached to the activated carbons), we calculated the radial distribution functions (RDF) for such interacting pairs of oxygen and hydrogen atoms (i.e., $g_{OH}(r)$) present in the drugs and block copolymers, respectively. Here, the RDF is

defined as the ratio of the local density of the intermolecular O-H pairs to their average density of the entire simulation system at various inter-atomic distances.

Since there are several H-bond acceptors on both sets of drugs, we adopt a numbering scheme as shown in Figure 7.7 to designate the oxygen atoms present on the drug molecules. Table 7.3 summarizes the locations of the first peak of the corresponding $g_{OH}(r)$ plots of the drug/block copolymer mixtures. For clarity, we do not show the original RDF plots here. The positions of the peaks in a RDF plot signify the preferred inter-atomic distances between the atoms of interest (intermolecular O and H in this case). According to the geometric definition of H-bond adapted in the present work, close proximity of H-bond acceptor/donor pair atoms (O-H pair) at distances less than or equal to 2.6 Å may possibly lead to H-bond formation [97, 98]. The bold figures in Table 7.3 represent the inter-O-H distances of the first peak locations that fall into the aforementioned H-bond definition. In other words, these pairs can be considered as probable H-bond sites. This allows us to count the approximate number of available H-bond sites between drugs and the block copolymers with respect to only H-bond acceptor groups on the drug molecules. It can be seen from Table 7.3 that for cucurbitacin drugs, there are approximately the same number of H-bond sites (about 2 to 3) in both PEO-*b*-PCL and PEO-*b*-3PCL cases, suggesting that the additional H-bonds formed in the PEO-*b*-3PCL system (Figure 7.5) is attributed to the ability of the H-bond donors on the PCL blocks to form H-bonds with individual H-bond acceptors on the cucurbitacin molecules.

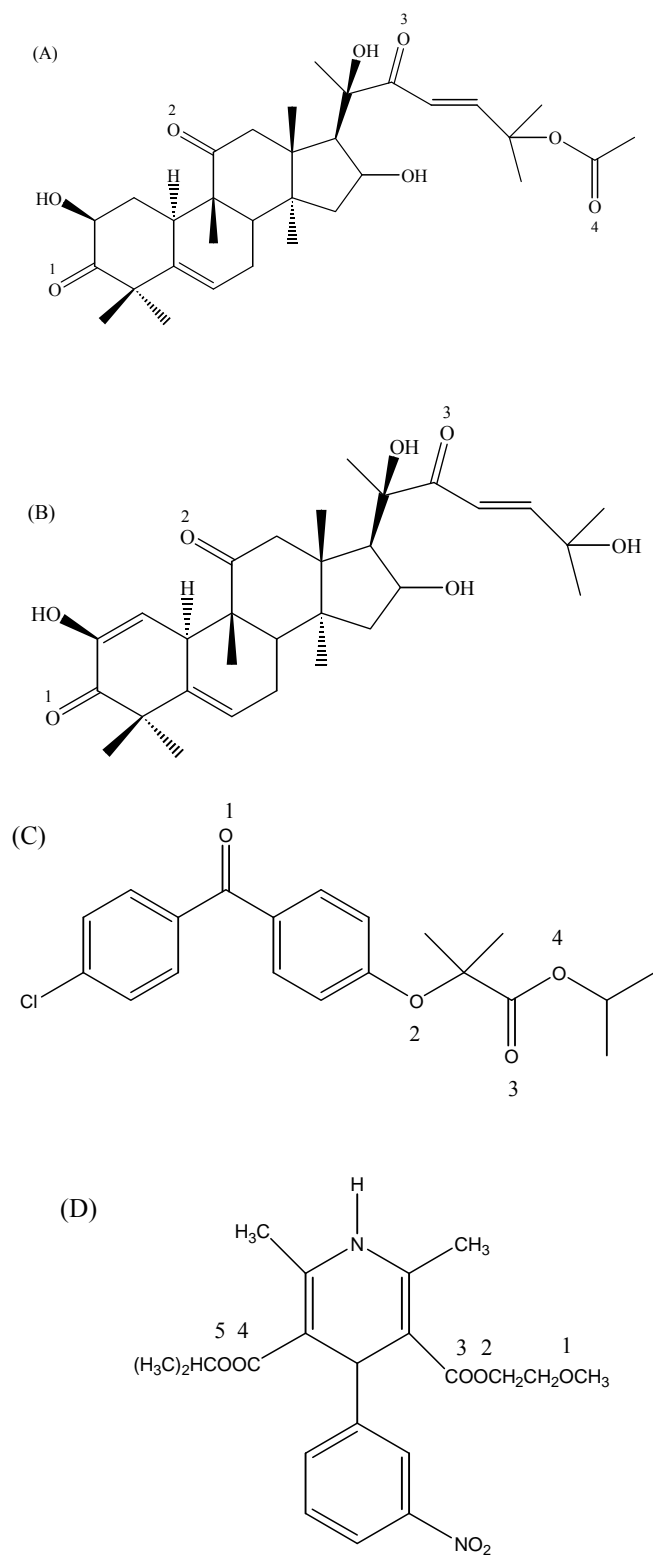


Figure 7.7 Numbering scheme of H-bond acceptor atoms of (A) CuB; (B) CuI; (C) Fenofibrate; and (D) Nimodipine.

Table 7.3 Locations of the first intermolecular OH peaks obtained from $g_{OH}(r)$ of mixtures containing 10 wt% drug (CuB, CuI, fenofibrate, and nimodipine) and remaining block copolymer – PEO(2500)-*b*-PCL(2500) and PEO(2500)-*b*-3PCL(2400).

Drug	Potential intermolecular hydrogen bonds	Position of first peak (Å) for PEO- <i>b</i> -PCL	Position of first peak (Å) for PEO- <i>b</i> -3PCL
CuB	(CuB)C=O(1)---H(PCL)	~ 2.45	~ 1.75
	(CuB)C=O(2)---H(PCL)	~ 2.25	~ 2.35
	(CuB)C=O(3)---H(PCL)	~ 2.75	~ 2.75
	(CuB)C=O(4)---H(PCL)	~ 2.45	~ 2.25
CuI	(CuI)C=O(1)---H(PCL)	~ 2.75	~ 5.55
	(CuI)C=O(2)---H(PCL)	~ 2.45	~ 5.05
	(CuI)C=O(3)---H(PCL)	~ 2.65	~ 1.95
Fenofibrate (F)	(F)O(1)---H(PCL)	~ 1.75	~ 1.75
	(F)O(2)---H(PCL)	~ 2.55	~ 4.25
	(F)O(3)---H(PCL)	~ 2.65	~ 2.55
	(F)O(4)---H(PCL)	~ 2.55	~ 3.25
Nimodipine (N)	(N)O(1)---H(PCL)	~ 3.05	~ 3.75
	(N)O(2)---H(PCL)	~ 2.65	~ 2.65
	(N)O(3)---H(PCL)	~ 2.35	~ 2.75
	(N)O(4)---H(PCL)	~ 2.35	~ 2.65
	(N)O(5)---H(PCL)	~ 2.65	~ 3.25

Note: O: Oxygen atom; H: Hydrogen atom. The bold figures in dark boxes represent inter-atomic distance capable of forming H-bond.

On the other hand, for fenofibrate and nimodipine drugs, the number of H-bond sites decreases significantly from approximately 4 (PEO-*b*-PCL) to 2 (PEO-*b*-3PCL) (See Table 7.3), leading to a decrease in the number of H-bonds formed (Figure 7.6). Results in Table 7.3 also suggest that only H-bond acceptors that are far apart from each other on the fenofibrate and nimodipine molecules could form H-bonds with the PCL blocks. In other words, clustering of H-bond acceptors restricts their interactions with the PCL blocks in the multi-block architecture. This is obviously not the case for the cucurbitacin drugs as their H-bond acceptors are evenly distributed on the drug molecules. The above findings suggest that multi-hydrophobic block architecture could potentially increase the drug loading for hydrophobic drugs with structures containing evenly distributed multiple H-bond donors and acceptors.

7.4 Summary

Molecular dynamics simulation was utilized to determine the drug encapsulation capability of PEO-*b*-3PCL by computing the χ parameters for the corresponding binary drug/multi-block copolymer mixtures (10 wt% of drug) containing hydrophobic drugs with very different spatial distribution of H-bond donors and acceptors on their molecular structures. The computed χ values were used to infer the solubility of the drugs in PEO-*b*-3PCL by comparing that for the most commonly used linear di-block PEO-*b*-PCL with comparable molecular weights. It was found that PEO-*b*-3PCL shows a great potential in encapsulating cucurbitacin drugs, which have an even distribution of H-bond donors and

acceptors on their molecules. The reason for such an observation was mainly attributed to the increase in the number of hydrogen bonds formed between the drugs and the PCL blocks, leading to much lower χ values. In the cases of fenofibrate and nimodipine, since they contain only clustered H-bond acceptors, the multi-hydrophobic block architecture of PEO-*b*-3PCL could not interact effectively through H-bonds with such drugs, leading to much higher χ values. This study shows the potential of using multi-block copolymers with multi-hydrophobic blocks as nano-carriers for encapsulating drugs that contain evenly distributed multi-H-bond donors and acceptors such as cucurbitacin drugs. By providing the atomistic details, the present study opens very interesting perspectives in drug delivery by showing the potential use of polymeric micelles made up of block copolymers with very different morphologies.

Chapter 8

Conclusion and Outlook

In this thesis, MD simulation approach was utilized to compute the Flory-Huggins interaction parameters (χ) between various water insoluble drugs and di-block copolymers in order to assess the power of this computational approach in predicting experimental solubility trends. The MD approach predicted the experimental solubility trends very well. Additionally, this approach provides useful atomistic details related to not only intermolecular interactions but also to intra-molecular interactions contributing to the thermodynamic compatibility. Based on the present work, the MD approaches outperformed the commonly used GCM in many aspects. MD simulation was able to capture most of the thermodynamic aspects of the drug solubility in di-block copolymers. It was evident from the study described in the Chapter 6 that the MD simulation can describe the effect of stereochemistry of the hydrophobic block on the polymer/drug miscibility. It is worth noting that the GCM fails to distinguish among different stereoisomers of block copolymers.

There are essentially two different approaches to calculate the χ values between drugs and di-block copolymers, as described in the Chapter 4. In one approach, the χ values were calculated using the solubility parameters (δ) derived from MD simulations of the drugs and di-block copolymers in their pure component form. This approach is still the most widely used approach to calculate the χ values in the pharmaceutical research, due to its ease of applicability. Even, the GCM method utilizes this basic approach to predict the miscibility. But, unfortunately, in this approach, the effect of concentration on the χ values, which allows us to study the effect of drug loadings, cannot be studied. Moreover, using this approach, one cannot predict negative χ values which generally results due to the presence of specific interactions in the mixture systems. Consequently, this approach completely neglects the presence of such intermolecular specific interactions. Because of these limitations, we adopted another approach in which the χ values are calculated based on the heats of mixing obtained from the simulation. The local packing of the drug molecules and segments of the block copolymers in a mixture environment is taken into account in the latter approach. In other words, the calculated χ manifests the behaviour of the drugs and PEO-*b*-PCL in the presence of each other.

The conventional compatibility studies focus on the interaction between the hydrophobic block of a block copolymer and the drug of interest. But the investigations of effect of local packing on compatibility (described in Chapter 4) supports the inclusion of hydrophilic block (PEO block) as well into the calculations of δ and χ . In other words, interactions of drug with the whole di-

block copolymer have to be considered. Our results confirm that both the interaction energy potential and the local molecular packing play vital roles in the correct prediction of δ and χ values. In the following Sections 8.1 and 8.2, we summarize the findings related to the Set-I (CuB and CuI) and the Set-II (fenofibrate and nimodipine) drugs, respectively.

8.1 Cucurbitacin Drugs

Two hydrophobic anti-cancer cucurbitacin drugs, CuB and CuI, with multiple H-bond donors and acceptors evenly distributed on their molecules were selected as model drugs to study the roles of polar and non-polar intermolecular interactions in the improvement of drug loading capacity of di-block copolymers. In the system of hydrophobic drugs, non-polar intermolecular interactions like short-range dispersive interactions are generally believed to be dominant forces influencing the drug loading capacity of di-block copolymers. But, our results in Chapter 5 confirm that besides these interactions, electrostatic intermolecular interactions also play a vital role in inducing compatibility in these drug/di-block copolymer systems. In fact, in the present set of hydrophobic drugs, we found that dispersive interactions did not contribute positively to inducing compatibility while electrostatic interactions, in the form of H-bonding, contributed positively, leading to lower χ values for the drug/PEO-*b*-PCL systems with high PCL/PEO (w/w) ratios. RDF and H-bond analysis of model mixtures performed in the Chapter 5, confirmed that the formation of H-bonds between multiple H-bond sites on the PCL block (hydrogen atoms of *activated carbons*) and single H-bond

sites on the drug molecules were responsible for inducing drug/ PEO-*b*-PCL affinity.

Further, we extended this study to functionalized di-block copolymers with substituent branches of benzyl carboxylate group, i.e., PEO-*b*-PBCL block copolymer with different tacticities. The tacticity of the di-block copolymer was found to influence significantly the solubility of cucurbitacin drugs in it. Based on MD simulation results obtained in the Chapter 6, the syndiotactic configuration was found to be the ideal stereo isomer for inducing the miscibility between these drugs and PEO-*b*-PBCL. The solubility of the drugs in the syndiotactic version of di-block copolymers was attributed to the favourable intramolecular interaction (π - π interaction) of the di-block copolymer and favourable intermolecular interaction between the di-block copolymer and the drugs. Favourable intermolecular associations/interactions are generally established through specific interactions which aid in achieving negative values of heats of mixing and hence negative χ values. The formation of such intermolecular specific interactions is largely hindered by the presence of intra-molecular π - π interactions. Hence, the syndiotactic version of the di-block copolymer which exhibits minimal π - π interactions succeeds in establishing favourable intermolecular specific interactions between the drug molecules and the di-block copolymer.

Finally, the multi-hydrophobic block architecture (PEO-*b*-3PCL) was able to encapsulate more cucurbitacin drugs compared to linear di-block copolymer PEO-*b*-PCL with the same PCL/PEO (w/w) ratio of 1.0. Analysis of the intermolecular interactions indicates that the number of hydrogen bonds formed between the

three PCL blocks and cucurbitacin drugs is significantly higher than that of the linear di-block copolymer. The study performed in Chapter 7 shows the potential of using multi-hydrophobic block copolymers as nano-carriers for encapsulating drugs that contain evenly distributed multi-H-bond donors and acceptors such as cucurbitacin drugs.

8.2 Fenofibrate and Nimodipine Drugs

Unlike cucurbitacin drugs, this set of drugs essentially contains only clustered H-bond acceptors. In the binary mixtures containing this set of drugs and PEO-*b*-PBCL, the absence of H-bond donors on their molecules was found to be responsible for their unfavourable interactions with substituent branches (benzyl carboxylate group) containing essentially only H-bond acceptors (e.g., -C=O(Chain) and Aromatic rings). Due to this, the strong intra-molecular interactions (e.g., π - π interactions and π - H(Chain) interactions) existing in such di-block copolymers could not be overcome, which consequently led to an increase in χ values for their binary mixtures.

In the multi-hydrophobic block architecture (PEO-*b*-3PCL), the clustering of H-bond acceptors restricted their interactions with the H-bond donors present on the PCL blocks, leading to much higher χ values. Thus, owing to the absence of hydrogen bond donors and the clustering of the H-bond acceptors on the fenofibrate and nimodipine molecules, this significantly reduces the number of hydrogen bonds formed in the multi-PCL block environment even though the

number of H-bond acceptors of this set of drugs is comparable to that of the cucurbitacin drugs (Set-I).

8.3 Limitations and Assumptions

There are various limitations and assumptions to the methodologies employed in the present research work. Few of them are related to the modeling part while others to the simulation part. Few most important of them will be discussed below along with their justification and treatment in the context of the purpose of the present work.

- (a) **Molecular Models**: The molecular models used throughout the thesis are thermodynamically different from the reality that the di-block copolymers form micelles in the presence of drugs and water molecules. Hence, ideally one would like to simulate di-block copolymer micelles to determine how block copolymer structures and its block lengths affect drug loadings and encapsulation efficiency for the drug of interest. Nevertheless, simulating such systems at the atomistic level is totally impossible at the time being as the computational costs are prohibitively high. Therefore, in the present work, we have focussed on investigating binary interactions between drugs and di-block copolymers of interest in their liquid state rather than in micelle environment. Additionally, simulating di-block copolymers, drug molecules, and their mixtures in amorphous state is relevant as such molecules should not exhibit any long range

order when they form micelles. Moreover, using such amorphous structures to represent the mixture systems to compute the χ values is consistent with the spirit of the Flory-Huggins solution theory and with the fact that the drug reside not only in the core but also in the corona of the micelles.

- (b) **Absence of Water**: Here, we are aware of the fact that in real micelle environment, the water molecules are present outside and inside the PEO corona of the micelles. Hence, there are chances of interactions of PEO with water as well, which will definitely affect the interactions between drug molecules and the PEO or even the PCL block. In fact, when PEO is dissolved into water, water molecules always wrap around the PEO molecules. And this is not the case for PPO and PMO. However, given the intention of the present work and the limitation of the available computational resources, we were not able to determine the effect of water on the computed χ parameters. In future, a systematic study might provide a key to deal with this problem efficiently.
- (c) **Equilibration issues**: MD simulations are computationally expensive and hence, in order to fulfill the condition of ergodic hypothesis (Refer Section 3.1), we have to run the simulation long enough to ensure the stability and equilibration of the systems so that the values of final property we obtain are statistically significant. The simulation times, we used were long enough to equilibrate the

systems of drug molecules. But, unfortunately, equilibration of block copolymers both in pure and mixture states could not be achieved over the simulation times we could practically use. Hence, to overcome this equilibration issue, we utilized the RIS theory to generate their initial conformations which could not be far from the equilibrated structures. Additionally, to render the collected sample uncorrelated for the mixture systems, we chose sampling interval based on the calculations of the velocity autocorrelation functions of the drug molecules.

8.4 Implications and Future Work

The contributions of the analysis of the discussed methods for designing polymeric drug delivery systems are of relevance to industrial practitioners and academicians alike. Various atomistic details available from the MD analysis gave useful information about the type and nature of existing inter as well as intra-molecular interactions. In the future, the methodologies discussed in the present thesis have great potential to provide an alternative to cumbersome and expensive “*trial and error*” type of formulation studies. By extending this approach to other block copolymer/drug systems, we can easily test the success of this approach as a predictive tool for defining the best block copolymer among the library of different block copolymers synthesized in lab.

Drug loading capacity and drug release kinetics are two critical functional properties of any drug carrier. In the present work, the molecular origin of the

increase/decrease of drug loading capacity of di-block copolymers was studied. The study of different types of specific interactions gave a better picture of the solubilisation of hydrophobic drugs in such di-block copolymers. In one of the study described in the Chapter 5, we briefly discussed the implications of the presence of hydrogen bonding between drugs and di-block copolymers on experimentally observed *in vitro* drug release kinetics of these drugs. In one of the studies by La *et al.* [116], the strength of interactions between the drug and the core-forming block was found to influence its release rate. Hence, a systematic study similar to one presented in this thesis, needs to be performed in order to find out the importance and influence of inter or intra-molecular interactions on *in vitro* drug release kinetics. In particular, the release of drugs from these block copolymer micelles will depend upon the rate of diffusion of the drugs from the micelles which will eventually depend on diffusion coefficients of these drugs. An ideal drug carrier possesses high drug loading with controlled release kinetics and minimum burst release. Polymer-drug compatibility measured using χ parameters tends to have opposite effects on both of these functional properties. The lower χ values give possibility of having higher drug loading with much slower drug release while, on the other hand, higher χ values generate lower drug loading with possibility of more burst release. Hence, an optimized χ value is required in order to have optimized functional properties. This thesis describes a qualitative method of estimating these parameters which compares performance based on comparison and/or experimental data. In the future, by extending methodologies described in the current thesis, one can come up with quantitative methods of estimating χ ,

which can relate drug loading and diffusion coefficient at the same time. This will probably help us to choose the right block copolymer having optimized χ values. During the diffusion of drug from core to targeted tissue, the drug has to pass through the water medium present outside the micelles and partly in the PEO corona. Hence, the diffusion study can be designed in two parts, one in the absence of water and the other in the presence of water on the side of PEO block. This will help us compare the diffusion processes in these two situations.

We studied the effect of tacticity of functionalized block copolymers (PEO-*b*-PBCL) on χ parameters of binary mixtures and/or drug loading capacities of these block copolymers. The methodologies used for studying stereoisomers can be readily extended to study constitutional isomers of PEO-*b*-PBCL, by placing functional groups on different carbon positions other than α -position used in the previous study. Several groups [117-119] have reported the synthesis of homopolymers of ϵ -caprolactone bearing benzyl carboxylate, carboxyl or benzyloxy group on the methylene group in the γ -position of ϵ -caprolactone by ring opening polymerization of the functionalized ϵ -caprolactone monomer. Hence, as a next step, it would be interesting to study the systems containing PEO-*b*-PBCL with benzyl carboxylate group substituted at the γ -position.

Based on the brief study on multi-block copolymers described in the Chapter 7, one would be highly interested in the molecular level study of drug loading capacity of other unique carriers like star shaped block copolymers and dendrimers which act as unimolecular micelles. The methodologies described in Chapter 7 can be readily applied to these types of carriers.

Bibliography

1. Allen, C.; Maysinger, D.; Eisenberg, A. *Colloids Surf. , B Biointerfaces* **1999**, *16*, 3-27.
2. Jones, M. C.; Leroux, J. C. *Eur. J. Pharm. Biopharm.* **1999**, *48*, 101-111.
3. Kwon, G. S. *Crit. Rev. Ther. Drug Carr. Syst.* **2003**, *20*, 357-403.
4. Adams, M. L.; Lavasanifar, A. *J. Pharm. Sci.* **2003**, *92*, 1343-1355.
5. Liu, J.; Lee, H.; Allen, C. *Curr. Pharm. Des.* **2006**, *12*, 4685-4701.
6. Liu, J.; Xiao, Y.; Allen, C. *J. Pharm. Sci.* **2004**, *93*, 132-143.
7. Lavasanifar, A.; Samuel, J.; Kwon, G. S. *Adv. Drug Deliv. Rev.* **2002**, *54*, 169-190.
8. Soo, P. L.; Luo, L.; Maysinger, D.; Eisenberg, A. *Langmuir* **2002**, *18*, 9996-10004.
9. Liu, H.; Finn, N.; Yates, M. Z. *Langmuir* **2005**, *21*, 379-385.
10. Letchford, K.; Liggins, R.; Burt, H. *J. Pharm. Sci.* **2008**, *97*, 1179-1190.
11. Hildebrand, J.; Scott, R. L. *The Solubility of Nonelectrolytes*; 3rd ed.; Reinhold: New York, 1950.
12. Hancock, B. C.; York, P.; Rowe, R. C. *Int. J. Pharm.* **1997**, *148*, 1-21.
13. Reuteler-Faoro, D.; Ruelle, P.; Nam-Tran, H.; De Reyff, C.; Buchmann, M.; Negre, J. C.; Kesselring, U. W. *J. Phys. Chem.* **1988**, *92*, 6144-6148.

14. Archer, W. L. *Ind. Eng. Chem. Res.* **1991**, *30*, 2292-2298.
15. Barton, A. F. M., (ed.). In *CRC Handbook of Solubility Parameters and other Cohesion Parameters*; 2nd ed.; CRC Press: Boca Raton, Florida, 1992.
16. Krevelen, D. V. Properties of Polymer: their correlation with chemical structure; their numerical estimation and prediction from additive group contributions. In Krevelen, D. V., (ed.); 3rd ed.; Elsevier Scientific Pub. Co.: New York: 1990; pp. 189-224.
17. Fedors, R. F. *Polym. Eng. Sci.* **1974**, *14*, 147-154.
18. Elbro, H. S.; Fredenslund, A.; Rasmussen, P. *Ind. Eng. Chem. Res.* **1991**, *30*, 2576-2582.
19. Tsibanogiannis, I. N.; Kalospiros, N. S.; Tassios, D. P. *Ind. Eng. Chem. Res.* **1994**, *33*, 1641-1643.
20. Ihmels, E. C.; Gmehling, J. *Ind. Eng. Chem. Res.* **2003**, *42*, 408-412.
21. Patel, S.; Lavasanifar, A.; Choi, P. *Biomacromolecules* **2008**, *9*, 3014-3023.
22. Kavassalis, T. A.; Choi, P.; Rudin, A. *Mol. Sim.* **1993**, *11*, 229-241.
23. Kavassalis, T. A.; Choi, P.; Rudin, A. Molecular Models and Three Dimensional Solubility Parameters of nonionic Surfactants. In *Molecular Simulation and industrial applications-methods, examples and prospects*; Gubbins, K. E., Quirke, N., (eds.); Gordon and Breach: Amsterdam, 1996; pp. 315-329.
24. Choi, P.; Kavassalis, T. A.; Rudin, A. *J. Colloid and interface Sci.* **1992**, *150*, 386-393.

25. Choi, P.; Kavassalis, T. A.; Rudin, A. *Ind. Eng. Chem. Res.* **1994**, *33*, 3154-3159.
26. Huynh, L.; Grant, J.; Leroux, J. C.; Delmas, P.; Allen, C. *Pharm. Res.* **2008**, *25*, 147-157.
27. Hill, T. L. *An Introduction to Statistical Thermodynamics*; Dover: New York, 1986.
28. Flory, P. J. *J. Chem. Phys.* **1941**, *9*, 660-661.
29. Flory, P. J. *J. Chem. Phys.* **1942**, *10*, 51-61.
30. Huggins, M. L. *J. Chem. Phys.* **1941**, *9*, 440.
31. Huggins, M. L. *Ann. N. Y. Acad. Sci.* **1942**, *43*, 1-32.
32. Olabisi, O.; Robeson, L. M.; Shaw, M. T. *Polymer-Polymer Miscibility*; Academic Press: New York, 1979; .
33. Cheung, Y. W.; Stein, R. S.; Wignall, G. D.; Yang, H. E. *Macromolecules* **1993**, *26*, 5365-5371.
34. Lau, C.; Mi, Y. *J. Polym. Sci. Part B: Polym. Phys.* **2001**, *39*, 2390-2396.
35. Hildebrand, J. H. *Proc. Natl. Acad. Sci. U. S. A.* **1927**, *13*, 267-272.
36. Hildebrand, J. H. *J. Am. Chem. Soc.* **1929**, *51*, 66-80.
37. Longuet-Higgins, H. C. *Proc. Royal Soc. Lond. A* **1951**, *205*, 247-269.
38. Guggenheim, E. A. *Trans. Faraday Soc.* **1948**, *44*, 1007-1012.
39. Flory, P. J. *Principles of Polymer Chemistry*; Cornell University Press: Ithaca, New York, 1953.
40. Coleman, M. M.; Graf, J. F.; Painter, P. C. *Specific Interactions and the Miscibility of Polymer Blends*; Technomic: Lancaster PA, 1991.

41. Dudowicz, J.; Freed, K. F. *Macromolecules* **1991**, *24*, 5076-5095.
42. Dudowicz, J.; Freed, M. S.; Freed, K. F. *Macromolecules* **1991**, *24*, 5096-5111.
43. Flory, P. J. *J. Am. Chem. Soc.* **1965**, *87*, 1833-1838.
44. Sanchez, I. C.; Lacombe, R. H. *Macromolecules* **1978**, *11*, 1145-1156.
45. Jain, R. K.; Simha, R. *Macromolecules* **1980**, *13*, 1501-1508.
46. Koningsveld, R.; Kleintjens, L. A.; Schoffeleers, H. M. *Pure Appl. Chem.* **1974**, *39*, 1-32.
47. Frenkel, D.; Smit, B. *Understanding Molecular Simulation*; 2nd ed.; Academic Press: San Diego, 2002.
48. Allen, M. P.; Tildesley, D. J. *Computer Simulation of Liquids*; Oxford University Press: New York, 1989.
49. Leach, A. R. *Molecular Modelling: Principles and Applications*; 2nd ed.; Prentice Hall: New York, 2001.
50. Mcquarrie, D. A. *Statistical Mechanics*; Harper & Row: New York, 1976.
51. Cho, K.; Joannopoulos, J. D. *Phys. Rev. A* **1992**, *45*, 7089-7097.
52. Ermer, O. *Structure and Bonding* **1976**, *27*, 161-211.
53. Mayo, S. L.; Olafson, B. D.; Goddard III, W. A. *J. Phys. chem.* **1990**, *94*, 8897-8909.
54. Rappe, A. K.; Casewit, C. J.; Colwell, K. S.; Goddard III, W. A.; Skiff, W. M. *J. Am. Chem. Soc.* **1992**, *114*, 10024-10035.
55. Weiner, S. J.; Kollman, P. A.; Case, D. A.; Singh, U. C.; Ghio, C.; Alagona, G.; Profeta, S.; Weiner, P. *J. Am. Chem. Soc.* **1984**, *106*, 765-784.

56. Brooks, B. R.; Bruccoleri, R. E.; Olafson, B. D.; States, D. J.; Swaminathan, S.; Karplus, M. *J. Comp. chem.* **1983**, *4*, 187-217.
57. Halgren, T. A. *J. Comp. chem.* **1996**, *17*, 490-519.
58. Allinger, N. L. *J. Am. Chem. Soc.* **1977**, *99*, 8127-8134.
59. Hwang, M. J.; Stockfisch, T. P.; Hagler, A. T. *J. Am. Chem. Soc.* **1994**, *116*, 2515-2525.
60. Sun, H. *J. Comp. Chem.* **1994**, *15*, 752-768.
61. Sun, H. *Macromolecules* **1995**, *28*, 701-712.
62. Sun, H. *J. Phys. Chem. B* **1998**, *102*, 7338-7364.
63. Rigby, D. *Fluid Phase Equilib.* **2004**, *217*, 77-87.
64. Wilson, E. B.; Decius, J. C.; Cross, P. C. *Molecular Vibrations*; Dover: New York, 1980.
65. Waldman, M.; Hagler, A. T. *J. Comp. Chem.* **1993**, *14*, 1077-1084.
66. Schreiber, H.; Steinhauser, O. *Biochemistry* **1992**, *31*, 5856-5860.
67. Sagui, C.; Darden, T. A. *Annu. Rev. Biophys. Biomol. Struct.* **1999**, *28*, 155-179.
68. Verlet, L. *Phys. Rev.* **1967**, *159*, 98-103.
69. Nose, S. *J. Chem. Phys.* **1984**, *81*, 511-519.
70. Nose, S. *Molec. Phys.* **1984**, *52*, 255-268.
71. Hoover, W. G. *Phys. Rev. A* **1985**, *31*, 1695-1697.
72. Andersen, H. C. *J. Chem. Phys.* **1980**, *72*, 2384-2393.
73. Theodorou, D. N.; Suter, U. W. *Macromolecules* **1986**, *19*, 139-154.

74. Flory, P. J. *Statistical Mechanics of Chain Molecules*; Hanser: New York, 1989.
75. Ewald, P. *Ann. Phys.* **1921**, *64*, 253-287.
76. Choucair, A.; Eisenberg, A. *J. Am. Chem. Soc.* **2003**, *125*, 11993-12000.
77. Nagarajan, R.; Barry, M.; Ruckenstein, E. *Langmuir* **1986**, *2*, 210-215.
78. Forrest, M. L.; Zhao, A.; Won, C. Y.; Malick, A. W.; Kwon, G. S. *J. Control. Release* **2006**, *116*, 139-149.
79. Jette, K. K.; Law, D.; Schmitt, E. E.; Kwon, G. S. *Pharm. Res.* **2004**, *21*, 114-119.
80. Ge, H.; Hu, Y.; Jaing, X.; Cheng, D.; Yuan, Y.; Bi, H.; Yang, C. *J. Pharm. Sci.* **2002**, *91*, 1463-1473.
81. Flory, P. J. *Macromolecules* **1974**, *7*, 381-392.
82. Mattice, W. L.; Suter, U. W. *Conformational Theory of Large Molecules: The Rotational Isomeric State Model in Macromolecular Systems*; J. Wiley: New York, 1994.
83. Flory, P. J. *J. Chem. Phys.* **1949**, *17*, 303-310.
84. Gadelle, F.; Koros, W. J.; Schechter, R. S. 1995, *28*, 4883-4892. *Macromolecules* **1995**, *28*, 4883-4892.
85. Aliabadi, H. M.; Elhasi, S.; Mahmud, A.; Gulamhusein, R.; Mahdipoor, P.; Lavasanifar, A. *Int. J. Pharm.* **2007**, *329*, 158-165.
86. Kohori, F.; Yokoyama, M.; Sakai, K.; Okano, T. *J. Control. Release* **2002**, *78*, 155-163.

87. Fournier, F.; Dufresne, M. H.; Smith, D. C.; Ranger, M.; Leroux, J. C.
Pharm. Res. **2004**, *21*, 962-968.
88. Chen, J. C.; Chiu, M. H.; Nie, R. L.; Cordell, G. A.; Qiu, S. X. *Nat. Prod. Rep.* **2005**, *22*, 386-399.
89. Miro, M. *Phytother. Res.* **1995**, *9*, 159-168.
90. Peters, R. R.; Farias, M. R.; Ribeiro-do-Valle, R. M. *Planta Med.* **1997**, *63*, 525-528.
91. Yesilada, E.; Tanaka, S.; Sezik, E.; Tabata, M. *J. Nat. Prod.* **1988**, *51*, 504-508.
92. Blaskovich, M. A.; Sun, J.; Cantor, A.; Turkson, J.; Jove, R.; Sebti, S. M.
Cancer Res. **2003**, *63*, 1270-1279.
93. Sun, J.; Blaskovich, M. A.; Jove, R.; Livingston, S. K.; Coppola, D.; Sebti, S. M. *Oncogene* **2005**, *24*, 3236-3245.
94. Jayaprakasam, B.; Seeram, N. P.; Nair, M. G. *Cancer Lett.* **2003**, *189*, 11-16.
95. Molavi, O.; Ma, Z.; Mahmud, A.; Alshamsan, A.; Samuel, J.; Lai, R.; Kwon, G. S.; Lavasanifar, A. *Int. J. Pharm.* **2008**, *347*, 118-127.
96. Mahmud, A.; Patel, S.; Molavi, O.; Choi, P.; Samuel, J.; Lavasanifar, A.
Biomacromolecules **2009**, *9*, 471-478.
97. Bertolini, D.; Cassettari, M.; Ferrario, M.; Grigolini, P.; Salvetti, G. *Adv. Chem. Phys.* **1985**, *62*, 277.
98. Geiger, A.; Mausbach, P. *Hydrogen-Bonded Liquids*; Dore, J. C., Teixeira, J., (eds.); Kluwer Academic Publishers: Dordrecht, Boston, 1991; pp. 171-183.

99. Senes, A.; Ubarretxena-Belandia, I.; Engelman, D. M. *Proc. Natl. Acad. Sci. U. S. A.* **2001**, *98*, 9056-9061.
100. Lee, J.; Park, K.; Chang, T.; Jung, J. C. *Macromolecules* **1992**, *25*, 6977-6979.
101. Lee, J.; Park, T.; Sung, J.; Park, S.; Chang, T. *Bull. Korean Chem. Soc.* **1991**, *12*, 569-574.
102. Lee, J.; Cho, E. C.; Cho, K. *J. Control. Release* **2004**, *94*, 323-335.
103. Lavasanifar, A.; Samuel, J.; Sattari, S.; Kwon, G. S. *Pharm. Res.* **2002**, *19*, 418-422.
104. Yokoyama, M.; Satoh, A.; Sakurai, Y.; Okano, T.; Matsumura, Y.; Kakizoe, T.; Kataoka, K. *J. Control. Release* **1998**, *55*, 219-229.
105. Latere Dwan'Isa, J. P.; Rouxhet, L.; Preat, V.; Brewster, M. E.; Arien, A. *Pharmazie* **2007**, *62*, 499-504.
106. Mahmud, A.; Xiong, X.; Lavasanifar, A. *Macromolecules* **2006**, *39*, 9419-9428.
107. Bai, F.; Li, F.; Calhoun, B. H.; Quirk, R. P.; Cheng, S. Physical Constant of Poly(propylene). In *Polymer Handbook*; Brandrup, J., Immergut, E. H. and Grulke, E. A., (eds.); A Wiley Interscience publications: New York, 1999; pp. V/21-V/30.
108. Kricheldorf, H. R.; Boettcher, C.; Tönnies, K. -. *Polymer* **1992**, *33*, 2817-2824.
109. Kricheldorf, H. R.; Kreiser-Saunders, I.; Boettcher, C. *Polymer* **1995**, *36*, 1253-1259.

110. Thakur, K. A. M.; Kean, R. T.; Hall, E. S.; Kolstad, J. J.; Lindgren, T. A.; Doscotch, M. A.; Siepmann, J. I.; Munson, E. J. *Macromolecules* **1997**, *30*, 2422-2428.
111. Thakur, K. A. M.; Kean, R. T.; Hall, E. S.; Kolstad, J. J.; Munson, E. J. *Macromolecules* **1998**, *31*, 1487-1494.
112. Burley, S. K.; Petsko, G. A. *Science* **1985**, *229*, 23-28.
113. Barlow, J. W.; Paul, D. R. *Polym. Eng. Sci.* **1981**, *21*, 985-996.
114. Cruz, C. A.; Barlow, J. W.; Paul, D. R. *Macromolecules* **1979**, *12*, 726-731.
115. Li, G.; Cowie, J. M. G.; Arrighi, V. *J. Appl. Polym. Sci.* **1999**, *74*, 639-646.
116. La, S. B.; Okano, T.; Kataoka, K. *J. Pharm. Sci.* **1996**, *85*, 85-90.
117. Trollsas, M.; Lee, V. Y.; Mecerreyes, D.; Lowenhielm, P.; Moller, M.; Miller, R. D.; Hedrick, J. L. *Macromolecules* **2000**, *33*, 4619-4627.
118. Lou, X.; Detrembleur, C.; Jérôme, R. *Macromolecular Rapid Communications* **2003**, *24*, 161-172.
119. Detrembleur, C.; Mazza, M.; Halleux, O.; Lecomte, P.; Mecerreyes, D.; Hedrick, J. L.; Jerome, R. *Macromolecules* **2000**, *33*, 14-18.

Appendix A

Flory-Huggins Lattice Theory of Polymer Solutions

Consider the lattice model of a polymer solution as shown in the Figure 2.3. This theory considers volume of each lattice site equal to the size of the solvent molecule and the segmental volume is considered to be approximately the same. If n_S is the number of solvent molecules and n_P and N are the number of polymer chains and the number of segments per polymer chain, respectively, then the total number of lattice sites, M , is equal to $(n_S + Nn_P)$. The volume fractions of polymer (ϕ_P) and solvent (ϕ_S) are given by following expressions:

$$\phi_P = \frac{Nn_P}{M} \tag{A.1}$$

$$\phi_S = \frac{n_S}{M}$$

Here, $\phi_P + \phi_S = 1$.

The change in the entropy of mixing (ΔS_{mix}) for polymer solutions can be calculated using:

$$\Delta S_{mix} = S_{mix} - S_p - S_s \quad (\text{A.2})$$

S_{mix} is entropy of the mixture while S_p and S_s are entropies of pure polymer and pure solvent, respectively. In the lattice model, the entropy of pure solvent is zero, i.e., $S_s = 0$. Now, utilizing the Boltzmann law of entropy ($S = k_b \ln \Omega$), the ΔS_{mix} can be given as:

$$\Delta S_{mix} = k_b [\ln \Omega_{mix} - \ln \Omega_p] \quad (\text{A.3})$$

where Ω_{mix} is the number of ways of arranging $(n_p + n_s)$ molecules into the lattice having M sites and Ω_p is the number of ways of arranging n_p molecules into the lattice with Nn_p sites. In general, Ω_{mix} can be expressed as follows:

$$\Omega_{mix} = \frac{\prod_{i=1}^{n_p} \omega_i}{n_p!} \quad (\text{A.4})$$

where ω_i is the number of ways of arranging the i -th polymer molecule in the lattice when there are already $(i - 1)$ polymer molecules in the lattice. The factor of $n_p!$ corrects for the over-counting since polymer chains are indistinguishable

and it is hard to tell the difference between the two configurations having same polymer distributions but different chain identities. The term $n_s!$ is not needed as there is only one way of placing the solvent molecules into the lattice after the placement of all polymer molecules.

Now, the next task is to derive a mathematical expression for the ω_i . Let us start with the calculation of placing a single polymer chain on the lattice, which will be denoted by ν_l . Since there are total M sites, the number of locations for placing the first segment of a polymer chain is M . With the first segment placed on the lattice, the fraction of available sites now becomes $M - 1/M$. If z is the coordination number describing the number of neighbouring sites then, the number of possible locations for placing the second segment will become $z\left(\frac{M-1}{M}\right)$. Similarly, for the third segment it becomes $(z-1)\left(\frac{M-2}{M}\right)$. The number of locations for placing the N^{th} segment of the chain would be $\left[(z-1)\left(\frac{M-(N-1)}{M}\right)\right]$. Hence, ν_l would be the product of all these expression,

which will be given by $\left(\frac{z-1}{M}\right)^{N-1} \frac{M!}{(M-N)!}$. Now, we follow the same above

procedure to obtain the number possible configurations for a set of n_p such chains in the whole lattice model. Hence, the number of configurations of placing the

first segment of all n_p chains (ω_1) would be $\frac{M!}{(N-n_p)!}$. Now, the number of

configurations for placing the remaining $(N-1)$ segments of all chains $\left(\prod_{i=2}^{n_p} \omega_i\right)$

would be given by $\left(\frac{z-1}{M}\right)^{n_p(N-1)} \frac{(M-n_p)!}{(M-Nn_p)!}$. Multiplying these two counts

together will give the expression for $\prod_{i=1}^{n_p} \omega_i$. Putting this in the equation (A.4)

along with $M = n_S + Nn_p$, we get the following expression for Ω_{mix} :

$$\Omega_{mix} = \left(\frac{z-1}{M}\right)^{n_p(N-1)} \frac{M!}{n_S!n_p!} \quad (\text{A.5})$$

Putting $M = Nn_p$, we get the expression for Ω_p :

$$\Omega_p = \left(\frac{z-1}{Nn_p}\right)^{n_p(N-1)} \left(\frac{(Nn_p)!}{n_p!}\right) \quad (\text{A.6})$$

Substituting (A.5) and (A.6) in (A.3), we get:

$$\Delta S_{mix} = k_b \ln \left(\frac{Nn_p}{M}\right)^{n_p(N-1)} \frac{M!}{n_S!(Nn_p)!} \quad (\text{A.7})$$

Apply the Stirling's approximation (Equation (2.12)) and simplify further using the expression (A.1) to get the following final expression for the entropy change on mixing:

$$\Delta S_{mix} = -k_b [n_S \ln \phi_S + n_p \ln \phi_p] \quad (\text{A.8})$$

Utilizing the random mixing assumption and utilizing the volume fractions in place of the mole fractions, we follow derivations similar to the one described in the Section 2.6.1, to get the following expression for the enthalpy change on mixing:

$$\Delta H_{mix} = Mz w \phi_p \phi_S \quad (\mathbf{A.9})$$

Appendix B

Prediction of the Molar Volume of the Repeating Units of Blocks of Copolymer

The group contribution method, GCVOL, first proposed by Elbro *et al.*[18], was used to predict the molar volumes of the repeating units of blocks of copolymer. According to this method, the molar volume V , is given by:

$$V = \sum n_i \Delta v_i \quad (\text{B.1})$$

where n_i is the number of groups i appearing in the compound, while Δv_i are group volume increments, which is given by the following polynomial function of absolute temperature:

$$\Delta v_i = A_i + B_i T + C_i T^2 \quad (\text{B.2})$$

where T is in Kelvin. The values of parameters A_i , B_i , and C_i are listed in the tables in the paper by Ihmels *et al.* [20].

The calculation of the molar volume of the repeating unit of PCL block at 413 K was taken as an example here. The following table shows the type and the number of groups present in the repeating unit of PCL block along with their A_i , B_i , and C_i values taken from the paper of Ihmels *et al.*

Group	Number of groups present	A cm ³ /mol	10 ³ B cm ³ /(mol K)	10 ⁵ C cm ³ /(mol K ²)
-COO	1	14.23	11.93	0.00
-CH ₂ - (chain)	5	12.52	12.94	0.00

(1) -COO group:

$$\begin{aligned}\Delta v_{-COO} &= 14.23 + 11.93 \times 10^{-3} \times 413 + 0 \\ &= 19.16 \text{ cm}^3 / \text{mol} .\end{aligned}$$

(2) -CH₂- (chain) group:

$$\begin{aligned}\Delta v_{-CH_2-} &= 12.52 + 12.94 \times 10^{-3} \times 413 + 0 \\ &= 17.86 \text{ cm}^3 / \text{mol} .\end{aligned}$$

$$\therefore V = 19.16 + 5 \times 17.86 = 108.46 \text{ cm}^3 / \text{mol} .$$

Appendix C

Calculations of Flory-Huggins Interaction Parameters from MD Data

The calculation of Flory-Huggins interaction parameter for binary system of PEO(2500)-*b*-PCL(2500)/CuB was taken as an example here. From NVT MD simulation, the average total energies were determined as follow:

	(Kcal/mol)
▪ Mixture of one PEO- <i>b</i> -PCL chain and one CuB molecule	: 473.03 ± 0.50
▪ PEO- <i>b</i> -PCL chain (Pure)	: 436.13 ± 0.85
▪ CuB drug (Pure)	: 40.54 ± 0.03

The enthalpy change on mixing for a mole of mixture, ΔH_m , can be calculated using the equation (4.5) and assuming ($\Delta PV \sim 0$) as follows:

$$\begin{aligned}\Delta H_m &= 473.0 - 436.13 - 40.54 \\ &= -3.64 \pm 0.99 \text{ kcal/mol}.\end{aligned}$$

We take the molar volume of the repeating unit of PEO block (V_{PEO}) as the reference volume, i.e., the volume of one site. Hence, we convert the above enthalpy change on mixing into the enthalpy change on mixing for a mole of lattice site, $\Delta H_{m,lattice}$, using the following expression:

$$\Delta H_{m,lattice} = \frac{\Delta H_m}{N_L}$$

where N_L is the total number of lattice sites in the mixture, which is calculated using the following equation:

$$N_L = \frac{V_{mixture}}{V_{PEO}}$$

At 473 K, V_{PEO} is 98.17 cm³/mol and $V_{mixture}$ for the mixture of one CuB, 56 repeating units of the PEO block, and 22 repeating units of the PCL block is 8470.28 cm³/mol. Using these values, N_L was found to be approximately 86. Hence,

$$\Delta H_{m,lattice} = \frac{-3.64 \pm 0.99}{86} = -0.042 \pm 0.011 \text{ kcal/mol}.$$

Putting this value in the equation (4.6), one can obtain the value of the Flory-Huggins interaction parameter (χ).